LBL-33961
UC-413

Lawrence Berkeley Laboratory
UNIVERSITY OF CALIFORNIA

On-Line Gas Chromatographic Studies of Rutherfordium (Element 104), Hahnium (Element 105), and Homologs

B. Kadkhodayan
(Ph.D. Thesis)

May 1993

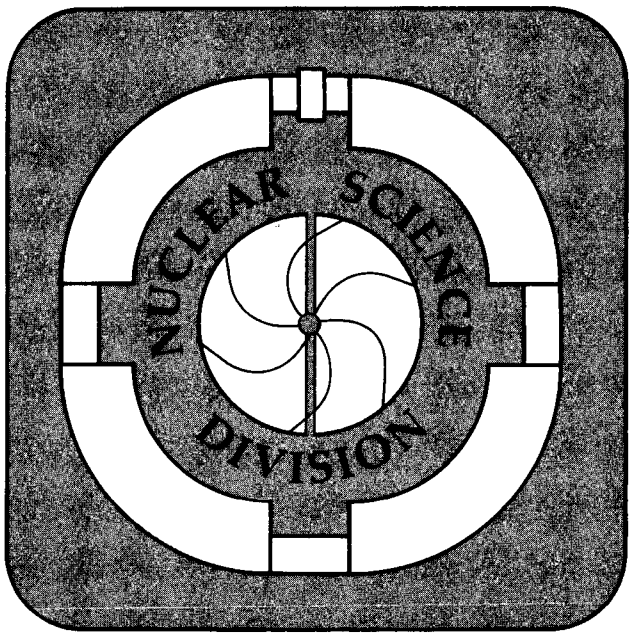

Prepared for the U.S. Department of Energy under Contract Number DE-AC03-76SF00098

DISCLAIMER

LBL-33961

On-line Gas Chromatographic Studies of Rutherfordium (Element 104), Hahnium (Element 105) and Homologs

Babak Kadkhodayan

Ph. D. Thesis

April 1, 1993

Department of Chemistry
University of California, Berkeley

and

Nuclear Science Division
Lawrence Berkeley Laboratory
University of California
Berkeley, CA 94720

This work was supported in part by the Office of Energy Research, Office of Basic Energy Sciences, Division of Chemical Sciences, U.S. Department of Energy, under Contract DE-AC03-76SF00098

Abstract

On-line Gas Chromatographic Studies of Rutherfordium (Element 104),

Hahnium(Element 105) and Homologs

by

Babak Kadkhodayan

Doctor of Philosophy in Chemistry

University of California at Berkeley

Professor Darleane C. Hoffman, Chair

Gas-phase isothermal chromatography is a method by which volatile compounds of different chemical elements can be separated according to their volatilities. The technique, coupled with theoretical modeling of the processes occurring in the chromatography column, provides accurate determination of thermodynamic properties (e.g., adsorption enthalpies) for compounds of elements, such as the transactinides, which can only be produced on an atom-at-a-time basis. In addition, the chemical selectivity of the isothermal chromatography technique provides the decontamination from interfering activities necessary for the determination of the nuclear decay properties of isotopes of the transactinide elements.

Volatility measurements were performed on chloride species of Rf and its group 4 homologs, Zr and Hf, as well as Ha and its group 5 homologs, Nb and Ta. Adsorption enthalpies were calculated for all species using a Monte Carlo code simulation based on a microscopic model for gas thermochromatography in open columns with laminar flow of the carrier gas. Preliminary results are presented for Zr- and Nb-bromides.

30.7-s ^{98}Zr, 7.1-s ^{100}Zr and 15-s ^{99}Nb were produced via the ^{235}U(n,f) reactions. 38-s ^{162}Hf, 1.7-min ^{165}Hf, 34-s ^{166}Ta, and 1.4-min ^{167}Ta were produced by the

$^{Nat}Eu + ^{147}Sm(^{20}Ne,xn)$ reactions. 65-s ^{261}Rf and 34-s ^{262}Ha were produced via the $^{248}Cm(^{18}O,5n)$ and $^{249}Bk(^{18}O,5n)$ reactions, respectively.

The Heavy Element Volatility Instrument (HEVI) was used for these volatility studies. HEVI is an on-line gas chromatography system which continuously separates halide species of short-lived nuclides according to their volatility. The following series in volatility and adsorption enthalpy of the group 4 element chlorides has been established: $ZrCl_4 \approx RfCl_4 > HfCl_4$, and $ZrCl_4 > RfCl_4 > HfCl_4$, respectively. Assuming similar molecular structures for chloride complexes within group 4 of the periodic table, a trend of decreasing volatility and ΔH_{ads} is observed as one moves down the group (noticed in Zr- and Hf-chlorides). Our results show a break in this expected trend. Further calculations are needed to assess whether this is due to relativistic effects in the transactinide region.

Dedication

This thesis is dedicated to my mother Soraya Afsar. Her constant love, support, and encouragement throughout my life has allowed me to achieve many of my goals and ambitions. I am fortunate to have a mother who is also one of my best friends.

I would also like to dedicate this work to my two sisters, Saloumeh and Miryam. I thank them for all their support.

Contents

List of Figures

List of Tables

Acknowledgements

First and foremost, I would like to thank my research advisor Dr. Darleane Hoffman. It has been a pleasure working in her group in the last five years. Darleane's constant guidance and support has made this work possible. I will always be grateful for her endless patience, generosity, and kindness.

I would like to thank Dr. Kenneth Gregorich not only for his scientific advise throughout the years, but for being my running buddy and my best friend. I have learned a great deal by observing Ken's calm, collected, and rational approach in solving problems and his general perspective on life. I also would like to thank Ken for keeping me in line and telling me "STOP IT Bobby, JUST STOP IT!!" when I needed it.

I thank Diana Lee for all her help with the many computer programs which were necessary for the analysis of my data. It has been very pleasant to start every working day with Diana's happy and cheerful greeting. I've enjoyed all our lunch conversations and her concern for my well being has always been appreciated.

I am also grateful to all the other members, past and present, of the LBL Heavy Element Nuclear and Radiochemistry Group [A. Türler (freely takes blame for anything and everything, "OK"), M. J. Nurmia (the walking encyclopedia), K. R. Czerwinski (Flipper), C. M. Gannett (Poopsey), H. L. Hall (Hoowerd), T. M. Hamilton (Boober), N. J. Hannink (Nasty), R. A. Henderson (uuhuum, need I say more), C. D. Kacher (Mr. fashion...NOT), S. A. Kreek (in one word, Obnoxious), M. R. Lane (the invisible man),

J. D. Leyba (Friar), M. F. Mohar (Biermeister), M. P. Neu (Sweety), and E. R. Sylwester (Sleepsalot)] for all their assistance.

I would like to thank all scientists from PSI and GSI involved in the hahnium experiments in Germany. I would specially like to thank Prof. Gäggeler for the opportunity to work at the PSI **SAPHIR** reactor.

I would like to thank the staff and crew of the LBL 88-Inch Cyclotron for providing me with the excellent heavy ion beams. I would specially like to thank Mr. Edward Chubak and Mrs. Ruth-Mary Larimer for all their assistance.

I am thankful to the U.S. Department of Energy for the use of the ^{248}Cm and ^{249}Bk, through the transplutonium element production facilities at the Oak Ridge National Laboratory. This work was supported in part by the Director, Office of Energy Research, Chemical Sciences Division, U.S. Department of Energy under contract number DE-AC03-76SF00098.

Chapter 1

Introduction

Ever since the discovery of periodic trends by the German chemist Lothar Meyer and the Russian Dmitri Mendeleev in 1869-70, the greatest tool for chemists in predicting the chemical properties of unknown elements has been the periodic table of the elements. The periodic table, as represented today, places elements into groups (columns) and periods (rows). As depicted in Fig. 1, there exists a period of elements from 58 to 71 called the lanthanide elements and a period of elements from 90 to 103 called the actinides, many of which are unstable and must be produced artificially. The periodic table shows elements 104 through 109, the transactinide elements, as homologs of hafnium through iridium. It is expected that this is a new transition series in which the 6d orbitals are being filled.

Recently there has been increased activity, both experimental and theoretical, in the study of the chemical properties of the transactinide elements. The special interest in this seventh row of the periodic table arises from predictions that due to relativistic effects the chemical properties of the heaviest elements might show deviations from periodic table trends. As early as 1969, Fricke and Greiner [FRI 69] predicted such deviations which may be understood if one considers that at very high atomic numbers the inner electrons attain relativistic velocities, thus leading to a contraction of the s and $p_{1/2}$ orbitals.

Periodic Table of the Elements

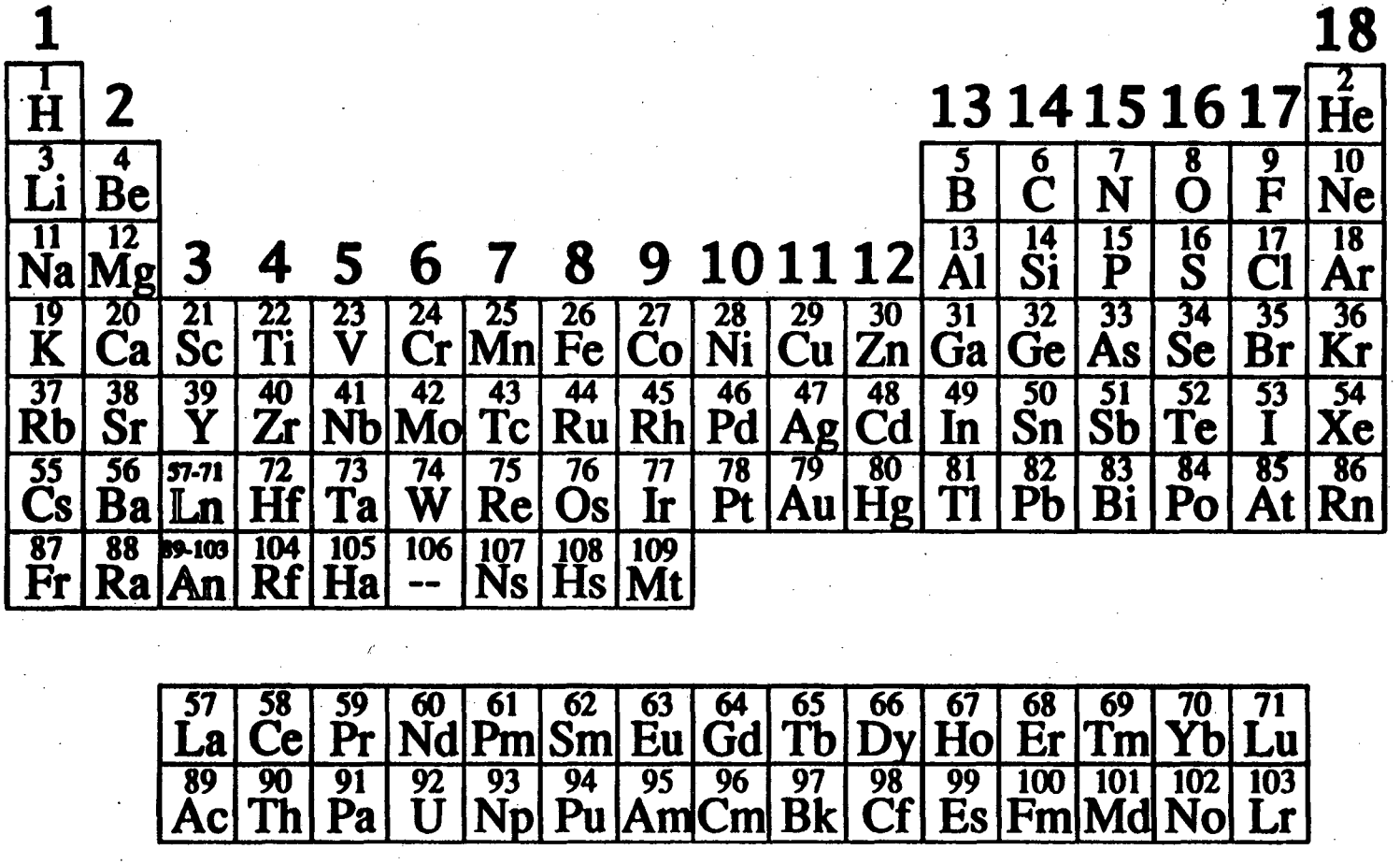

Fig. 1.1 The periodic table of the elements

The $p_{3/2}$ orbitals are relatively unchanged because the contraction effect is counteracted by spin-orbit effects. Consequently, the d and f electrons are more efficiently screened from the nuclear charge, resulting in an increase in energy and a radial extension for these orbitals. In transactinide elements relativistic effects may alter the relative stability of the 7s, 6d, and 7p valence electrons to such an extent that other oxidation states than those expected from periodic table extrapolations become important.

In the transition region at the end of the actinide series and beginning of the transactinide series, the role of the $7\Gamma_{p1/2}$ and 6d orbitals in the chemistry of the region is difficult to predict. Therefore, it is possible that some of these elements may exhibit p rather than d character. Recent extensive theoretical calculations [BRE 84, DES 80, KEL 84, PYY 88, ZHU 90] have provided chemists with predictions on how the relativistic rearrangements of valence electrons may affect the chemical properties of the heaviest elements. Multiconfiguration Dirac-Fock (MCDF) calculations [BRE 71, BRE 84, DES 80, ZHU 90] have predicted a ground state electron configuration for Lr^o of $[Rn]5f^{14}7s^27p^1$ instead of $[Rn]5f^{14}6d7s^2$ as expected by analogy with Lu^o. Based on extrapolations from this result Keller [KEL 84] suggested that the ground state configuration of Rf should be $7s^27p^2$ rather than $6d^27s^2$ analogous to the $5d^26s^2$ configuration of its lighter homolog, Hf. This prediction may imply that element 104 should behave like a heavy p-element similar to Pb. In recent more accurate MCDF calculations using 468 jj-configurations, Glebov et al. [GLE 89] determined that the ground state of Rf should be a J=2 level, Fig. 2, consisting of the $6d7s^27p$ configuration (80%) with a level only 0.5 eV higher consisting of the $6d^27s^2$ configuration (95%), while the $7s^27p^2$ state (predicted to be the ground state by Keller) is 2.9 eV above the ground state. Based on their calculations, Glebov et al. concluded that Rf should show no distinctive p-character. In fact Rf should behave like Hf, a typical d-element. In the case of Ha, MCDF calculations [FRI SUB] have predicted a ground state electronic configuration of $7s^26d^3$.

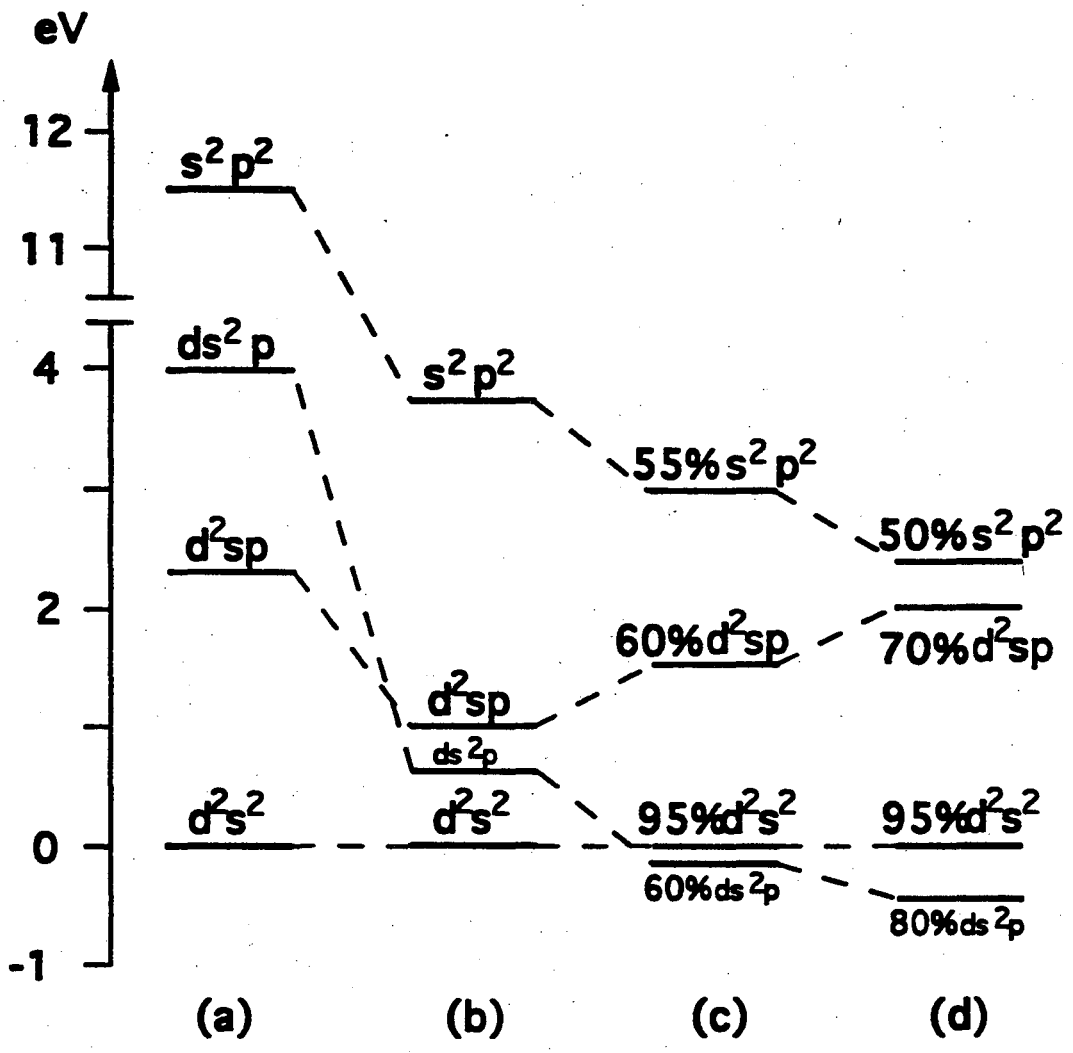

Prepared from [GLE 89]

Fig. 1.2 Energies of low-lying states of Rf:
a) nonrelativistic calculations; b) relativistic single-configuration calculations;
c) relativistic calculations involving 30 configurations; d) relativistic calculations involving 468 configurations.

An intense effort in MCDF calculations relevant to the volatilities of halides of transactinide elements and the lighter homologs is being carried out by Perishina [PER 93], presently at the Gesellschaft für Schwerionenforschung (GSI), Germany. Perishina et al. are using the MCDF method in molecular orbital calculations to arrive at the degree of ionic or covalent character in the transactinide and homolog halides. A more covalent (less ionic) character corresponds to a more volatile halide species. These calculations arrive at adsorption enthalpy values of halides on various surfaces. From these values volatility temperatures for the halides are calculated. While the absolute values of the adsorption enthalpies or the volatilities from the MCDF calculations may not be accurate, the trends within a given group of the periodic table should be valid.

The experimental verification of the predictions of these calculations is desirable. Various chemical procedures have been devised to investigate the influence of relativistic effects on the chemical properties of the transactinides. These experiments include volatility studies of both the elemental form [ZHU 89] and of the halides [GAG 91, JOS 88, TUR 90, ZVA 66,69,70,76,89] using on-line gas chromatographic techniques, and solution chemistry using chromatographic and solvent extraction techniques. Volatility experiments by Zhuikov et al. [ZHU 89] in 1989 indicated that Rf and Hf did not behave like p-elements. These experiments are based on the large differences in the heats of sublimation between p and d elements. For example [KAT 86], the heats of sublimation of Hf (611 KJ/mol), Ta (782 KJ/mol), and W (849 KJ/mol) are 3 to 4 times higher than those of Tl (180 KJ/mol), Pb (197 KJ/mol), and Bi (209 KJ/mol). These large differences are based on the difference of bond strengths associated with the p and d elements. In another work published in 1990, Zhuikov et al. [ZHU 90] evaluated various experimental approaches for investigating relativistic effects in Rf involving volatilities in the elemental state, thermochromatography of Rf tetrahalides, and the stability of lower oxidation states. It was stated that in gas chromatography experiments (elemental forms) it is hardly possible to distinguish

between "relativistic" and "non-relativistic" atoms as it would be extremely difficult to stabilize the elements like Hf and Rf in the atomic state at the required high column temperatures of up to 1500 °C. Thermochromatography of the tetrachlorides or tetrabromides appeared most promising.

Rudolph [RUD 80] has investigated the validity of "on-line" gas chromatography measurements of inorganic halides and oxides as a tool in determining adsorption enthalpies and entropies for short-lived nuclides. Adsorption enthalpies and entropies on quartz surfaces were measured, for $NbCl_5$ and $NbOCl_3$, using the 54 s $^{97}Nb^m$. These results were compared with results from "off-line" gas chromatography measurements. As shown in Table 1, on-line measurements of adsorption enthalpies and entropies were found to provide reliable and reproducible results.

Table 1.1 Comparison of adsorption enthalpies and entropies from on-line and off-line measurements.

Compound	ΔH_{ads} (kJ mole^{-1})		ΔS_{ads} (J mole^{-1} K^{-1})	
	on-line	off-line	on-line	off-line
$NbCl_5$	-69 ± 3	-68 ± 3	-7 ± 5	-15 ± 5
$NbOCl_3$	-96 ± 3	-94 ± 13	-31 ± 5	-34 ± 14

Data from [RUD 80]Table 1.1

The short half-lives and low production rates of the transactinide elements make on-line gas chromatography an invaluable technique in the investigation of nuclear and chemical properties of these elements. The study of the nuclear properties of these elements is made possible due to a very fast and efficient chemical separation of transactinides from interfering actinide activities. Furthermore, chemical properties, such

as volatility of halide species of the transactinides and homologs can be studied. From these measurements, adsorption enthalpies on various solid surfaces are calculated, and trends in the periodic table are investigated. A sudden break or change in a continuing trend within a periodic group may indicate the presence of relativistic effects.

Chapter 2

Instrumentation Development

Experimental investigation of the chemical properties of the transactinide elements is extremely difficult. The longest-lived known isotopes of the transactinide elements have half-lives of 65 s or less. These elements have only been produced in heavy ion fusion reactions at rates of a few atoms per minute or less. Furthermore, actinide activities which are produced in high yields in these reactions interfere in the detection of the transactinides, further complicating chemical studies. Due to the low production rates and short half-lives of these nuclides, very specific and unique chemical procedures have been devised. Some procedures are designed to operate continuously, whereas others allow fast reproducible separations with high repetition rates in order to obtain statistically significant results. On-line isothermal gas chromatography is one of the most unique chemical procedures designed to investigate the properties of these elements. This method takes advantage of the high volatilities of the halides of the group 4, 5 and 6 transition elements to efficiently separate transactinide halides and their lighter homologs from the less volatile trivalent actinides. This chemical separation allows the investigation of nuclear and chemical properties of the transactinide elements.

2.1 Previous work

2.1.1 Zvara et al. (Gas Thermochromatography)

On-line gas thermochromatography experiments with transactinide elements were performed in 1966 by Zvara et al. [ZVA 66]. Their studies have continued until today [BEL 75, ZHU 89, ZVA 69,70,76]. Taking advantage of the fact that bromides and chlorides of the group 4 and 5 elements, and possibly Rf and Ha, form rather volatile species, they performed gas-solid thermochromatography. A schematic of their apparatus is given in Fig. 2.1. The reaction $^{242}Pu(^{22}Ne,4n)^{260}104$ was used to form the Rf atoms. In some experiments a Sm target was irradiated, along with the Pu target, to produce Hf activities simultaneously. Recoiling products formed in the nuclear reaction (section I) were carried in a flow of N_2 carrier gas to the chlorinating section of the apparatus (section II), and the reaction products were subjected to a mixture of $NbCl_5$ and $ZrCl_4$ vapors. The volatile halides were carried with the nitrogen flow down a 4 m long chromatography column (section III). Different materials, such as glass, Teflon, or stainless steel, were used in this section as exchange surfaces. An inert filter (section IV) was placed before a series of mica fission track detectors (section V), to prevent any large particles from entering the detector chamber. Sections VI and VII served as a trap for chloride vapors that passed through previous sections. Two series of experiments were conducted. All sections of the apparatus were maintained at a preselected uniform temperature. In the first series, the temperature was maintained at approximately 220-250 °C. Four fission tracks were observed, and were attributed to the decay of ^{260}Rf. In the second series of experiments, the temperature of the column was kept at approximately 300-350 °C. Eight fission tracks were observed. Based on various justifications involving a detector efficiency which was optimized for a 0.3 sec half life (which was thought at the time to be correct for ^{260}Rf) and the behavior of the Hf

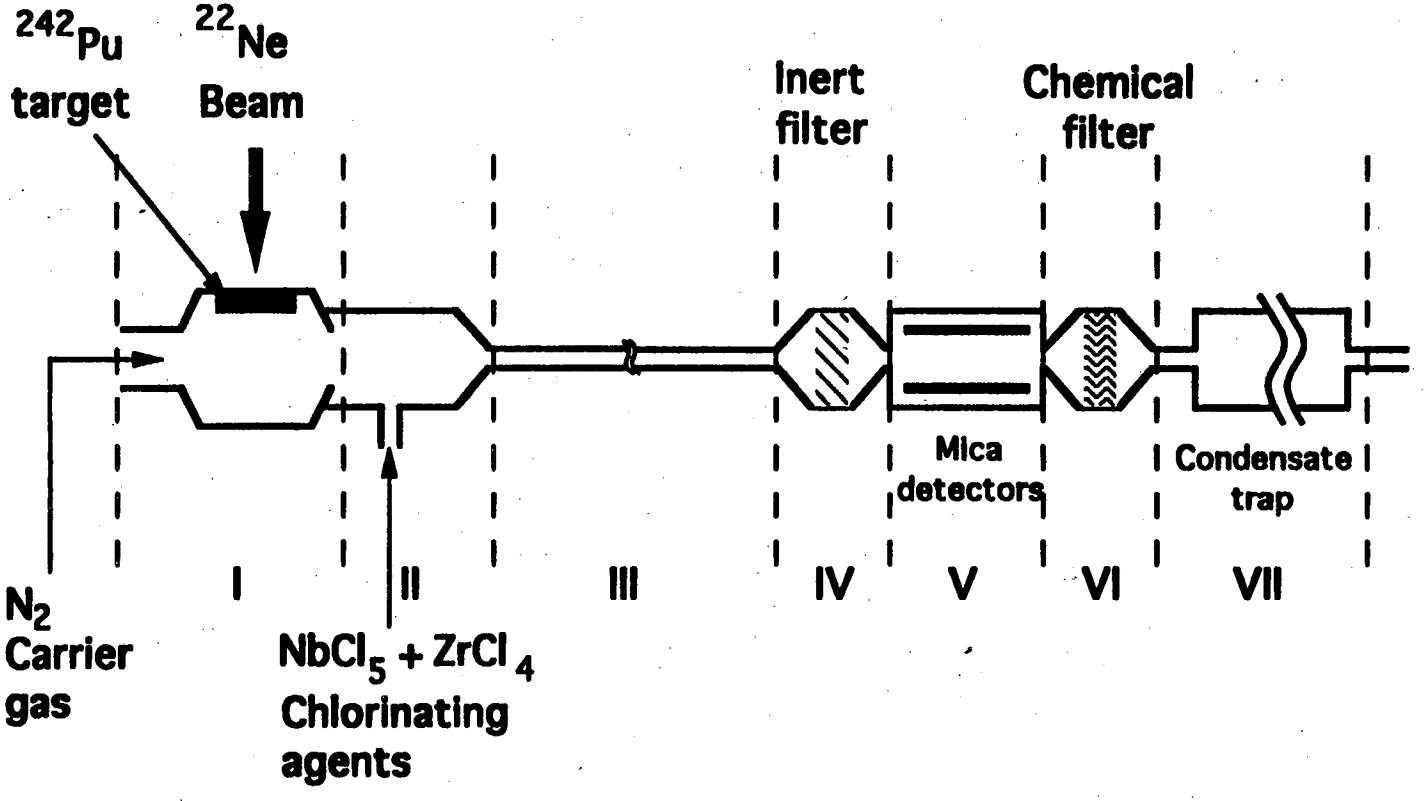

Fig. prepared from [HYD 87]

Fig. 2.1 Schematic of the type of chromatographic apparatus used by Zvara et. al for chemical studies of Rf chlorides.

activities [HYD 87], Rf halides were claimed to have been made and separated from the actinide activities. However, the mere observation of fission tracks is insufficient for identifying the atomic number (Z) or mass number (A) of a fissioning species since all information concerning the Z, A and the half-life of the fissioning nucleus is lost. These results have also been the subject of controversial discussions [HYD 87, GAG 88] in relation to the claim of the discovery of element 104.

2.1.2 Rudolph et al. (Isothermal Chromatography)

In 1980, Rudolph et al. [RUD 80] developed an on-line isothermal chromatography system for the determination of adsorption enthalpies and entropies of short-lived inorganic halides and oxides on quartz surfaces. Adsorption enthalpy and entropy results were obtained by this method for $NbCl_5$ and $NbOCl_3$ using the 54 sec ^{97m}Nb. Fig. 2.2 illustrates a schematic of the apparatus used by Rudolph et al. The source of $^{97}Nb^{m}$ was ^{97}Zr (from ^{235}U fission products) in a KCl/CsCl melt. The melt was kept at 1000 K (section 1). Nb was volatilized as pentachloride, in a nitrogen gas stream containing CCl_4 vapors. The volatile $NbCl_5$ molecules were carried with the gas flow down an isothermal quartz chromatography column (section 2), 80 cm in length and 8 mm in diameter. The column was packed with quartz glass particles. At the end of the isothermal section of the column, a section was gas cooled (section 3) to room temperature and the 744 keV γ-radiation of $^{97}Nb^{m}$ was measured with a Ge(Li)-detector system (sections 4 and 5). As illustrated in Table 1.1, their results agreed with data from conventional off-line measurements [RUD 79,80b]. Rudolph et al. concluded that on-line measurements are suitable for the study of heavy elements with $Z \geq 100$, which can only be produced in very small amounts and have short-lived isotopes.

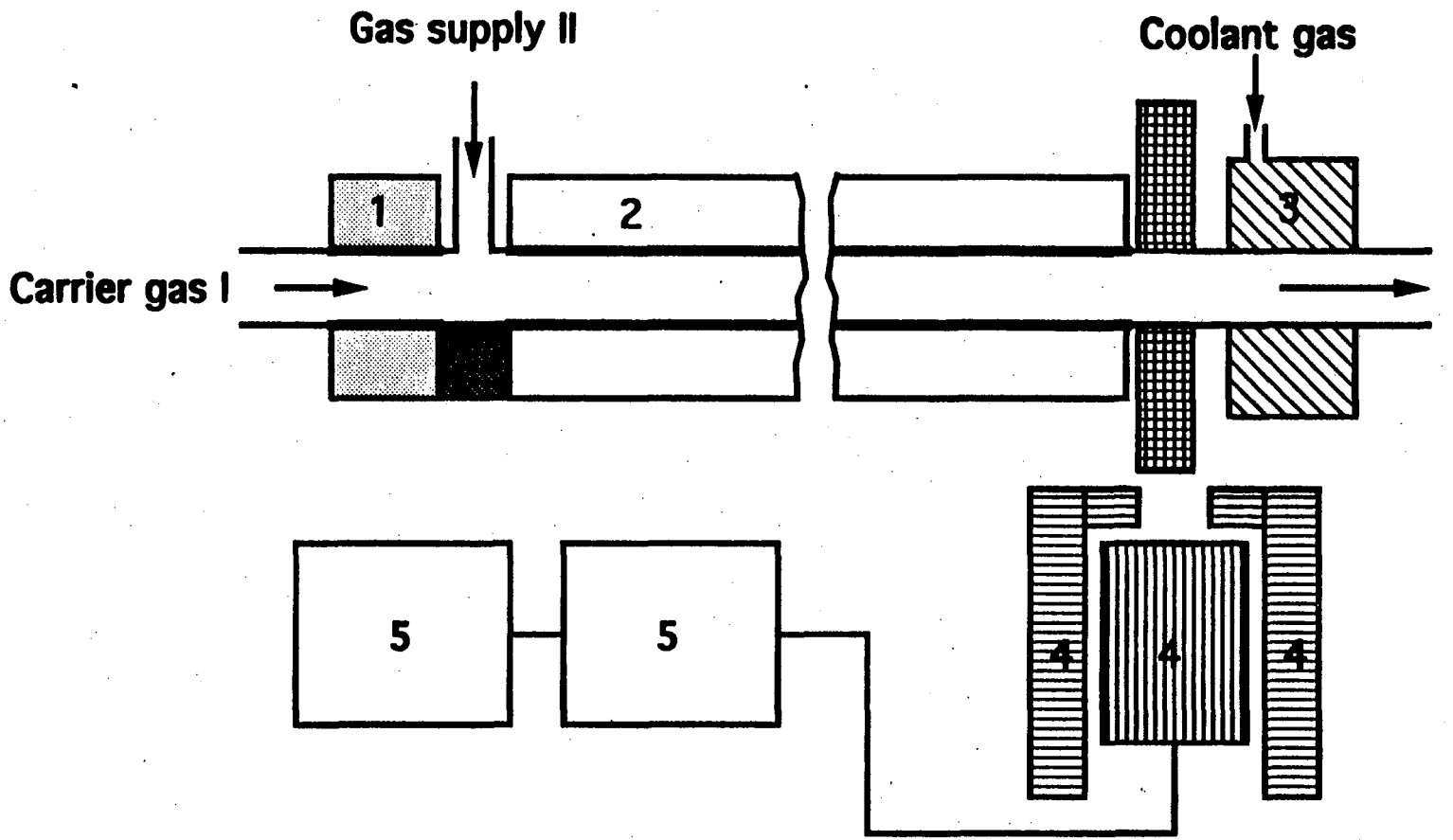

Fig. prepared from [RUD 80]

Fig. 2.2 Schematic of the type of chromatographic apparatus used by Rudolph et. al 1) Injection port oven;2) Column oven; 3) Gas cooling for detector section; 4) Detector with shielding; 5) Single or multi-channel-analyzer with data storage and printout.

2.1.3 Gäggeler et al. (OLGA)

In 1985 Gäggeler et al. [GAG 85] developed an on-line gas chemistry apparatus which was used to investigate adsorption enthalpies for the element polonium with various metal surfaces (the apparatus was later called OLGA). In 1986 [BRU 86], OLGA was used to search for volatile superheavy elements. OLGA was capable of separating volatile elements in their oxide or hydroxide forms. This system had the advantage of performing alpha spectroscopy while measuring the half-lives, making it possible to identify the decaying nuclide. Soon after, Gäggeler et al. developed OLGA II [GAG 91], which was especially designed for the separation of volatile halide species of short-lived nuclides. This system was also equipped with an improved detection system and was used in several studies of the halides of hafnium, niobium, tantalum, protactinium, rutherfordium and hahnium [GAG 92, TUR 90, YA 89]. The OLGA systems (Fig. 2.3) were very similar in design to the system used by Rudolph et al, with some exceptions. The reaction products were attached to KCl aerosols in He and transported to a quartz wool plug kept at 900 °C, inside the chromatography column. The chlorinating agents were added at this point and the volatile species formed were carried down an isothermal section of the column. After the volatile species moved through this section, they were attached to new KCl aerosols in N_2, in a recluster chamber, and collected on a tape which was moved in front of a series of alpha detectors or a gamma detector. HBr and HCl were used as halogenating agents. The main differences between this system and the system used by Rudolph et al., are the much shorter chromatography column (30 cm), the addition of a recluster chamber, and the tape detection system.

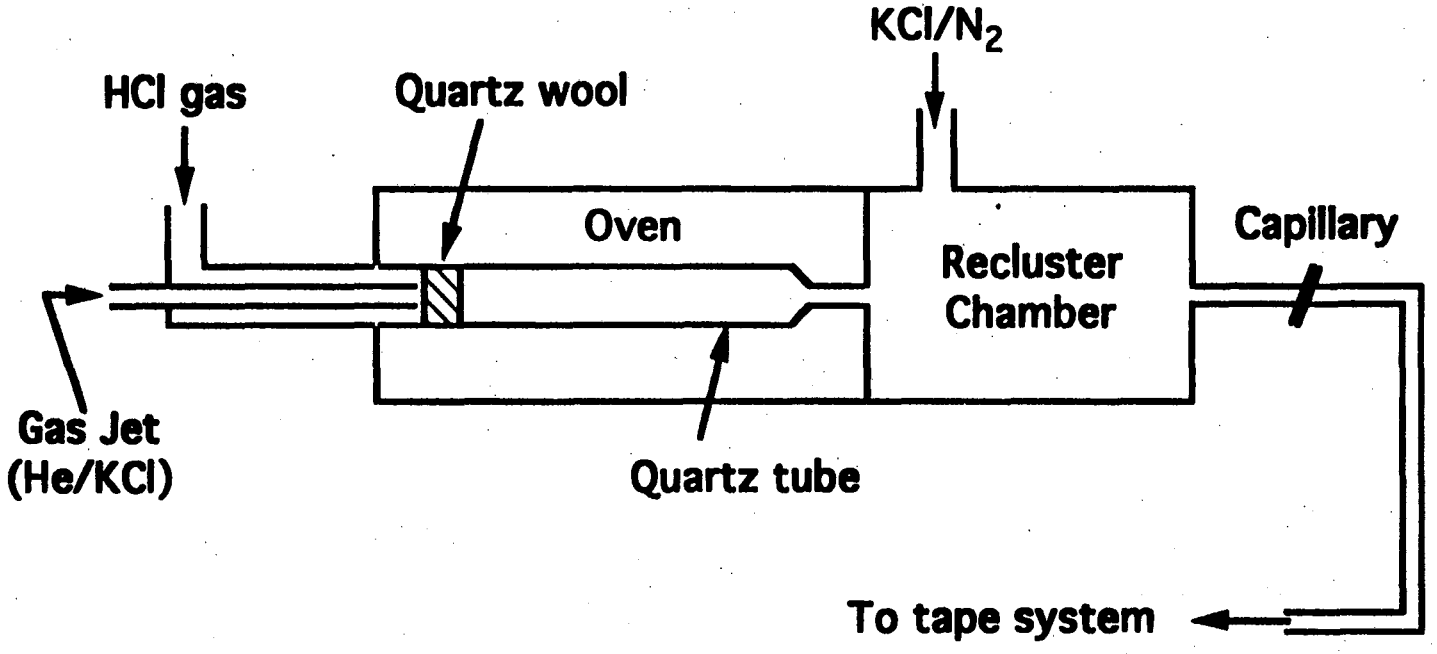

Fig. prepared from [TUR 90]
Fig. 2.3 Schematic of the type of chromatographic apparatus used by Gaggeler et. al (OLGA).

2.2 New Instrumentation

Motivated by this pioneering research, an improved system called the Heavy Element Volatility Instrument (HEVI) was designed and constructed. HEVI [KAD 92] is an on-line gas chromatography system which continuously separates halide species of short-lived nuclides according to their volatilities. Although the OLGA systems were an improvement over Rudolph's system, they also had several shortcomings. The isothermal section of the column was very short, the temperature profiles lacked uniformity (Fig. 2.4), and the design of the system permitted the corrosion of the heating units, leading to the break down of the system. Major improvements in the HEVI system include a longer chromatography column with superior temperature profiles which result in more distinct separation of the volatile species. Addition of a controlled gas flow system prevents salt buildup inside the column from the He/KCl aerosol gas transport system and allows continuous use of the system without periodic replacement of the column. The new system is designed to prevent or reduce corrosion. Both gaseous HBr and HCl have been used as halogenating agents in experiments with HEVI.

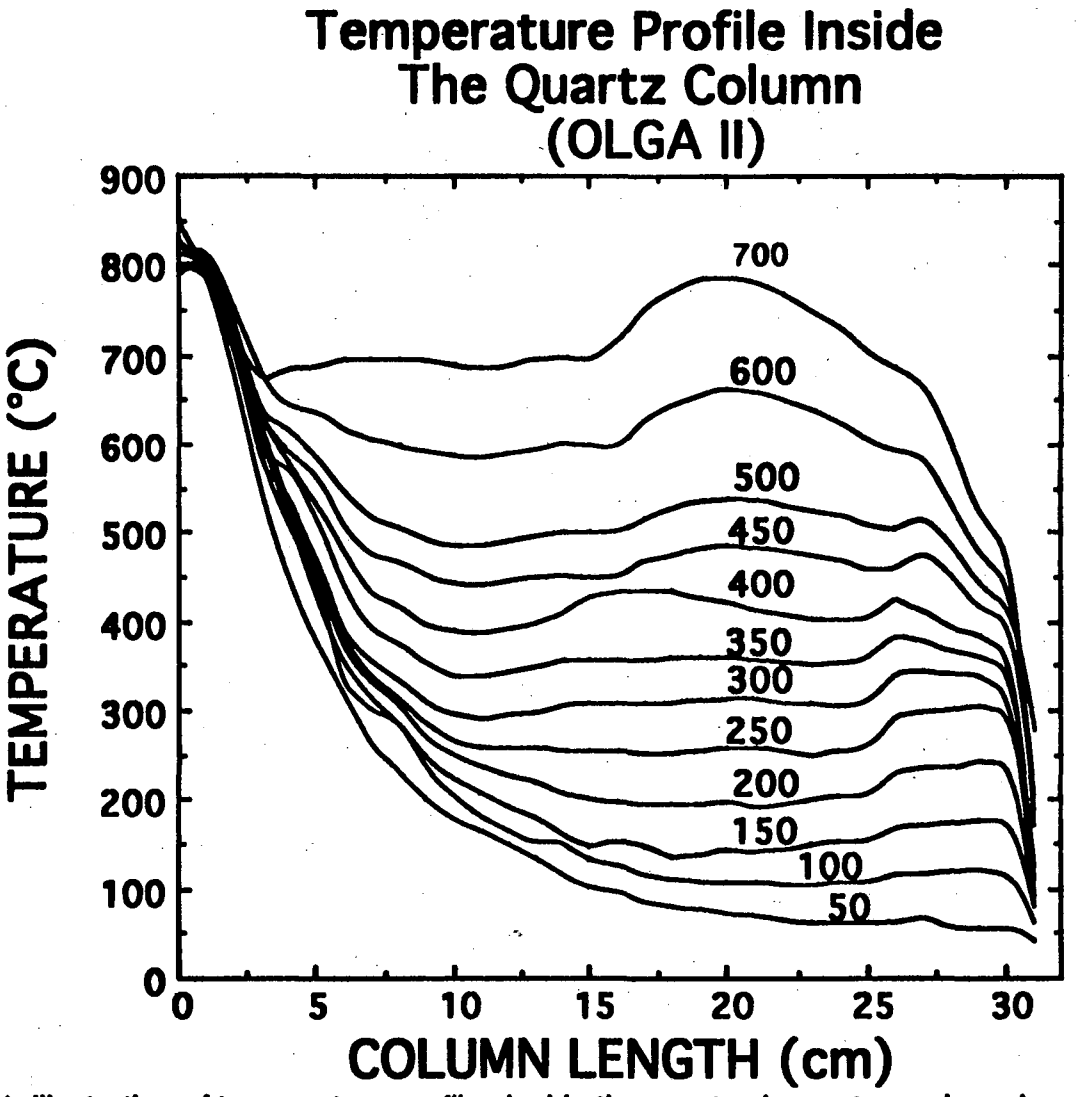

Fig. 2.4 Illustration of temperature profiles inside the quartz chromatography column for OLGA. Isothermal temperature settings are indicated above the curves.

2.2.1 Operation Principle

Activity is transported from the target chamber (see section 3.2) to HEVI via an aerosol gas-jet transport system. The aerosols are generated by sublimation of crystalline KCl or MoO_3 inside a quartz tube. Helium gas is passed over the crystals at the rate of 2 liters per minute to sweep the aerosols into a presorter capillary, where the larger aerosol particles are allowed to settle out of the He flow. The presorted aerosols are then transported directly into the target chamber through a 4.8-mm i.d. Teflon capillary. Products of nuclear reactions between an ion beam from the LBL 88-Inch Cyclotron and a fixed target, recoil out of the target (Fig. 2.5) and are stopped in helium. The products are then collected on aerosols in helium which sweeps out the volume behind the target continuously. The activity-laden aerosols are then rapidly transported by the helium through a 1.6-mm i.d. Teflon capillary tube to the chromatography system.

The activity-laden aerosols enter the first section of the quartz column and are stopped on a quartz wool plug placed at the entrance to the chromatography section of the column. This first section of the quartz column is kept at approximately 900°C to vaporize the aerosols, leaving the activity on the quartz wool. Reactive gases are added to the quartz wool plug to form halide compounds. The volatile species are then carried down a cooler, isothermal section of the column by the helium gas flow. The species that leave the column, enter a recluster chamber, where they are attached to new KCl aerosols in N_2 (section 2.2.2.4), and are transported to the detection system. The N_2/KCl transport system is similar to the described He/KCl transport system.

The retention time of a molecule in the isothermal section of the column is related to the number of adsorption/desorption steps between the molecule and the column surface and also the period of time the molecule spends in the adsorbed state. The retention time is then dependent on the adsorption enthalpy, the column temperature, the true volume

Operation Principle

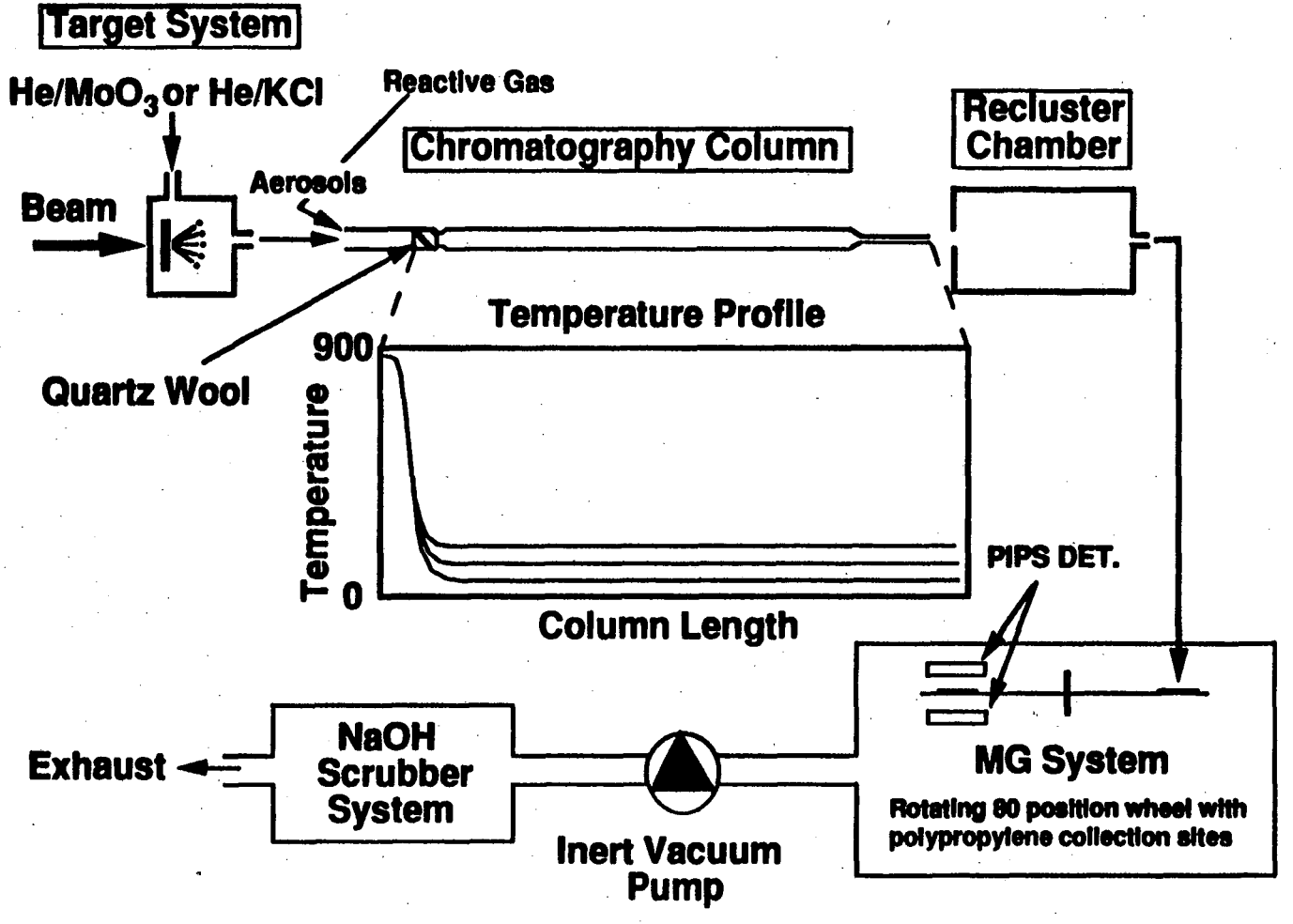

Fig. 2.5 Illustration of the different parts of the experimental setup. The experimental process has been followed from production to chromatography and finally to detection.

flow rate of the carrier gas and the column length. If the retention time is relatively long in comparison to the half-life of a species, it will remain on the surface of the quartz column and decay. However, if the species has a relatively short retention time compared with its half life, it will leave the column and enter the recluster chamber where it is attached to new aerosol particles and transported to a detection system. So retention time as a function of column temperature is measured using the species half-life as a clock.

Two detection systems are used to detect alpha/spontaneous fission (SF) activities and a separate system to detect gamma-ray activities. The horizontal rotating wheel system [HOF 80], the MG, and the OLGA II tape counting system [GAG 91] can be used to detect alpha/SF activities. A Ge detector in conjunction with a special collection site is used to detect gamma or X-ray activities. All systems are described in detail in subsequent sections of this thesis. All detector chambers and the collection site were evacuated with an inert vacuum pump. The exhaust gases, still containing the reactive halogenating agents, were neutralized in a NaOH scrubber system before release to the building exhaust.

2.2.2 Design Description

HEVI consists of several components (Fig. 2.6): (i) the split shell furnaces (Fig. 2.7), and controllers, which heat the various sections of the quartz column; (ii) the chromatography column assembly consisting of the Inconel jacket (Fig. 2.8), the quartz chromatography column and the graphite/ceramic pieces; (iii) the heat sink, which provides cooling between the high temperature section of the system and the cooler isothermal section; (iv) the recluster components (Fig. 2.9), which allow the transport of the separated volatile species to the detection system; (v) the gas flow system consisting

Gas Chemistry Setup

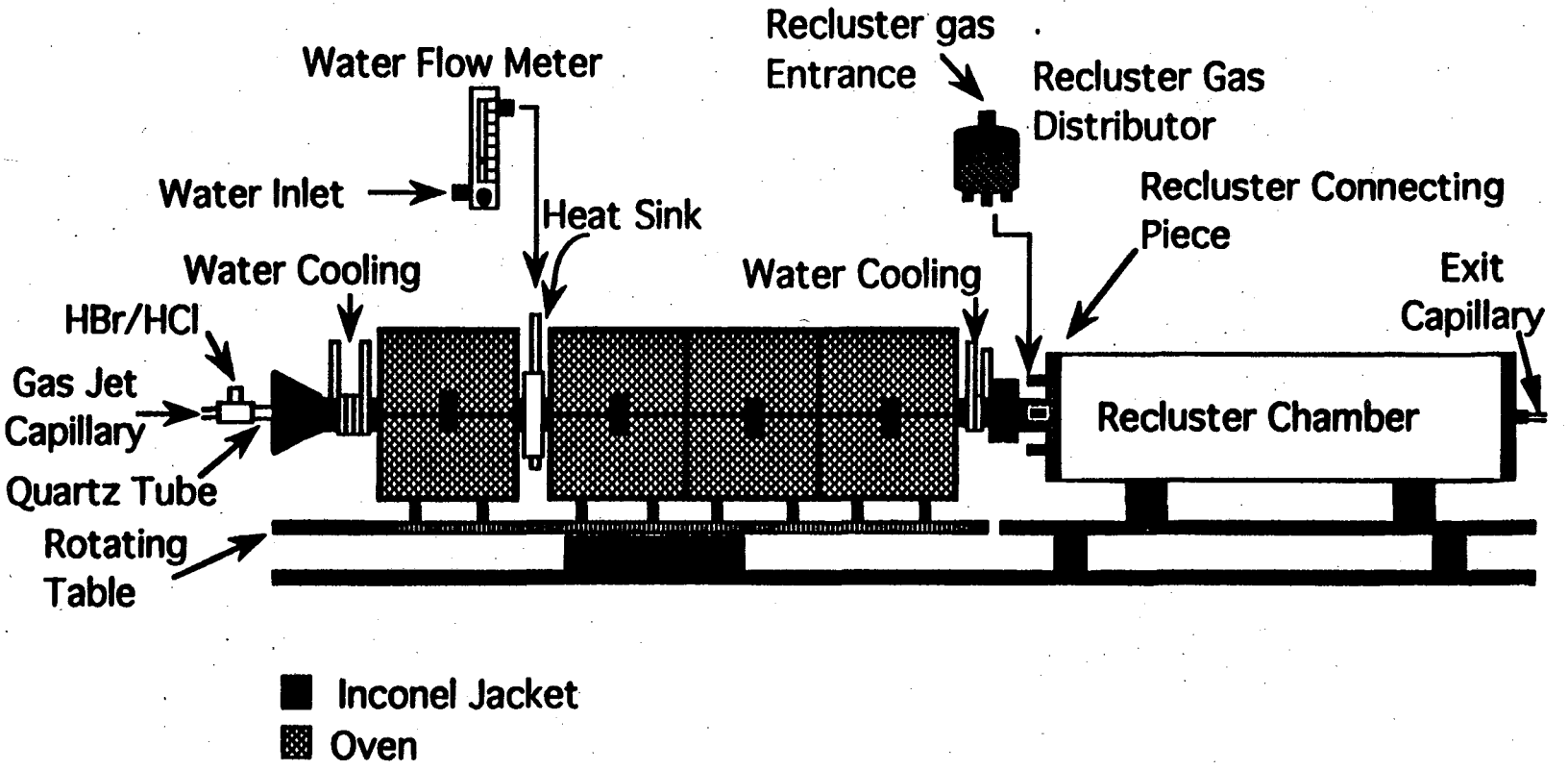

Fig. 2.6 Illustration of the Heavy Element Volatility Instrument (HEVI). Shown here is the side view of the chromatography and recluster segments.

of the mass flow controllers and gas switches (Fig. 2.10), which control the continuous flow of gases to the system; and (vi) the detection systems.

2.2.2.1 Split Shell Furnaces and Controllers

The system is heated by four split shell furnaces (Teco F-6-1000-H-1.5-1V-SSL)* mounted end to end on a 15 x 94 cm rotating table, (Fig. 2.6). The furnaces are 16.51-cm in length with a 12.8-cm o.d., (Fig. 2.7). The heated length in each furnace is 15.2-cm. The furnaces are designed for operation up to a maximum temperature of 1000°C. They are provided with a 2.54-cm i.d. vestibule to allow clearance for the Inconel jacket. The control device for each furnace (Teco/Sigma MDC4E) is capable of accurately controlling the rate of ascent or descent to appropriate temperature settings.

2.2.2.2 Chromatography Column Assembly

Inconel alloy 600 is a good material for use in severely corrosive environments at elevated temperatures. It is resistant to oxidation at temperatures up to 1180°C. The alloy has excellent mechanical properties at cryogenic as well as elevated temperatures. Because of its resistance to chloride-ion stress-corrosion cracking and corrosion by high purity water, it is also used in nuclear reactors. The Inconel jacket is a tube approximately 78-cm long with a 2.54-cm o.d. and a 2.21-cm i.d. (Fig.2.8). Stainless steel flanges are welded on the ends of the Inconel jacket and copper water cooling coils have been soldered to both ends of the tube. Cooling of the flanges is essential for vacuum tight connections with adjacent system components.

* Teco Manufacturing Company, 108 Baywood Ave. #100, Longwood, Florida 32750

Split Shell Furnace

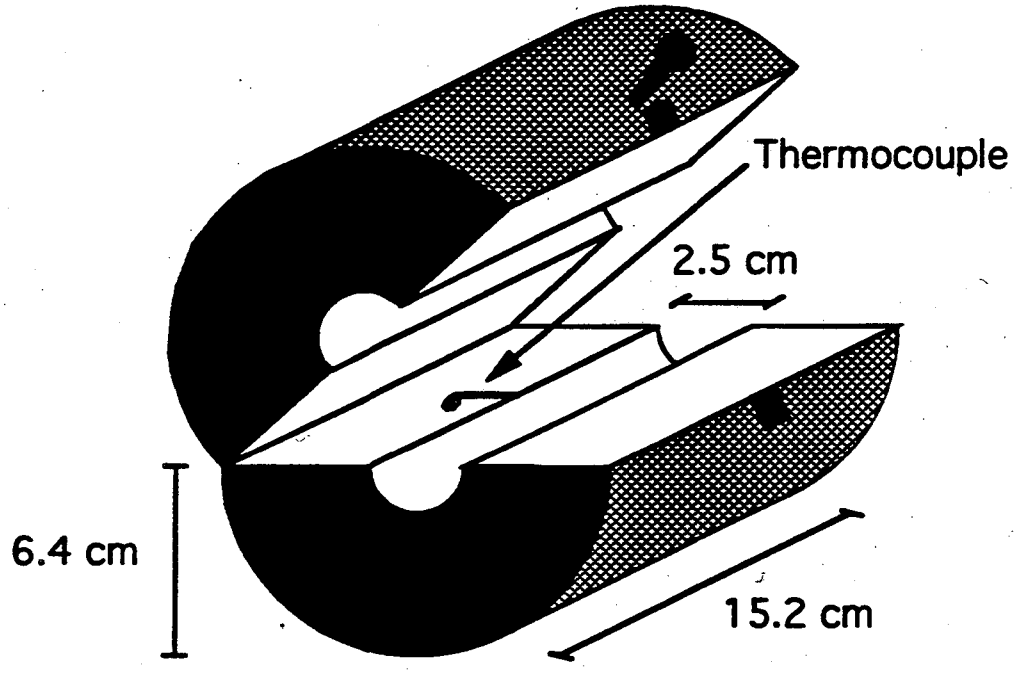

Fig. 2.7 Split shell furnace (Teco F-6-1000-H-1.5-1V-SSL) designed for operation up to a maximum temperature of 1000 °C.

Graphite/Ceramic Arrangement Inside the Inconel Jacket

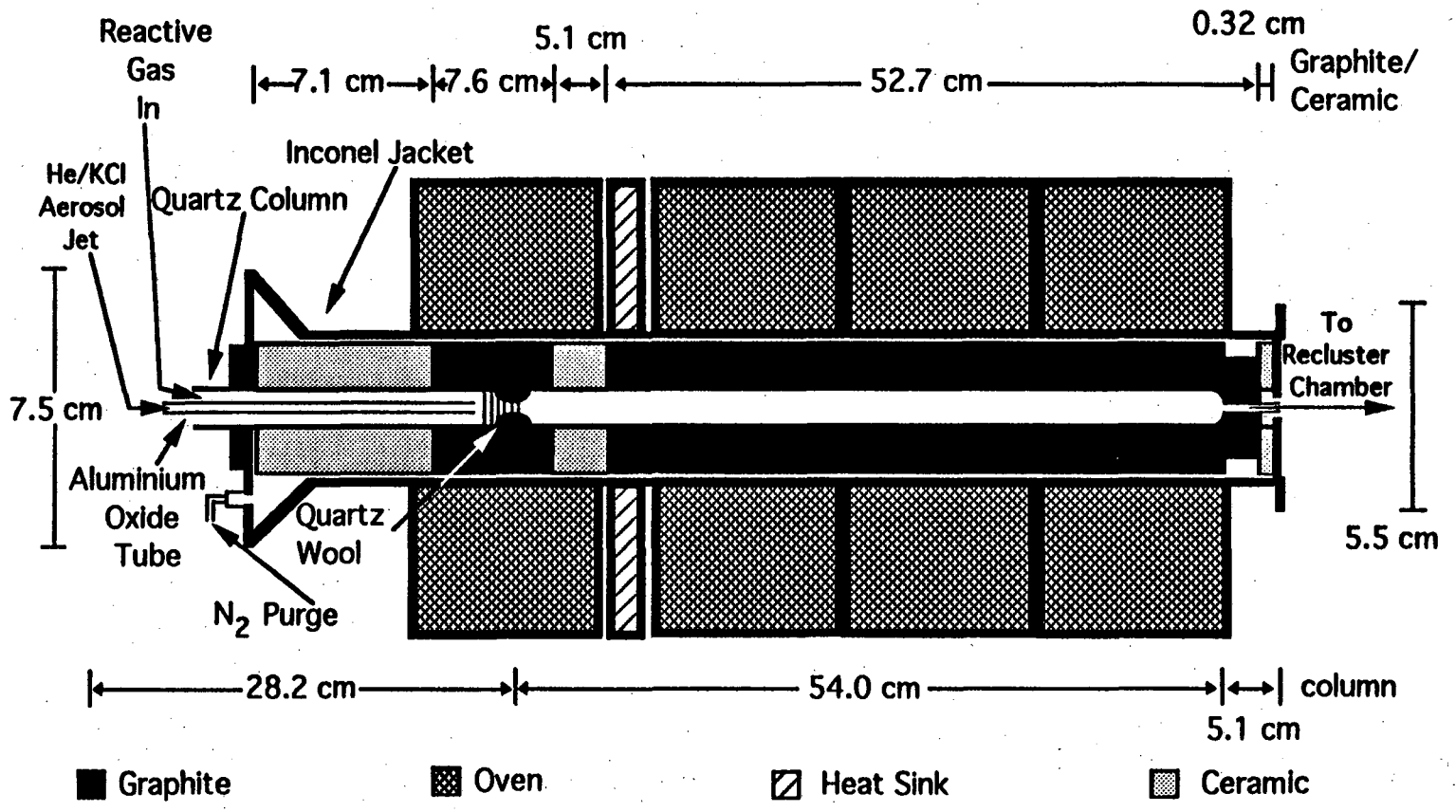

Fig. 2.8 Horizontal cross-sectional view of the graphite/ceramic arrangement inside the Inconel jacket. High density graphite is used for its excellent heat conductivity properties and ceramic is used for its good insulation properties. This arrangement ensures uniform isothermal temperature profiles in the quartz chromatography column.

A tube adapter has been connected to the upstream end of the Inconel jacket to increase its diameter from 2.5-cm to 7.5-cm, in order to allow clearance to insert and seal the 8-mm o.d. quartz chromatography column. The length of the 6-mm i.d. quartz column is 82.2-cm. At the downstream end, there is a 5.1-cm tip of 1-mm i.d.. A 3-mm i.d. indentation is placed 28.2-cm from the beginning of the column (Fig. 2.8) to hold a small amount of quartz wool. The quartz wool acts as a filter for the activity laden aerosols, which are transported from the target chamber via the He gas jet, as explained above. This section of the quartz column is kept at approximately 900°C by the first furnace, and the remaining 59.1-cm length of the column is kept isothermal at lower temperatures, ranging from 50°C to 650°C by the other three furnaces. The activity-laden aerosols are transported directly to the quartz wool by a 27-cm long x 2.0-mm i.d. aluminium oxide tube, in the quartz column. The aerosols are collected on the quartz wool, and are vaporized at 900°C, leaving the activity on the quartz wool. Brominating or chlorinating agents, such as HBr or HCl gases, are added at this point at a rate of 100 ml/min. Volatile halide species which are formed will then flow down the isothermal length of the column at the appropriate isothermal temperature and enter the recluster chamber. Nonvolatile species decay inside the quartz column.

To keep uniform isothermal temperature profiles in our quartz chromatography column, a series of graphite and ceramic tubes, with a 2.10-cm o.d. and a 9.0-mm i.d., are carefully arranged inside the Inconel jacket (Fig. 2.8). High-density graphite is used for its excellent heat conductivity properties and ceramic is used for its good heat insulation properties. A 7.1-cm ceramic piece insulates the 900°C section from the upstream end of the Inconel jacket. This piece is followed by a 7.6-cm graphite piece which assures a uniform temperature at the quartz wool position. Next is a 5.1-cm ceramic piece which insulates the isothermal section from the 900°C section. Finally a 52.7-cm graphite tube surrounds the isothermal section of the quartz tube insuring a uniform temperature. The last 2.54 cm of this graphite tube is reduced to a 1.55-cm o.d.

and a 3.2-mm ceramic washer is placed between the graphite and the Inconel wall, to avoid contact between the graphite and the water cooled Inconel tube. This reduces cooling of the graphite (and the column) and ensures uniform temperature profiles at the tip of the column. A 100 ml/min flow of nitrogen gas is maintained inside the Inconel jacket and around the graphite/ceramic arrangement. This assures a slight positive pressure inside the Inconel jacket, preventing the back flow of corrosive gases inside the jacket.

2.2.2.3 Heat Sink

To further minimize the transfer of heat from the 900°C section to the adjacent isothermal section a removable heat sink was constructed. The heat sink is a water cooled 6.5 x 6.0 x 1.0-cm copper block. It is used around the Inconel jacket between the 900°C furnace and the isothermal section for all temperature settings below 250°C and is removed at higher temperatures. The control of the water flow through the heat sink regulates the heat transfer from the 900°C section to the isothermal section. The water flow through the system is controlled by a water flowmeter (RMA Rate-Master, * Dwyer Instruments, Inc.). The meter controls flow from 7 l/hr to 91 l/hr. Appropriate water flow settings have been determined for each isothermal temperature.

2.2.2.4 Recluster Components

The volatile species, after leaving the chromatography column, enter the recluster chamber, where they are attached to KCl aerosols in nitrogen to be transported through a capillary to the detection system. The recluster unit consists of the connecting piece,

* Dwyer Insturments, Inc., P.O. Box 373, Michigan City, Indiana 46360

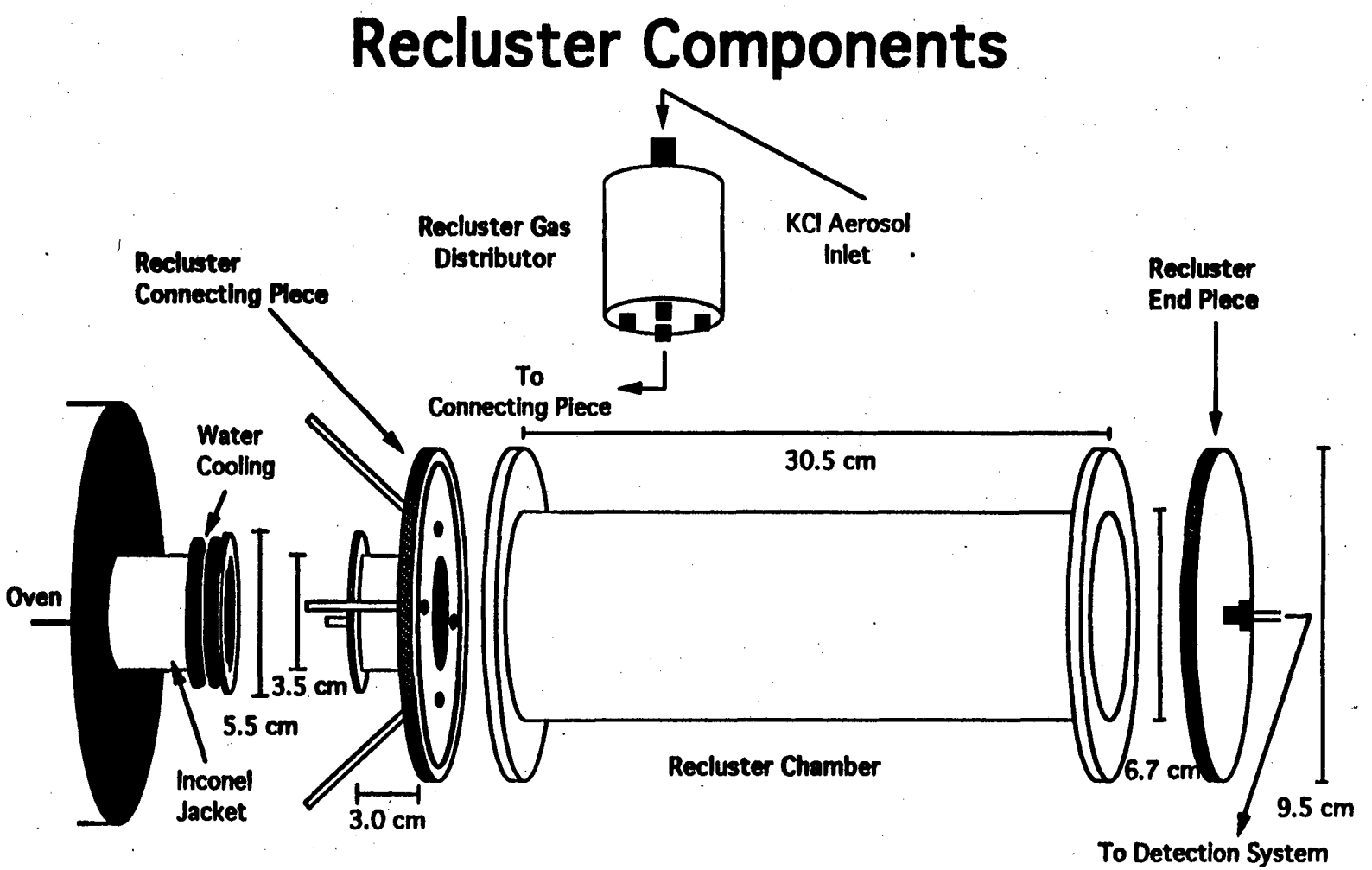

Fig. 2.9 Illustration of the recluster components. The recluster unit consists of the recluster connecting piece, which connects the Inconel jacket to the recluster unit, the recluster gas distributor, which distributes the recluster gas equally to the four inlets on the connecting piece, the recluster chamber and the recluster end piece.

the gas distributor, the recluster chamber and the end piece (Fig. 2.9).

The KCl aerosols for the N_2/KCl gas jet system are generated by sublimation of crystalline KCl at approximately 650°C inside a quartz tube. Nitrogen gas, at the rate of 1.5 liters per minute, is used to sweep the aerosols out of the tube and into a 'presorter' capillary, where the larger aerosol particles are allowed to settle out. The presorted aerosols are transported directly into the recluster gas distributor via a 4.8-mm i.d. polypropylene tube. The recluster gas distributor is a 9.0-cm long stainless steel cylindrical piece with a 6.5-cm o.d.. The recluster gas exits the distributor through four 2.4-mm i.d. polypropylene capillaries and is introduced to the recluster unit through four inlets on the recluster connecting piece. The stainless steel recluster connecting piece, illustrated in Fig. 2.9, connects the Inconel jacket to the recluster unit. The recluster chamber is a 30.5-cm long cylindrical piece of 2.5-mm thick Pyrex glass with a 6.7-cm i.d.. The species entering the recluster chamber through the tip of the quartz chromatography column are collected on the aerosols in nitrogen. The activity-laden aerosols are then swept out of the chamber into a 2.4-mm i.d. polypropylene capillary from the center of the recluster end piece and transported to the detection system. The recluster unit typically operates at an absolute pressure of 0.85 atm.

2.2.2.5 Gas Flow System

During an experiment two types of measurements are performed. The activity-laden aerosols which exit the target system are either injected into the chromatography system, where chromatography is performed before transport to the detection system for a 'chemistry' measurement, or the chromatography system is bypassed and the activities are sent directly to the detection system where a 'direct catch' measurement is performed. A direct catch is simply a measurement of the amount of activity from specific nuclides

under study, without chemical separation. A comparison of the activities from a direct catch measurement and a chemistry measurement gives the relative yield of a species. In order to perform the above two measurements, it is crucial to maintain the uninterrupted flow of gases in the system to maintain the temperature profiles in the quartz column and to maintain a constant gas-jet efficiency.

The controlled flow of gases in HEVI is obtained through several mass flow controllers and two direction control switches. Fig. 2.10 shows a schematic of the controlled flow of gas through the entire system. The two bypass-switches are made out of Lucite with dimensions of 9.0 x 9.0 x 3.5-cm. The first bypass-switch enables the aerosols to bypass the chromatography oven to perform a yield check measurement. At the same time, pure helium is directed into the chromatography column at a rate of 2 l/min, to maintain the temperature profiles. The second switch enables the aerosols to either enter the detection system or bypass the detection system and proceed directly to waste. All corrosive gases are neutralized by a scrubber system as shown in Fig. 2.10.

2.2.3 Temperature Profiles

Fig. 2.11 illustrates temperature profiles inside the quartz chromatography column for each of the thirteen isothermal temperature settings from 50°C to 650°C in 50°C increments. To obtain these profiles, a thermocouple was inserted inside the column and pulled back in 1-cm increments from the column tip to the quartz wool plug and the temperature at each point was recorded. The flow of gases through the system was regulated to produce exact experimental gas flow conditions. As previously mentioned, the heat sink was removed at temperatures above 250°C. This is the cause of the sudden increase in temperature observed in Fig. 2.11 at the region from 5-cm through 15-cm between the 250°C setting and all higher temperature settings. The length of the

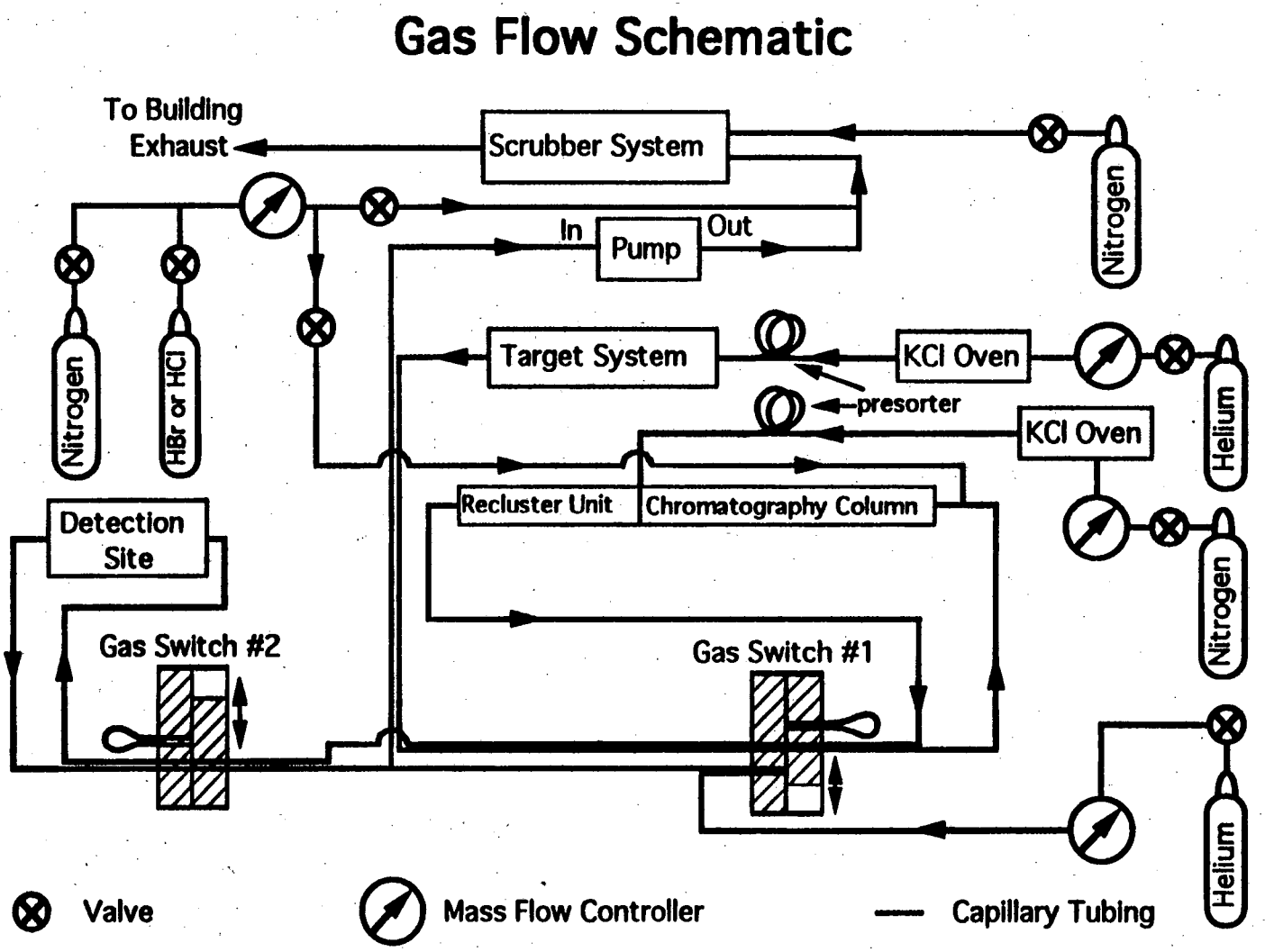

Fig. 2.10 Illustration of the gas flow schematic of the system. The flow of gases in the system is controlled through several mass flow controllers and two direction control switches.

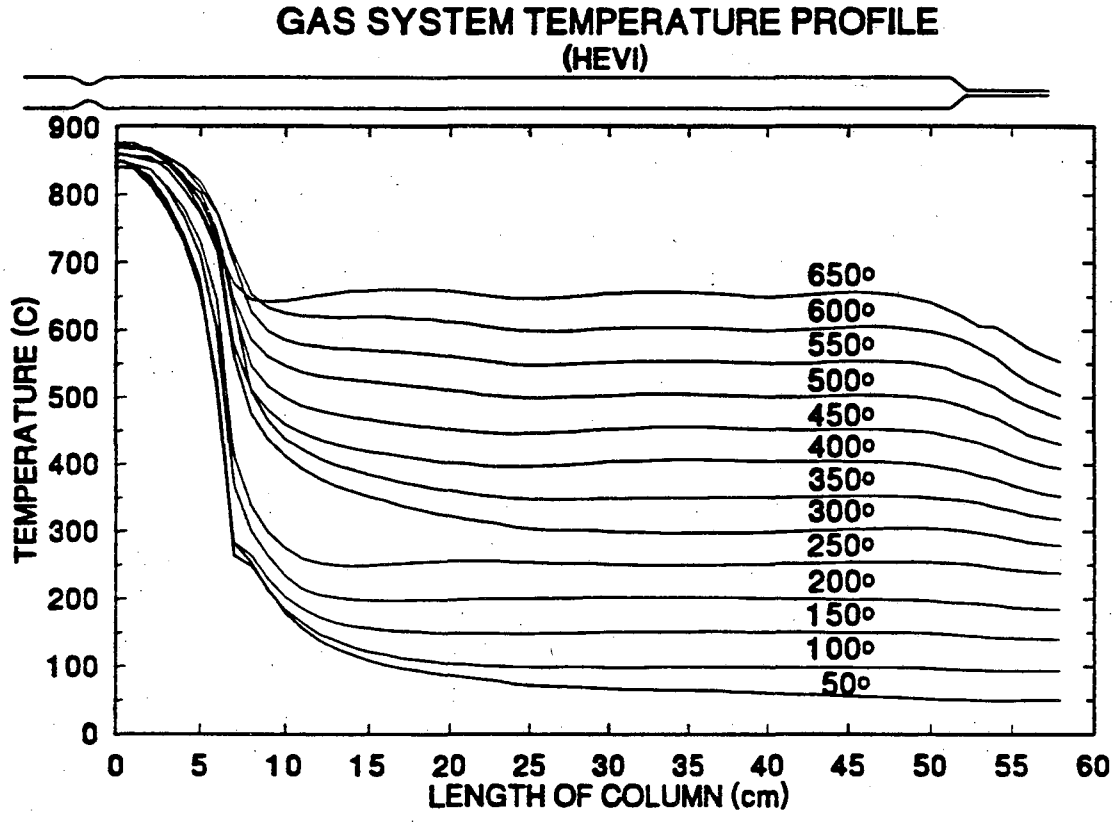

Fig. 2.11 Illustration of temperature profiles inside the quartz chromatography column for each of the thirteen isothermal temperature settings from 50 to 650°C in 50°C steps. The sudden increase in temperature observed at the region from 5 through 15 cm between 250°C settings and all higher temperature settings is due to the removal of the heat sink.

isothermal section part in the chromatography column is about 15-cm at 50°C settings, approximately 40-cm at 100°C through 250°C settings, and approximately 30-cm at 300°C or higher. The term 'isothermal' implies T±5°C. The greater lengths of HEVI's isothermal sections are a major improvement over OLGA II (Fig. 2.4), whose isothermal lengths are 20-cm at 700°C, 18-cm at 600°C, 16-cm at 400°C and 500°C, 15-cm at 300°C, 11-cm at 200°C and only 6-cm at 100°C. This improvement should lead to more distinct separations.

Chapter 3

Production of Isotopes

Transactinide elements can only be produced in "heavy ion" fusion reactions at rates of a few atoms per minute or less. The production of these elements requires neutron-rich actinide elements, with relatively long half lives, as target material and heavy ion beams. Isotopes such as ^{248}Cm (element 96) and ^{249}Bk (element 97) are ideal target materials for such heavy ion fusion reactions. A combination of such targets with an accelerated beam of ^{18}O yields detectable amounts of transactinides, via a compound nucleus reaction mechanism.

As mentioned before, on-line isothermal gas chromatography is a method by which volatile compounds of different chemical elements can be separated according to their volatilities. Our investigation of periodic table trends is based on a comparison of the volatilities of transactinide halides with halides of their lighter homologs. This comparison may only be valid when study of the volatilities of homologous elements are performed under the same conditions as for the transactinide elements. Consequently, short-lived isotopes of the lighter homolog elements were also produced in tracer quantities via heavy ion fusion reactions.

3.1 Target Preparation

Several targets were used in this work for the production of transactinide elements and their lighter homologs. All targets were prepared via a molecular deposition technique [AUM 74, EVA 72, MUL 75] from an isopropanol solution. This method ensures a thin, adherant, and uniform target. Target materials in NO_3^- form are dissolved in pure isopropanol and electroplated on thin metal foil backings at high voltage. Fig. 3.1 illustrates a special electroplating cell developed for the preparation of targets. The plating cell has an aluminum base which holds the circular (o.d. 12-mm) beryllium (2.75-mg/cm^2) metal foil used as target backing. The Be foil serves as the cathode. A Teflon chimney (i.d. 6-mm), which holds the isopropanol solution containing known amounts of the target material to be plated, is placed directly on top of the Be foil. A platinum foil with a 4-mm center hole, acts as the anode, and is placed in between the mid ring and the top section of the plating cell. The solution is stirred continuously with a 2-mm o.d. glass rod attached to a small electric motor. Deposition is carried out by applying several hundred volts across the electrodes. The voltage is adjusted so that the current does not exceed 6-mA/cm^2, since at this point the solution will begin to bubble resulting in a poor deposit. A layer of approximately 75-μg/cm^2 is deposited on the Be foil in a 6-mm diameter circle, as defined by the chimney of the plating cell. The Be foil is then dried under a heat lamp and baked in a quartz tube inside a split shell furnace at 500°C for approximately thirty minutes to convert the deposit to the oxide. The exact target thickness is determined using an α-spectrometer system utilizing a Si(Au) solid state surface barrier detector. The plating and baking process is repeated until the desired target thickness is achieved.

Plating Cell

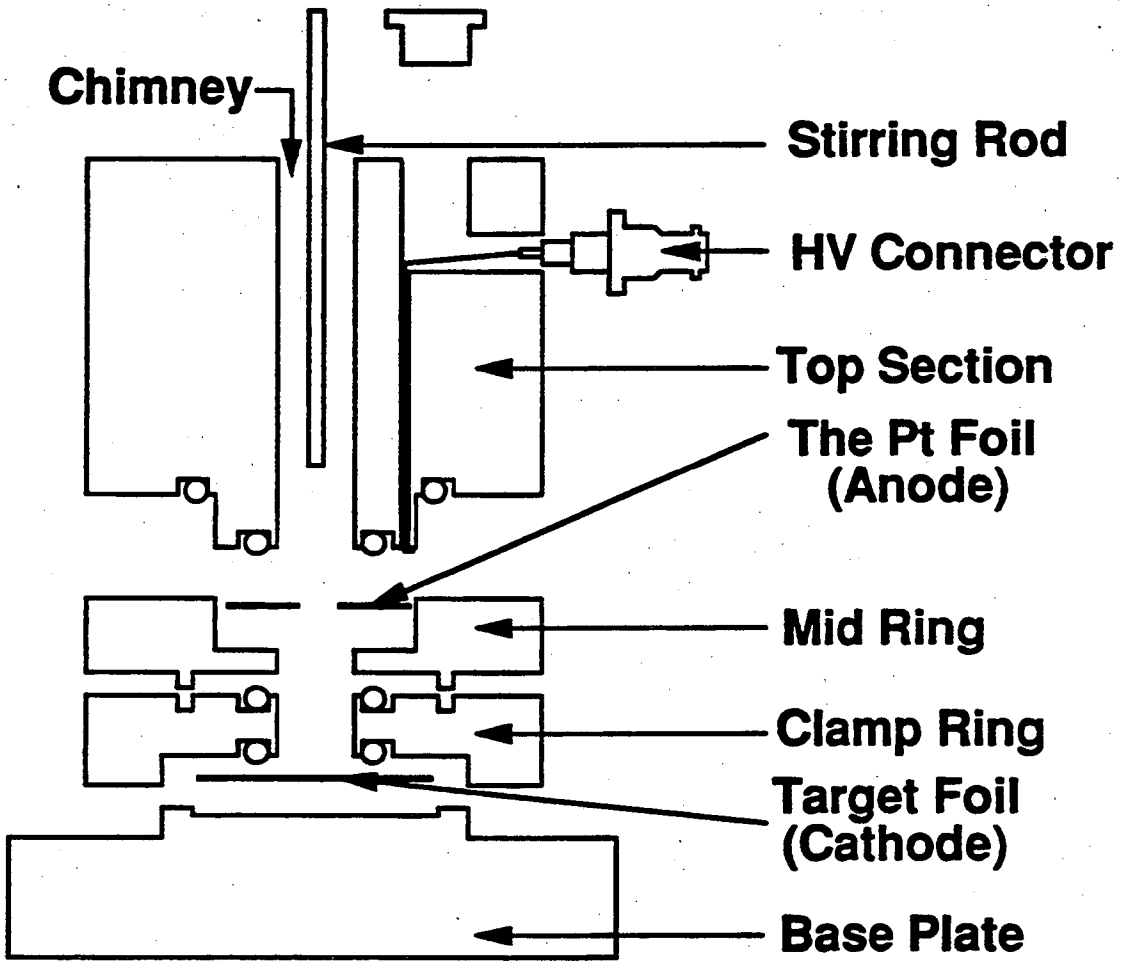

Fig. 3.1 Schematic of the plating cell used in target preparation

3.1.1 Mixed ^{nat}Eu and ^{147}Sm Target

A mixed target of ^{nat}Eu (47.8% ^{151}Eu, 52.2% ^{153}Eu) and ^{147}Sm was prepared for the Hf and Ta isotope production. Europium oxide powder was purchased from K & K Laboratories Inc. at Plainview, NY. Isotopically pure $^{147}Sm_2O_3$ was purchase from Oak Ridge National Laboratory. Known amounts of both materials were dissolved in an appropriate quantity of 3 M nitric acid. The solutions were then evaporated to dryness several times from a 3 M nitric acid solution to convert the Eu_2O_3 and the $^{147}Sm_2O_3$ to nitrate form. Stock solutions of Eu and ^{147}Sm were prepared by dissolving the resulting NO_3^- salts in appropriate amounts of pure isopropanol. In order to measure the target thickness after each plating procedure, ^{241}Am and ^{248}Cm tracers were added to the Sm and the Eu solutions, respectively. Known amounts of both solutions were added to the plating cell before each plating interval. The final thicknesses of Sm and Eu metal in the final metal-oxide deposit was 0.365-mg/cm^2(0.214-mg/cm^2, ^{147}Sm and 0.151-mg/cm^2, ^{nat}Eu).

3.1.2 ^{248}Cm Target

A ^{248}Cm target was prepared for the production of ^{261}Rf via the ^{248}Cm(^{18}O,5n) reaction at the Lawrence Berkeley Laboratory (LBL) 88-Inch Cyclotron. First, a $3^+/2^+$ separation (Fig. 3.2) was conducted in order to isolate the Cm from lead impurities. The Cm^{3+} in a 0.20 M HNO_3 aqueous phase was extracted into an organic phase of 0.5 M di-2-ethylhexylorthophosphoric (HDEHP) acid in heptane [HOR 69]. Two back extraction procedures were performed on the organic phase. First, a $3^+/2^+$ separation was performed by a back extraction of the 2^+ ions into a 0.2 M HNO_3 solution. Second, a $4^+/3^+$ separation was performed by a back extraction of the Cm^{3+} into a 3M HNO_3

Cm Separation Flowchart

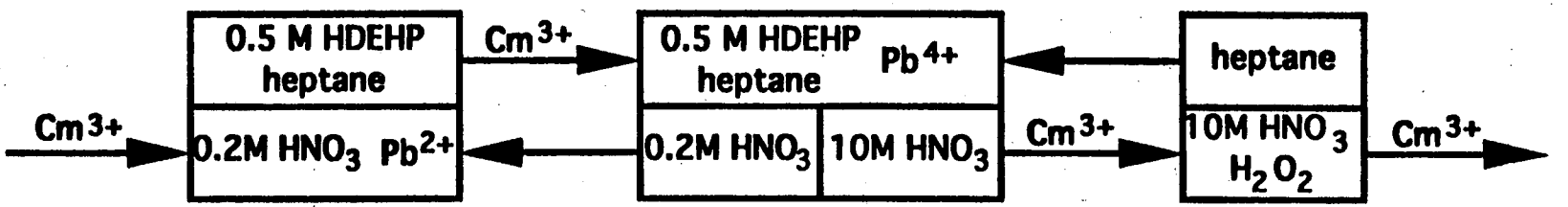

Fig. 3.2 Flow chart of the purification chemistry for the Cm target. The Cm^{3+} in a 0.20 M nitric acid aqueous phase was extracted into an organic phase of 0.5 M HDEHP in heptane and back extracted into an aqueous phase of 10 M nitric acid.

solution. This procedure isolated Cm from 2^+ and 4^+ lead ion impurities. The 3M HNO_3 aqueous phase was washed several times with heptane to remove residual HDEHP. The solution was then evaporated, and the resulting NO_3^- salt was dissolved in appropriate amount of pure isopropanol. Each extraction was performed twice to assure high separation yield. The target was then prepared via the electrodeposition method described in section 3.1. The final thickness of ^{248}Cm in the Cm_2O_3 deposit was 0.81-mg/cm^2.

3.1.3 ^{249}Bk Target

A ^{249}Bk target was prepared for the production of Ha isotopes via the $^{249}Bk(^{18}O,5n)$ reaction at the Gesellschaft für Schwerionenforschung (GSI) **UNILAC** accelerator in Darmstadt, Germany. The 325-day ^{249}Bk was purified from ^{249}Cf, the beta decay daughter, via a $4^+/3^+$ separation (Fig. 3.3). The Bk^{3+} in a 10 M HNO_3 aqueous phase was converted to the 4+ oxidation state using saturated $KBrO_3$. The Bk^{4+} was extracted into an organic phase of 0.5 M HDEHP in heptane. Two back extraction procedures were performed on the organic phase. Each aqueous phase used for the back extractions contained a small amount of H_2O_2 to reduce Bk^{4+} to Bk^{3+}. First, a $3^+/2^+$ separation was performed by a back extraction of the 2^+ ions into a 0.2 M HNO_3 solution. Second, a $4^+/3^+$ separation was performed by a back extraction of the Bk^{+3} into a 3M HNO_3 solution. This procedure isolated Bk from 2^+ and 4^+ lead ion impurities. The 3M HNO_3 aqueous phase was washed several times with heptane to remove residual HDEHP. Each extraction was performed twice to assure high separation yield. The target was then prepared via the electrodeposition method described in section 3.1. The final thickness of ^{249}Bk in the Bk_2O_3 deposit was 0.70-mg/cm^2.

Bk Separation Flowchart

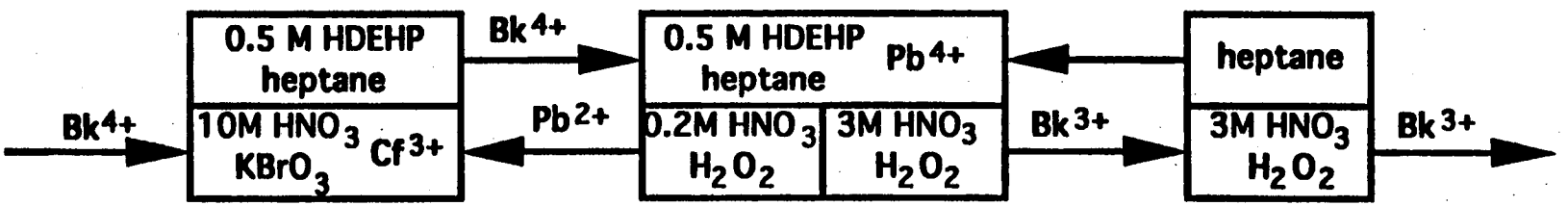

Fig. 3.3 The Bk^{3+} in a 10 M HNO_3 aqueous phase was converted to the 4^+ oxidation state using saturated $KBrO_3$. The Bk^{4+} was extracted into an organic phase of 0.5 M HDEHP in heptane and back extracted with a 3 M HNO_3 solution containing a small amount of H_2O_2 to reduce Bk^{4+} to Bk^{3+}.

3.1.4 ^{235}U Target

A ^{235}U target was prepared for the production of Zr and Nb isotopes via the $^{235}U(n,f)$ reaction at the **SAPHIR** reactor at the Paul Scherrer Institute (PSI) in Switzerland. A stock solution of ^{235}U was prepared in pure isopropanol and electrodeposited on a 4.05 mg/cm^2 thick, 60-mm i.d. circular aluminum foil. A plating cell and plating procedures, similar to those described in section 3.1, were used in the production of this target. However, a larger plating cell was used to give a target with a 50-mm diameter. The glass stirring rod was replaced with a platinum wire shaped in the form of a flat spiral, which acted both as the anode and a stirrer. The final thickness of ^{235}U in this target was 0.180 mg/cm^2.

3.2 Target Systems

3.2.1 LBL

All irradiations carried out for the production of Hf, Ta, Bi, Po, and Rf isotopes were performed at the LBL 88-Inch Cyclotron in Cave 0, the high-radiation level irradiation facility. This facility is equipped with a target system (Fig. 3.4) capable of utilizing non-radioactive or radioactive targets. When using a radioactive target, a fast-closing "slammer valve" is used to ensure that the 88-Inch Cyclotron is protected from contamination with target material in the case of a catastrophic target failure. During these irradiations, the pressure inside the beam line between the accelerator and the target system is continuously monitored. In the event of a vacuum failure, the "slammer valve" simply seals the beam line between the target system and the cyclotron, isolating the

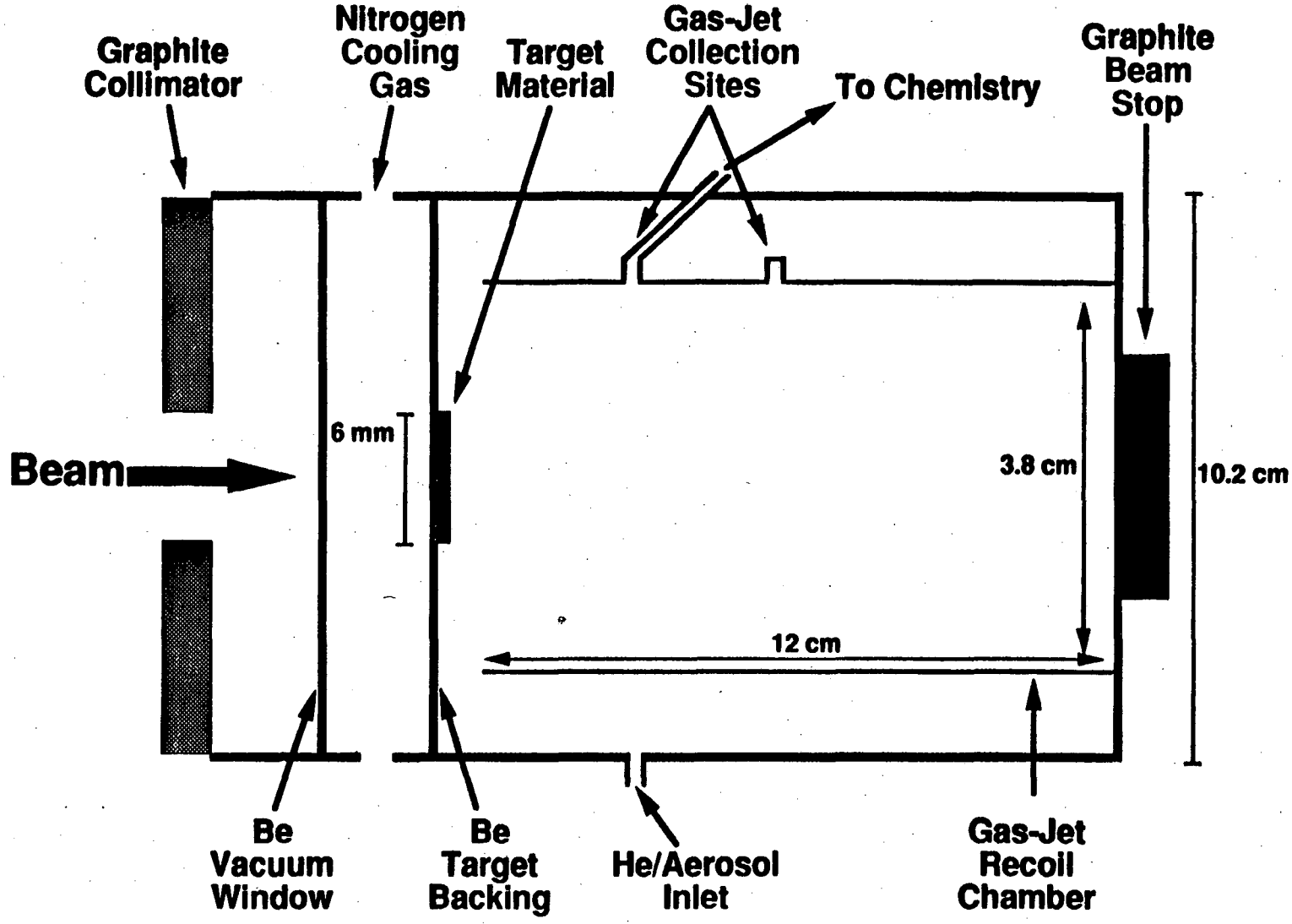

Fig. 3.4 Schematic of the LBL target system at the cyclotron.

cyclotron. A "beam wobbler" [MOO 83] is also used to spread the beam intensity over the entire target area to prevent local overheating in the target.

After a positive ion beam exits the cyclotron and passes through the "beam wobbler", it passes through a water-cooled graphite collimator (6-mm i.d.), a 2.75-mg/cm^2 Be vacuum window which separates the target system from the cyclotron vacuum, 0.2-mg/cm^2 nitrogen cooling gas, which cools the target backing placed 2-mm from the vacuum window, the 2.75-mg/cm^2 Be target backing, and finally the target material. The beam is stopped in a water cooled graphite beam stop, 15 cm from the target.

The reaction products which recoil out of the target are stopped in 1.3 atm He in the recoil chamber. The products are then attached to aerosols in the He and are transported to the gas chromatography system through a 2.4-mm i.d. x 5-m long capillary.

3.2.2 GSI

All irradiations carried out for the production of Ha isotopes were performed at the GSI UNILAC accelerator. The target system (Fig. 3.5) used at this facility is very similar to the system used at LBL. To protect the accelerator from possible contamination during bombardments of radioactive targets, a "quick valve" is used. The design and the principle of operation of this valve is similar to the "slammer valve" used at LBL.

The positive ion beam passes through the same materials as in section 3.2.1 but it is stopped in a water cooled copper beam stop. It is possible to adjust the distance between the gas-jet recoil chamber and the target. The recoiling reaction products are attached on aerosols in He, which sweeps the front of the target continuously, and are transported to the gas chromatography system through a 2.4-mm i.d. x 15-m long capillary.

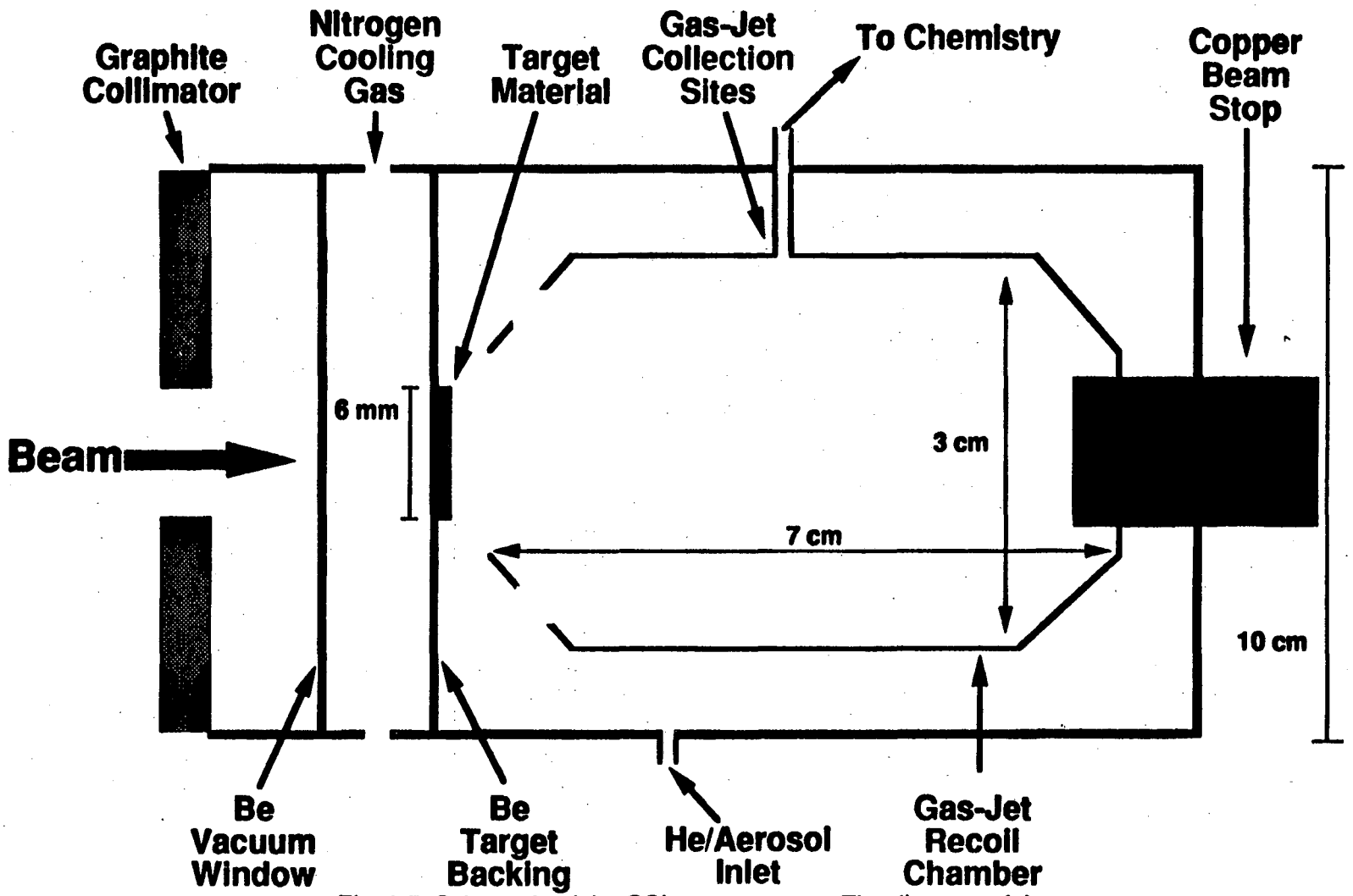

Fig. 3.5 Schematic of the GSI target system. The distance of the recoil chamber to the target may be adjusted by moving the chamber back and forth on the copper beam stop.

3.2.3 PSI

All irradiations carried out for the production of Zr and Nb isotopes were performed at the PSI **SAPHIR** reactor. The reactor is of the light-water moderated swimming pool type with a thermal power of 10 MW. A helium-filled beam line provides $(4.6\pm0.5)\times10^6$ thermal neutrons/$(s\cdot cm^2)$ over a beam spot size of 50 mm in diameter at the site of the target. Fig. 3.6 illustrates the schematic of the target system. The target chamber is made of titanium to keep the neutron-induced activity of the assembly as low as possible [YA 89]. The Ti(n,γ) reaction produces only the 5.1-min ^{51}Ti with a low cross section of 0.2 barn. The 6-mm thick aluminum-boron carbide chopper is used to reduce the neutron flux out of the reactor by a factor of 100. The production of the fission product nuclides can be precisely timed with this mechanical shutter. The target chamber can be vented through a relief valve into the waste air stream. The waste air from the outer tube of the capillaries and from the target chamber housing is pumped through an activated charcoal filter and then released into the building ventilation system. The level of activity in the filter is continuously monitored. The recoiling fission products are attached to aerosols in He, which sweeps the front of the target continuously, and are transported to the gas chromatography system. If the monitored activity exceeds the preset limits, an interlock is triggered, closing the reactor beam line and the gas supply to the gas-jet transport system and opening the relief valve to the target chamber.

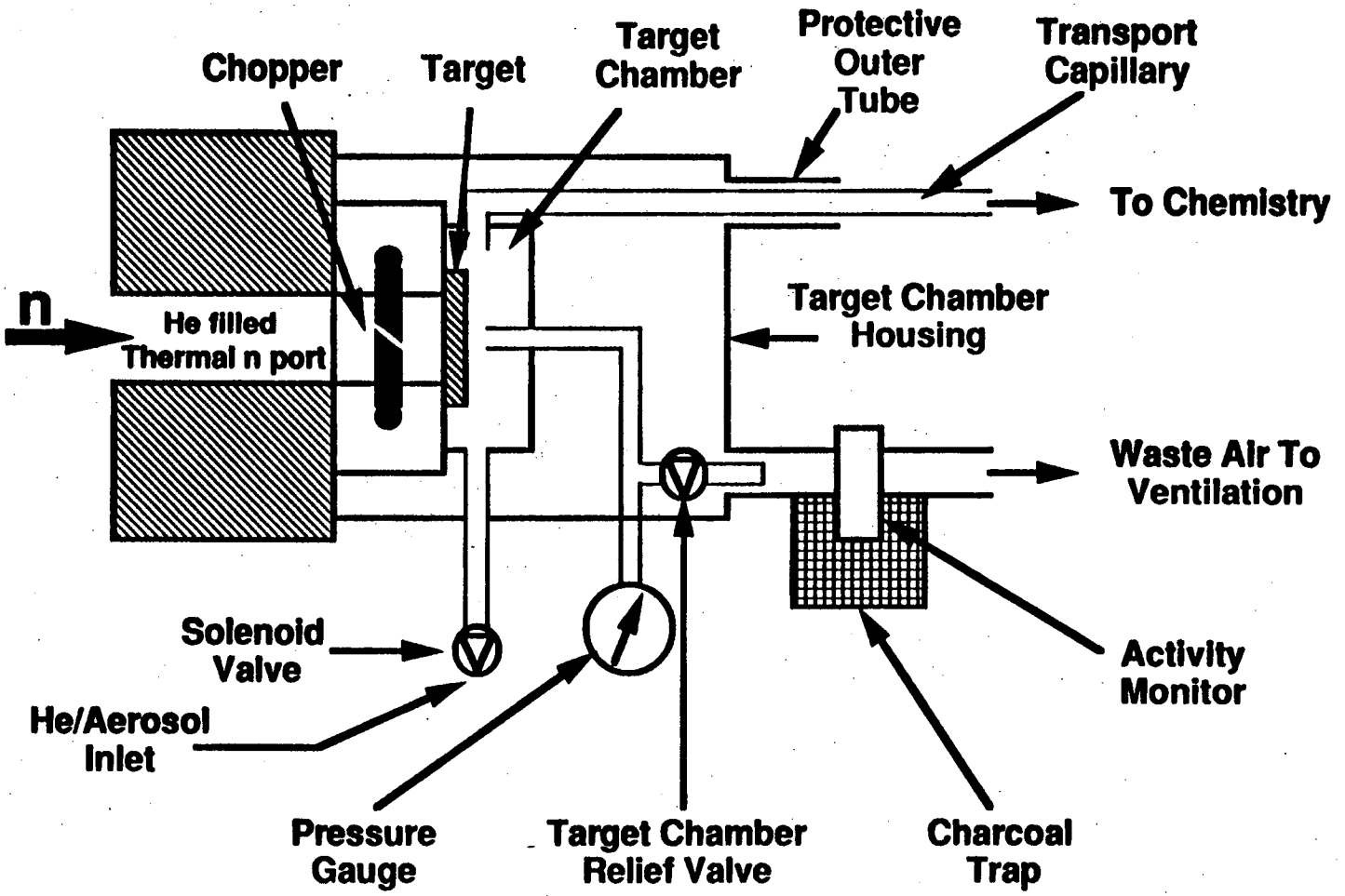

Fig. 3.6 Schematic of the PSI target system

3.3 Irradiations

3.3.1 $^{Nat}Eu + ^{147}Sm(^{20}Ne,xn)$ Reactions

Isotopes of Hf and Ta were produced by ($^{20}Ne^{6+}$,xn) reactions with a mixed ^{nat}Eu + ^{147}Sm target. The 140-MeV (laboratory system) $^{20}Ne^{6+}$ beam from the LBL 88-Inch cyclotron, after passing through the 2.75-mg/cm^2 Be vacuum window, 0.2-mg/cm^2 nitrogen cooling gas and the 2.75-mg/cm^2 Be target backing, was degraded to 122 MeV before striking the target material. Typical beam currents of 0.1 pμA were used throughout the experiments. The isotopes 41-s ^{162}Hf, 1.7-min ^{165}Hf, 32-s ^{166}Ta and 1.3-min ^{167}Ta were produced with cross sections of hundreds of milibarns. Typical γ-spectra of a 'direct catch' and a 'chemistry' experiment are illustrated in Fig. 3.7. The 'direct catch' measurement is simply a 5-min survey of photopeaks from the reaction products transported directly from the target system to the detection system. During a 'chemistry' measurement the reaction products are transported to the chromatography system where a chemical separation based on volatility is performed. The separated volatile species are then transported to the detection system as previously explained in section 2.2.2.5. The 'chemistry' spectrum illustrated in Fig. 3.7 was measured after separation at 500°C where both the Hf and the Ta halides are volatile. In both types of measurements, samples were collected for 5 min and surveyed during the collection period for characteristic photopeaks. The 173.7-keV and 195-keV γ-peaks were observed for ^{162}Hf. The 179.9-keV [BRU 81] γ-peak was observed for ^{165}Hf. The 158.7-keV and 311.7 KeV γ-peaks were observed for ^{166}Ta, and the 113.7-keV and 139.5-keV γ-peaks for ^{167}Ta [SHI 78].

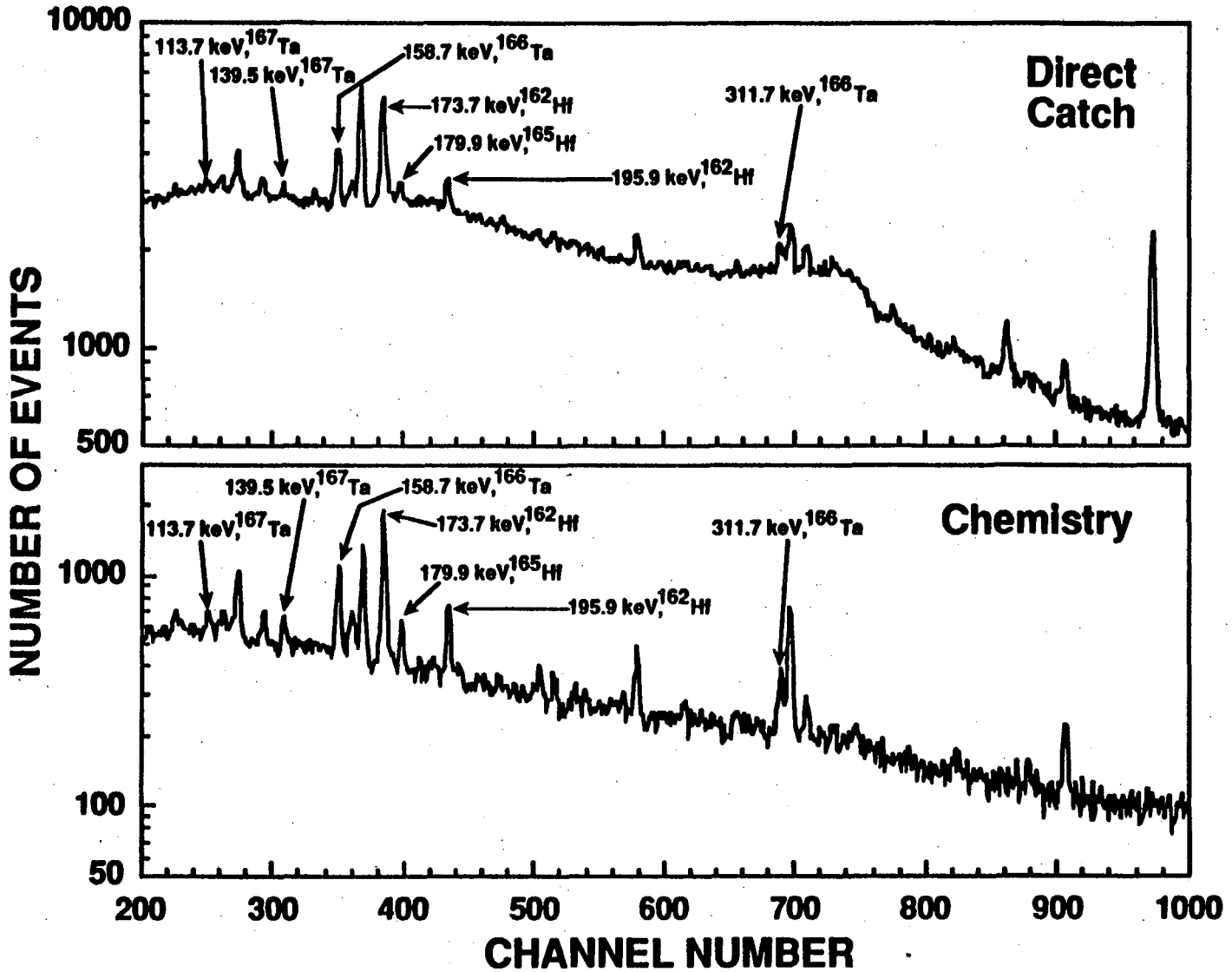

Fig. 3.7 Typical 5-min γ-spectra of 'direct catch' and 'chemistry' measurements for Hf and Ta experiments.

3.3.2 $^{248}Cm(^{18}O,5n)$ Reaction

The 78^{+11}_{-6} s ^{261}Rf (half-life measured in this work) was produced by the $^{248}Cm(^{18}O^{5+},5n)$ reaction with a cross section of 5 nb [GHI 70]. The 117-MeV (laboratory system) $^{18}O^{5+}$ beam from the LBL 88-Inch cyclotron, after passing through the 2.75-mg/cm^2 Be vacuum window, 0.2-mg/cm^2 nitrogen cooling gas and the 2.75-mg/cm^2 Be target backing, was degraded to 99 MeV before striking the target material. Typical beam currents of 0.5 pμA were used throughout the experiments. Each sample was collected for one minute and surveyed for 6 min for characteristic alpha-particle events. Fig. 3.8 shows the sum spectrum of all alpha particles observed in the chemistry experiments for the first 3 minutes of counting. The major activities in this spectrum are from Bi and Po isotopes. The chloride species of these elements are highly volatile (chromatographic properties discussed in chapter 6). These isotopes are produced with cross sections of tens to hundreds of millibarns from the reaction of ^{18}O with trace lead impurities in the target material. The 8.15-MeV to 8.38-MeV region in the alpha spectrum contains all events due to ^{261}Rf and its 25-s daughter ^{257}No. A weak alpha line at 8.305 MeV (0.25%) from the 25.2-s $^{211}Po^{m}$ also falls in this region. However, the number of events in this region attributable to this alpha line can be deduced using its known intensity relative to the 7.275-MeV (91.05%) $^{211}Po^{m}$ alpha line [ShI 78].

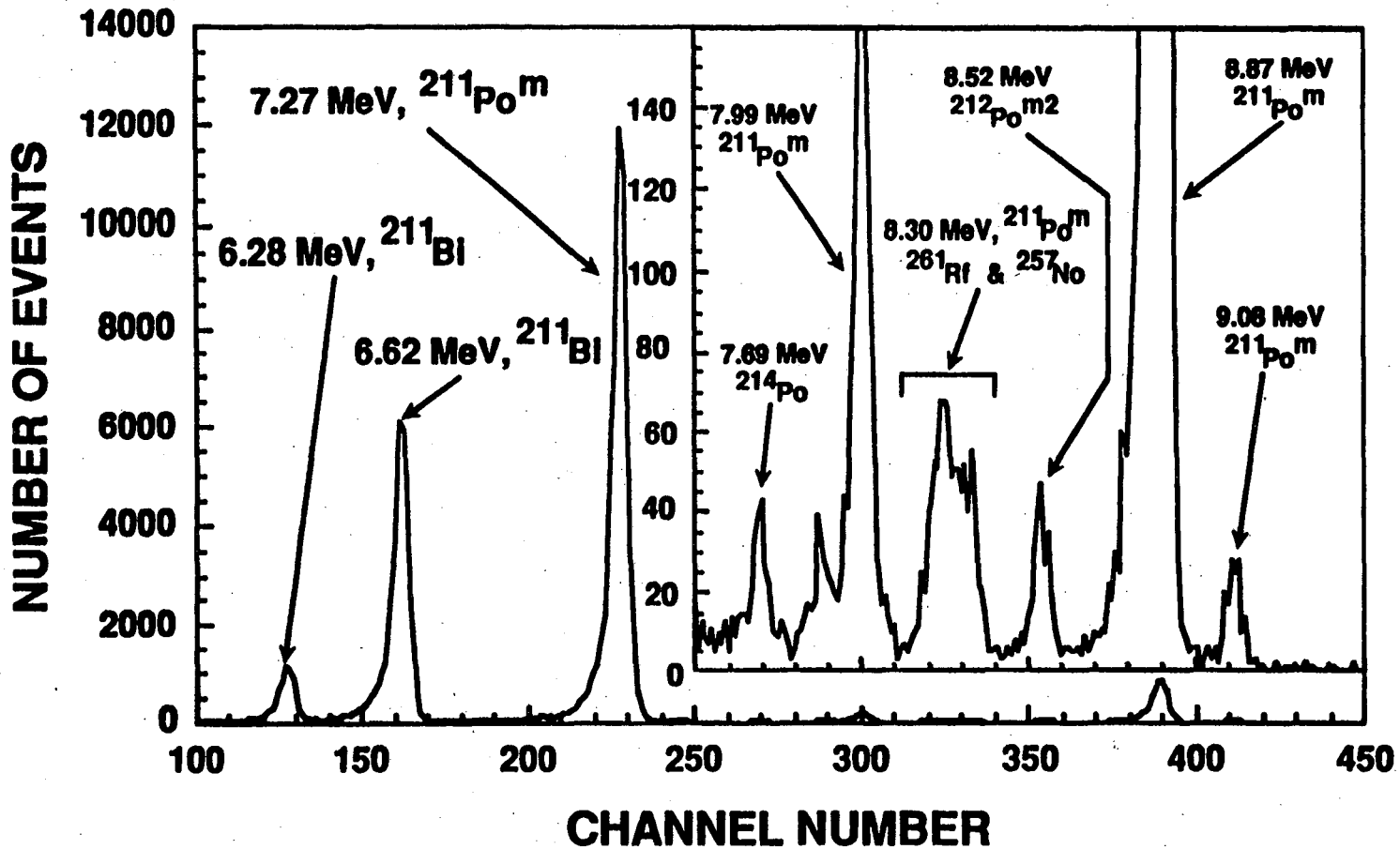

Fig. 3.8 Sum spectrum of all alpha particles observed in the Rf chemistry experiments for the first 3 minutes of counting.

3.3.3 ^{249}Bk(^{18}O,5n) Reaction

34-s ^{262}Ha was produced at the **UNILAC** accelerator at GSI by the ^{249}Bk($^{18}O^{5+}$,5n) reaction, at a beam energy of 99-MeV (laboratory system), with a cross sections of 6±3 nb [KRA 92]. Typical beam currents of 0.5 pμA were used throughout the experiments. Each sample was collected for 20 s and surveyed for 2 min for characteristic alpha-particle and spontaneous fission events. Fig. 3.9 shows the sum spectrum of all alpha particles observed in the chemistry experiments. As explained in section 3.3.2, the major activities in this spectrum are from Bi and Po isotopes. The 8.40 MeV to 8.70 Mev region in the alpha spectrum contains all events due to ^{262}Ha and its 3.93-s daughter ^{258}Lr.

3.3.4 ^{235}U(n,f) Products

Neutron-rich isotopes of Zr and Nb were produced at the **SAPHIR** reactor at PSI via the neutron-induced fission of ^{235}U. The ^{235}U target was covered with a 3.24-mg/cm^2 thick aluminum foil in order to suppress products from the heavy fission fragment mass peak relative to the light one. The former products, having a significantly lower recoil energy and range, are stopped in this foil, simplifying the identification of the light Zr and Nb fission isotopes. Typical γ-spectra of a 'direct catch' and a 'chemistry' experiment are illustrated in Fig. 3.10. The 504.3-keV γ-peak for the 7.1-s ^{100}Zr was observed. The 787.3-keV and 1024.0-keV γ-peaks for 2.9-s ^{98}Nb were observed. The 97.7-keV and 139.8-keV γ-peaks for 15-s ^{99}Nb, and 1429-keV γ-peak for the 1.25-min ^{94}Sr [SHI 78] were observed. The 'chemistry' spectrum illustrated in Fig. 3.10 was measured after separation at 400°C where both the Zr and the Nb halides are volatile. Strontium has no volatile chloride species, as observed by the disappearance of the 1429-keV γ-peak of

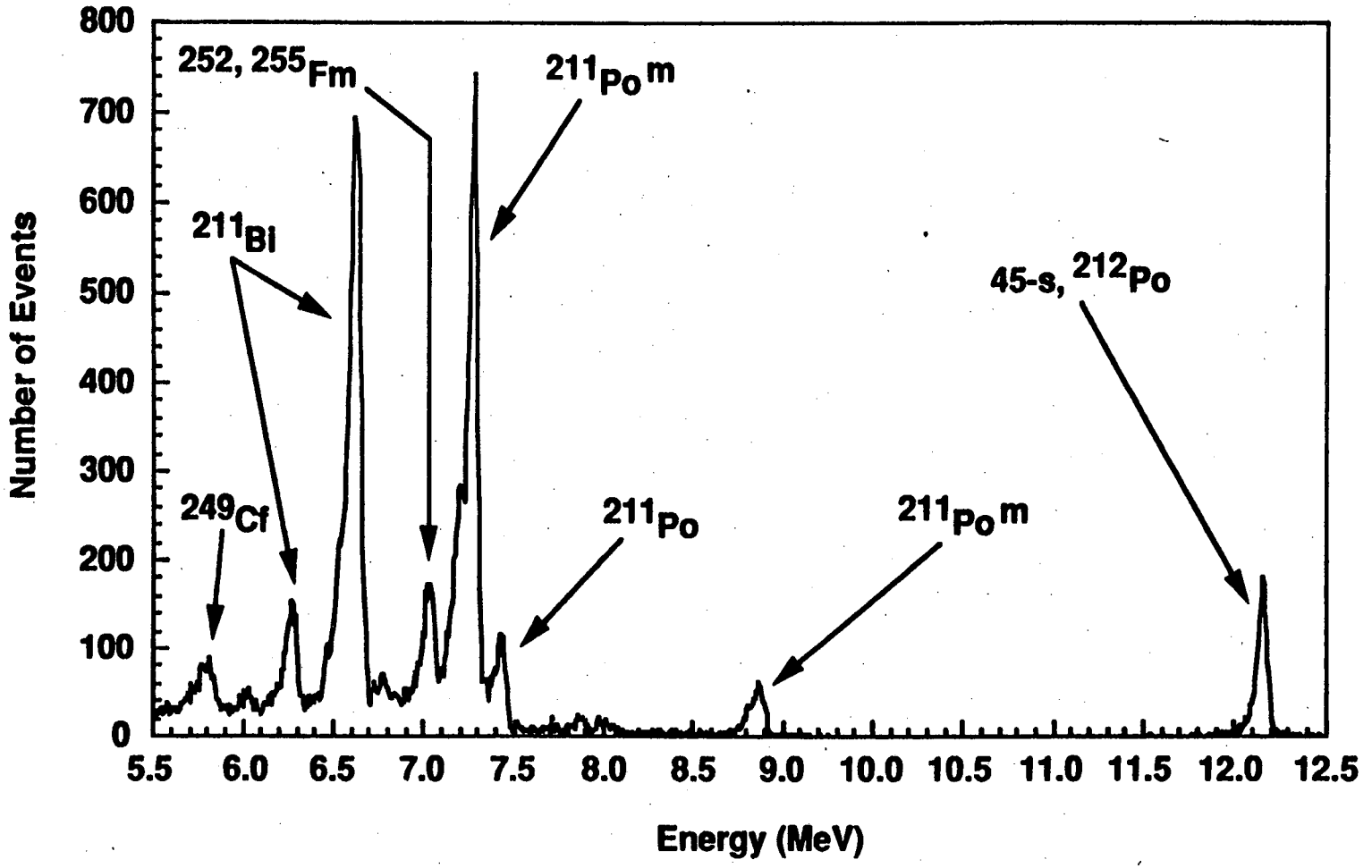

Fig. 3.9 Sum spectrum of all alpha particles observed in the Ha chemistry experiments for the first 2 minutes of counting.

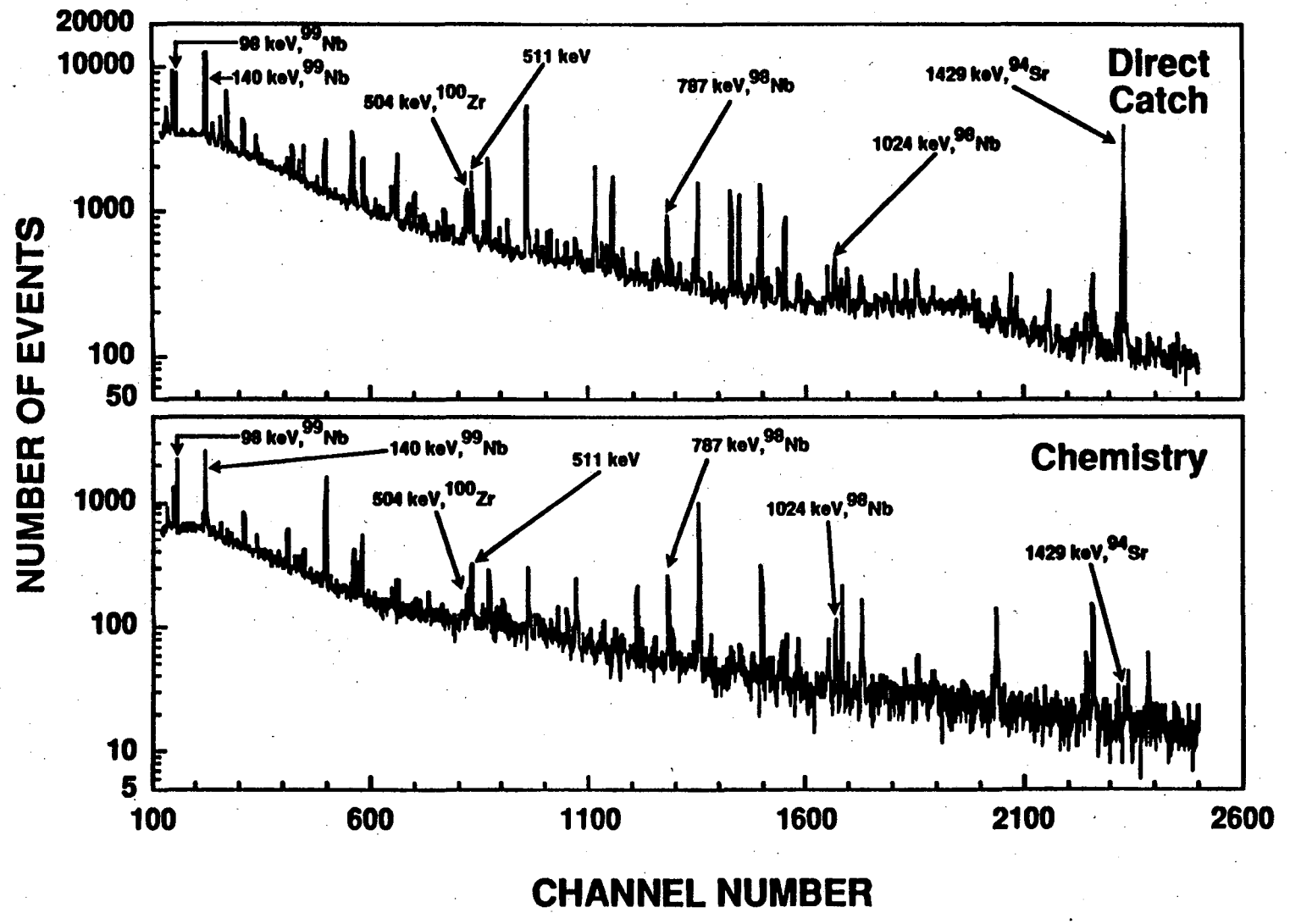

Fig. 3.10 Typical 5-min γ-spectra of 'direct catch' and 'chemistry' measurements for Zr and Nb experiments.

1.25-min ^{94}Sr, . The 30.7-s ^{98}Zr, which has no γ-peaks, was detected by the γ-peaks of its 2.9-s ^{98}Nb daughter. It was assumed that all ^{98}Nb detected was produced by the decay of ^{98}Zr since the recluster time, period of time from separation to detection, was on the order of 20 s. Gamma peaks not labeled in Fig. 3.10 include those due to the decay of ^{141}Ba, ^{142}Ba, ^{145}Ce, ^{140}Cs, ^{134}I, ^{144}La, ^{101}Mo, ^{90}Rb, ^{130}Sb, ^{132}Sb, ^{104}Tc, ^{133}Te, ^{134}Te, etc..

Chapter 4

Experimental Procedures

4.1 Gas Transport Systems

All products from nuclear reactions were transported to the gas chromatography system (HEVI) via a He/aerosol gas transport system. Two aerosol systems, He/KCl and He/MoO_3, were used in this work. The aerosols for each gas-jet system were generated by heating crystalline KCl or MoO_3 to 640°C or 620°C, respectively, inside a quartz tube heated by a split shell furnace. Helium gas flowing at a rate of 2 l/min, was used to sweep the aerosols out of the tube and into a 'presorter' capillary, where the larger aerosol particles were allowed to settle out of the He flow. The presorter is a 5 meter length of 4.8-mm i.d. Teflon capillary tube which has been wound into several coils of about 15 cm diameter. The 'presorted' aerosols were transported directly into the target chamber via a 4.8-mm i.d. Teflon capillary tube. The recoiling reaction products were stopped in the He and collected on the aerosols in the helium, which continuously swept out the volume behind each target. The activity-laden aerosols were transported by the helium through a 1.6-mm i.d. Teflon capillary tube to the gas chromatography apparatus. All capillaries used in the transport process of the products to HEVI were made of Teflon to eliminate any exchange of oxygen through the capillary walls. The yield of volatile

halides was found to be sensitive to oxygen. The total transportation yield of both systems ranges from 60-80%. In experiments conducted at the 88-Inch cyclotron at LBL, the length of the transport capillary from the target chamber to the gas chromatography apparatus was 5 meters with a transport time of one second or less. The length of this capillary at the **UNILAC** accelerator at GSI was 15 meters with a comparable transport time. At the **SAPHIR** reactor at PSI, a 130 meter long polyethylene capillary (2-mm i.d.) was used to transport the activity from the reactor building to the chemistry building. A transportation time of approximately 12 s was measured [YA 89] at a gas flow of 2 l/min.

4.1.1 Aerosol Oven Temperatures

The aerosol oven temperatures given in section 4.1 represent conditions of maximized gas-jet yield for each system. To arrive at these temperatures gas-jet yield measurements were conducted at preselected temperature intervals. For these measurements an ^{225}Ac recoil source, made from a ^{229}Th source, on a flat brass pin was used in conjunction with a recoil chamber. The flat side of the brass pin was placed 1 cm away from a ^{229}Th source in 1 atm of He (Fig. 4.1). Three hundred volts were applied between the source and the pin to collect the positive ^{225}Ra ions, recoiling from the ^{229}Th alpha decay, on the brass pin (the high ionization potential of He prevents neutralization of the ^{225}Ra). The Ac source was held inside the recoil chamber (Fig. 4.2) and the recoiling products from the ^{225}Ra decay chain (Fig. 4.3) were attached to the aerosols which were then transported to a collection site. One hundred volts were applied between the source and a metal pin to aid the recoiling of products. The recoiling ^{221}Fr attached to the aerosols which were transported via the gas-jet system and collected on thin Al foils. These foils were measured with an α-spectrometer system

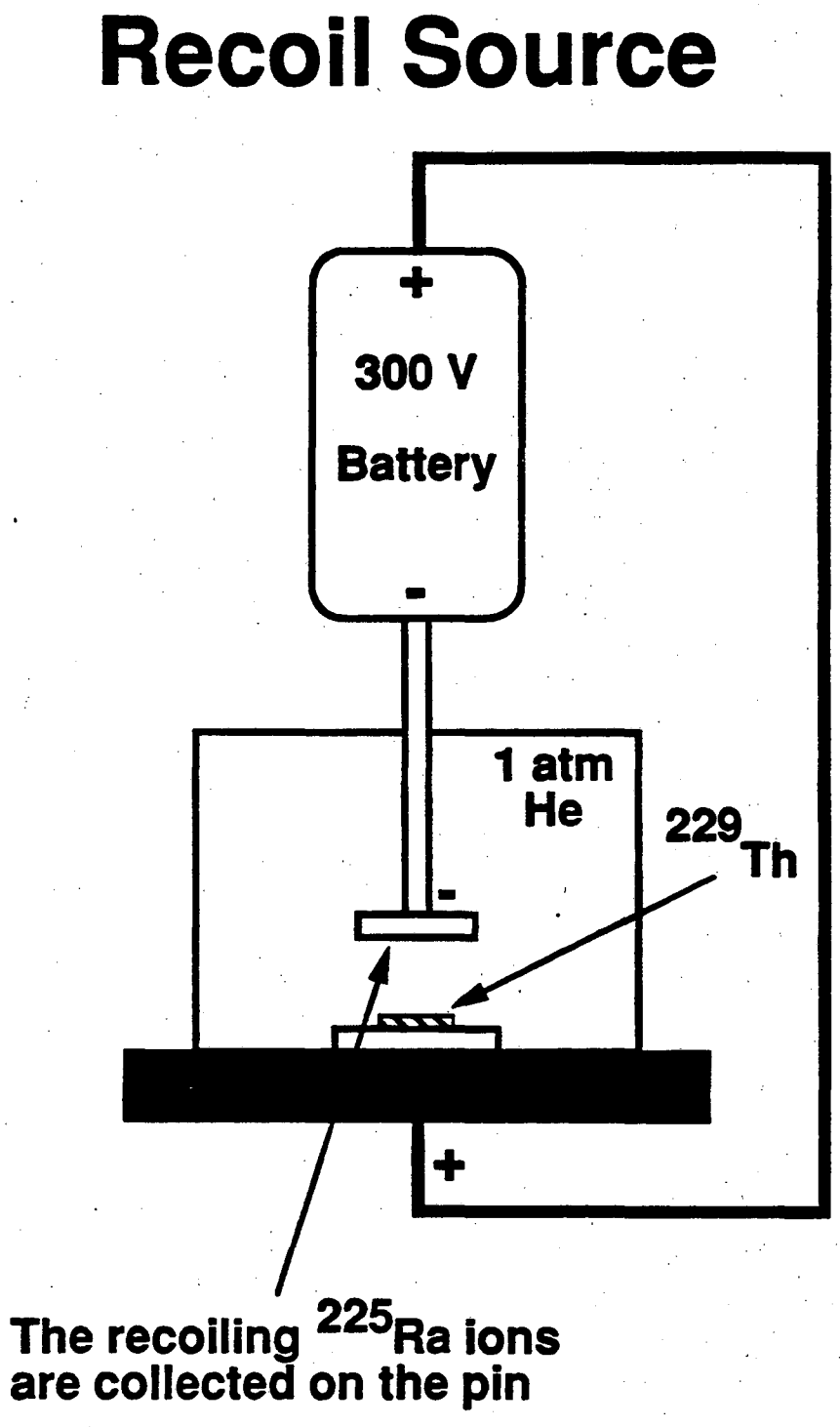

Fig. 4.1 Illustration of the ^{229}Th recoil source.

Ac Recoil Chamber

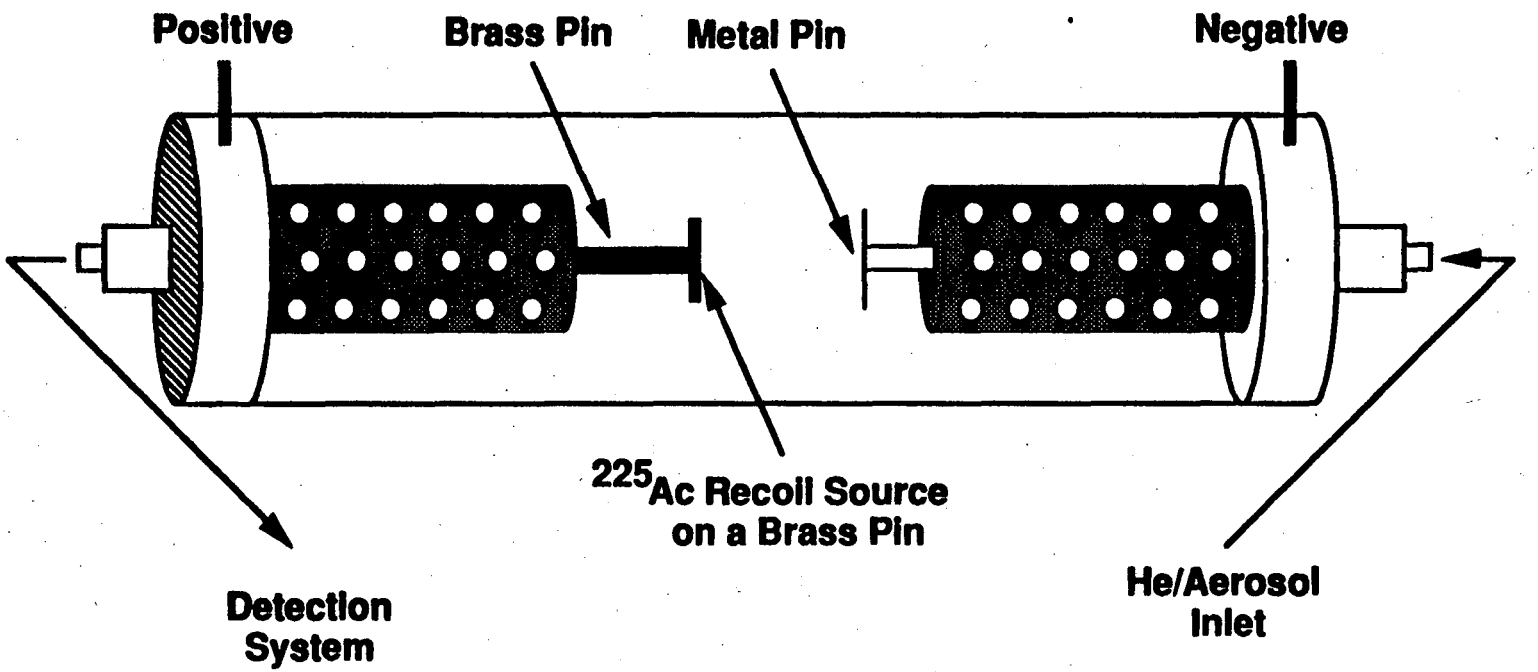

Fig. 4.2 Illustration of the Ac recoil chamber used in gas-jet yield measurements. One hundred volts are applied between the source pin and the metal pin to aid in collecting the recoiling products.

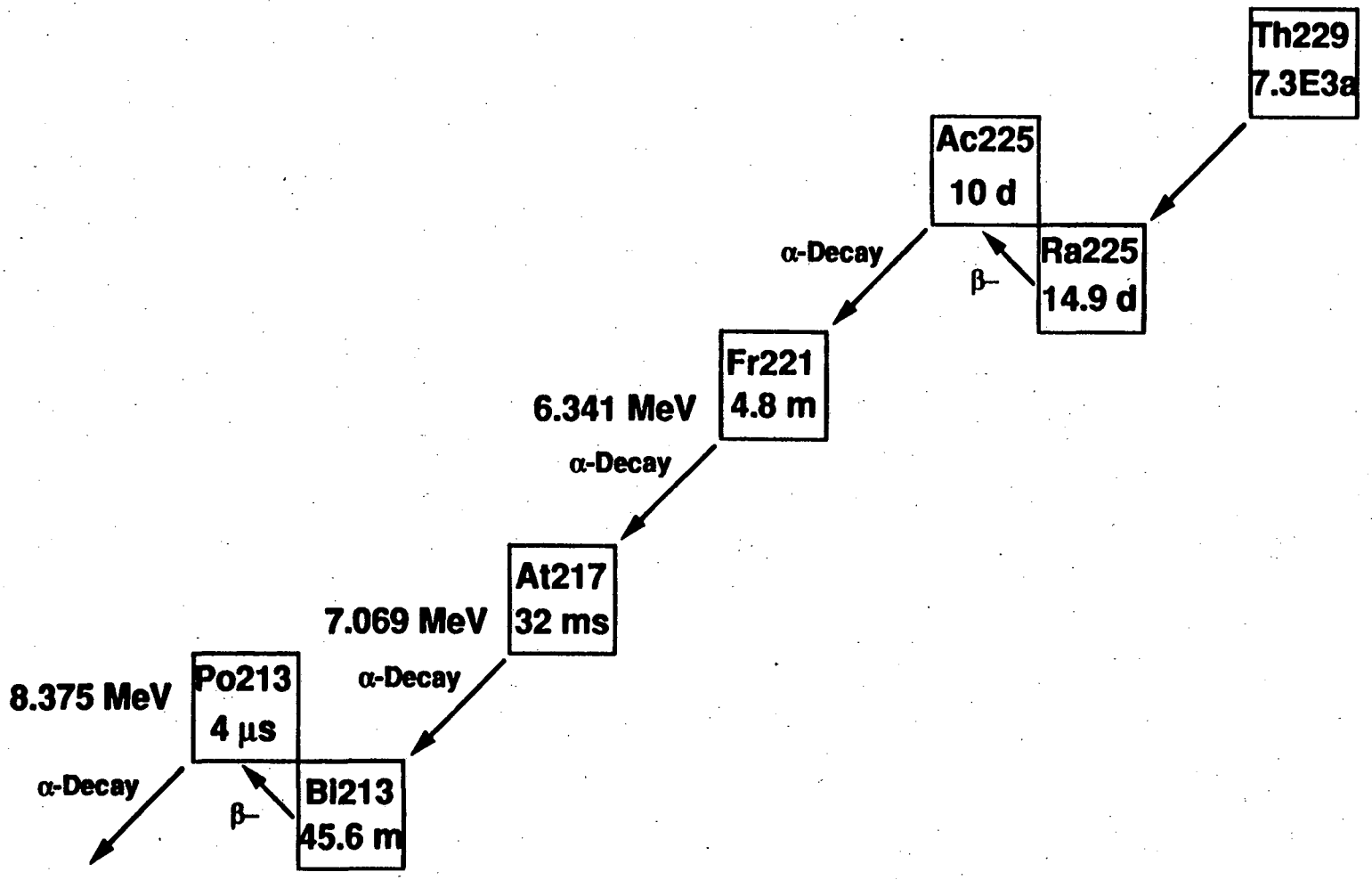

Fig. 4.3 Decay chain of the recoil source.

utilizing a Si(Au) solid state surface barrier detector. Gas-jet transport yields were determined using the 6.341-MeV, 7.069-MeV and 8.375-MeV alpha particles from ^{221}Fr, ^{217}At, and ^{213}Po, respectively. Figs 4.4 and 4.5 show yield versus aerosol oven temperature plots for the He/KCl and the He/MoO_3 systems, respectively. A temperature of 620°C was used for the He/MoO_3 system since at the maximized yield temperature of 650°C excess amounts of MoO_3 aerosols overload the system. Aerosol oven temperatures were elevated by ≈100°C [YA 89] at GSI and PSI since a stainless steel tube was used, in place of a quartz tube, and there was an addition of a sintered glass filter after the 'presorter' loop. The glass filter further discriminated against large aerosol particles and was cleaned daily to insure constant transport conditions.

4.1.2 Aerosol Material

Two types of aerosols were used. KCl aerosols were used in the early development stages of this chemical separation since the He/KCl system was a well-established method of transporting reaction products from heavy ion nuclear reactions. This is the preferred transport system for aqueous chemistry since KCl readily dissolves in aqueous solutions. However, after prolonged gas chemistry experiments with this system, the quartz surface of the chromatography column is partially coated with a thin layer of KCl causing the chromatography to be performed on KCl rather than on SiO_2. Our volatility measurements are strongly dependent on the chromatography surface and therefore a new transport system had to be established to resolve this problem.

The He/MoO_3 transport system is the preferred system for our on-line isothermal gas chromatography. Reactions between MoO_3 and a variety of chlorinating agents produce molybdenum-chloride ($MoCl_5$) and -oxychloride ($MoOCl_3$) which are volatile at temperatures as low as 100°C. After the transport of reaction products to the

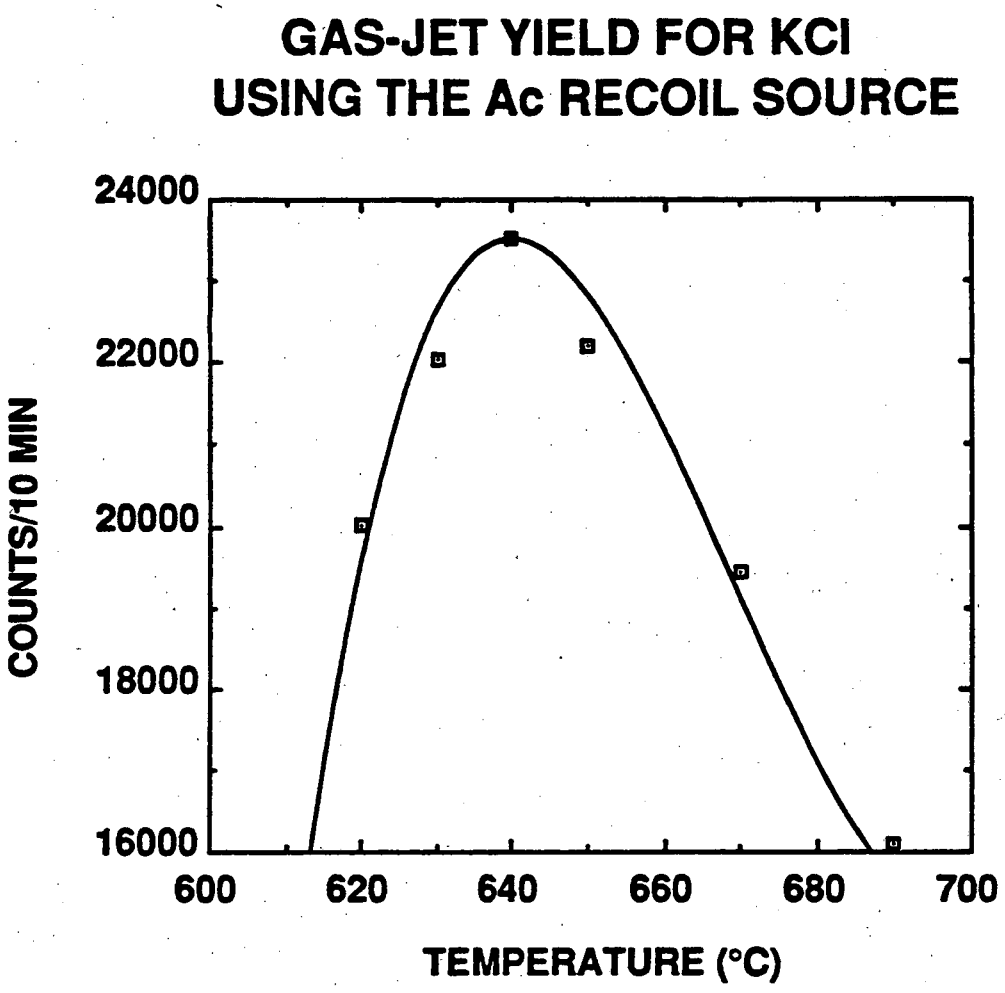

Fig. 4.4 Yield versus aerosol oven temperature for the He/KCl transport system.

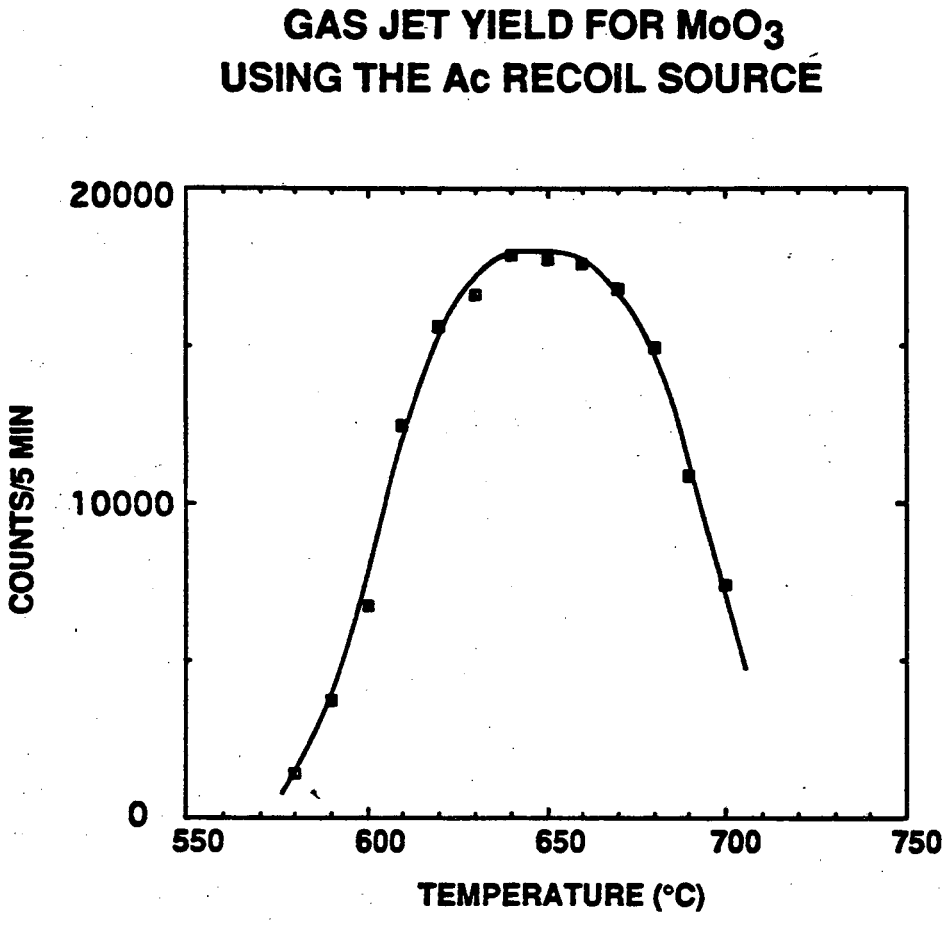

Fig. 4.5 Yield versus aerosol oven temperature for the He/MoO_3 transport system.

chromatography system, the aerosols are converted to volatile species which leave the column without coating the quartz (SiO_2) chromatography surface.

As stated above, the He/MoO_3 transport system is very new and not completely understood. For example, certain chlorinating agents such as HCl and HBr gas produce non-volatile molybdenum-oxyhalides (MoO_2Cl_2, MoO_2Br_2) which coat the chromatography column (found in this work). Intensive studies of this system are being conducted at PSI [TUR 93].

4.2 Halogenating Agents

Various halogenating systems were used in order to find the optimum conditions for the gas chromatography process. Halogenating agents in both gaseous and gas/vapor phases were utilized. All gases were supplied to the chromatography system by a (Model # SCH-0118) *Matheson 7-valve panel. The flow rate of gases to the system was controlled by a Matheson mass flow controller. The panel was used in conjunction with a gas bubbler (Fig. 4.6) for gas/vapor phase halogenating systems. Gases supplied from the mass flow controller entered the gas bubbler through the reactive gas inlet. The gas bubbled through the liquid phase to create vapor, and exited the bubbler through the reactive gas outlet to the chromatography system. The bubbler was designed to allow the bypass of liquid agents by a clockwise and a counterclockwise rotation of valves 1 and 2, respectively.

All gases were purchased from Matheson Gas Company Inc. and all other chemicals were purchased from Aldrich Chemical Company Inc.. The HCl, HBr, and Cl_2 gases were 99.995%, 99.8%, and 99.99% in purity. The thionyl chloride ($SOCl_2$), carbon

* Matheson Gas Products, 8800 Utica Avenue, Cucamonga, California 91730

Gas Bubbler

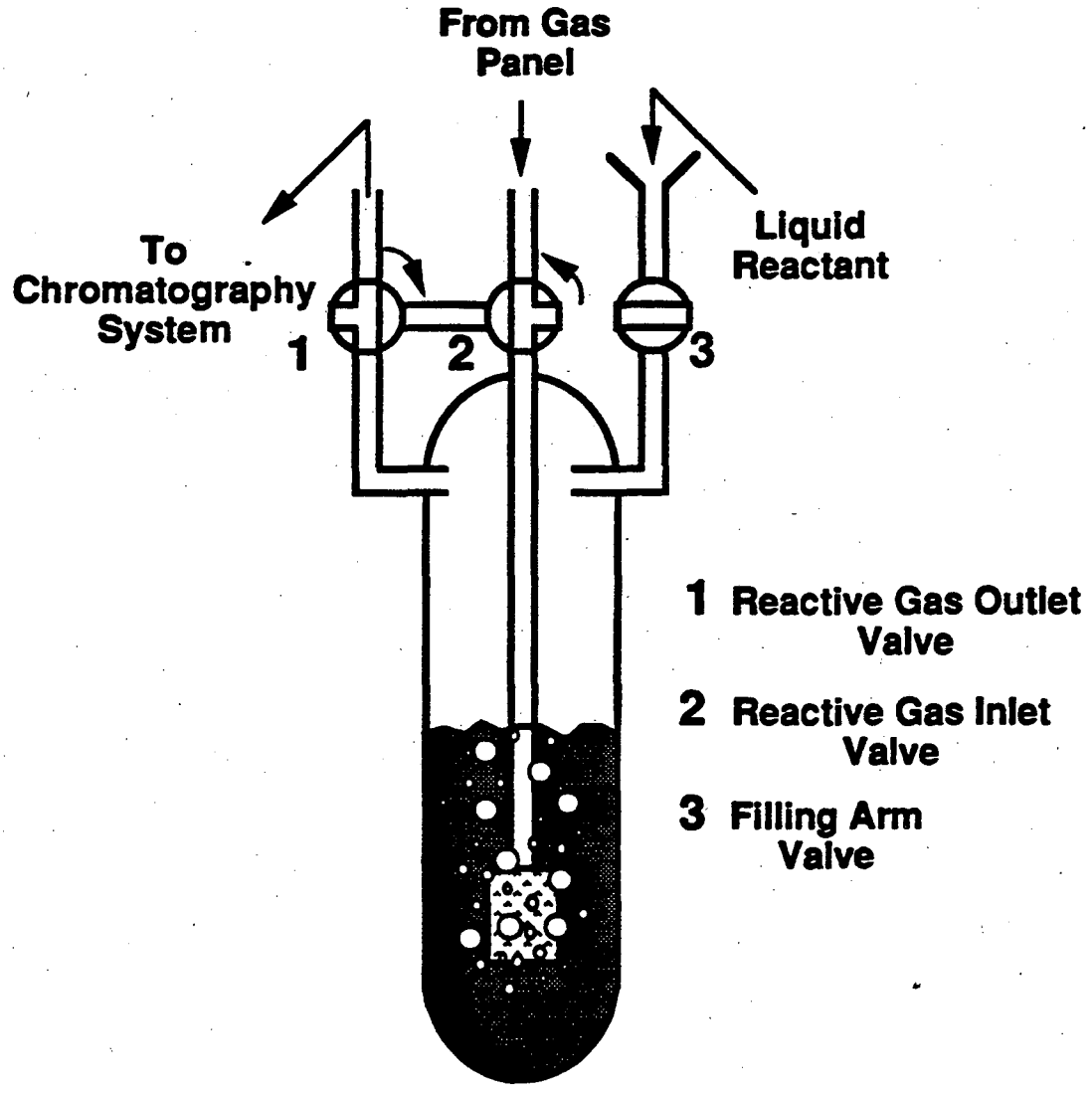

Fig. 4.6 Illustration of the gas bubbler used in experiments with mixtures of liquid and gaseous reactive agents. Liquid reactants may be bypassed by a clockwise and a counterclockwise rotation of valves #1 and #2, respectively.

tetrachloride (CCl_4), and boron tribromide (BBr_3), were 99+%, 99%, and 99.99% in purity. Experiments were conducted with the following halogenating systems: HCl gas, mixtures of HCl gas and $SOCl_2$ and HCl gas and CCl_4, Cl_2 gas, mixture of Cl_2 gas and CCl_4, and HBr gas.

4.3 Chromatography Surfaces

Two types of chromatography surfaces, SiO_2 and KCl, were utilized. The quartz columns used in HEVI provided a SiO_2 chromatography surface. The total length of the column was 82.2 cm with an inner diameter of 6 mm. The column ended in a 5.1-mm tip with an inner diameter of 1 mm. The total length of the isothermal column surface available for chromatography was approximately 48 cm including the tip. The shape and the column temperature profiles are illustrated in Fig. 2.11. To create the KCl surfaces, a small amount of KCl crystals was introduced inside the column. The crystals were melted with a heat gun until a liquid phase was observed. The column was rotated slowly as the liquid moved along the surface coating the column. This resulted in a visible crystalline layer of KCl. The chromatography temperatures in these measurements did not exceed 450°C to insure the presence of a KCl surface.

4.4 Detection and Data Acquisition Systems

In the subsequent sections of this paper, references will be made to 'direct catch' or 'chemistry' measurements. Please refer to section 2.2.2.5 for an explanation of these terms. For experiments conducted in all accelerator facilities the integrated beam current

was recorded for each direct catch and chemistry measurement to correct for any beam current fluctuations.

4.4.1 Ge Spectrometer System

For detection of species with characteristic gamma activities, a high-purity Ge gamma-ray spectrometer system using a PC-based ORTEC ACE 4K system was used in conjunction with a Teflon collection site. The activity-laden aerosols which were transported to the collection site for a 'direct catch' or a 'chemistry' measurement were collected on a 2.54 cm diameter glass fiber filter inside a Teflon collection site placed in front of a Ge detector (Fig. 4.7). The glass fiber filter was supported by a glass frit. The filter was surveyed for characteristic gamma activities and was replaced with a new filter after each measurement.

4.4.2 Merry-Go-Round and Realtime Data Acquisition and Graphics System

The Merry-Go-Round (MG) and Realtime Data Acquisition and Graphics System (RAGS) [HOF 80, LER 87] were used for the detection of alpha/SF activities from the (^{18}O,5n) reaction with ^{248}Cm at the LBL 88-Inch Cyclotron. The MG (Fig. 4.8) was located approximately 15 m away from the gas system. The 25.4-cm radius horizontal wheel of the MG had 80 equally spaced collection positions about its circumference. A steel ring with a 0.63-cm i.d. hole, which was covered with a 40±10 μg/cm^2 film of polypropylene, was placed in each collection position. The activity-laden aerosols were deposited on the polypropylene film. The wheel was stepped at one-minute time

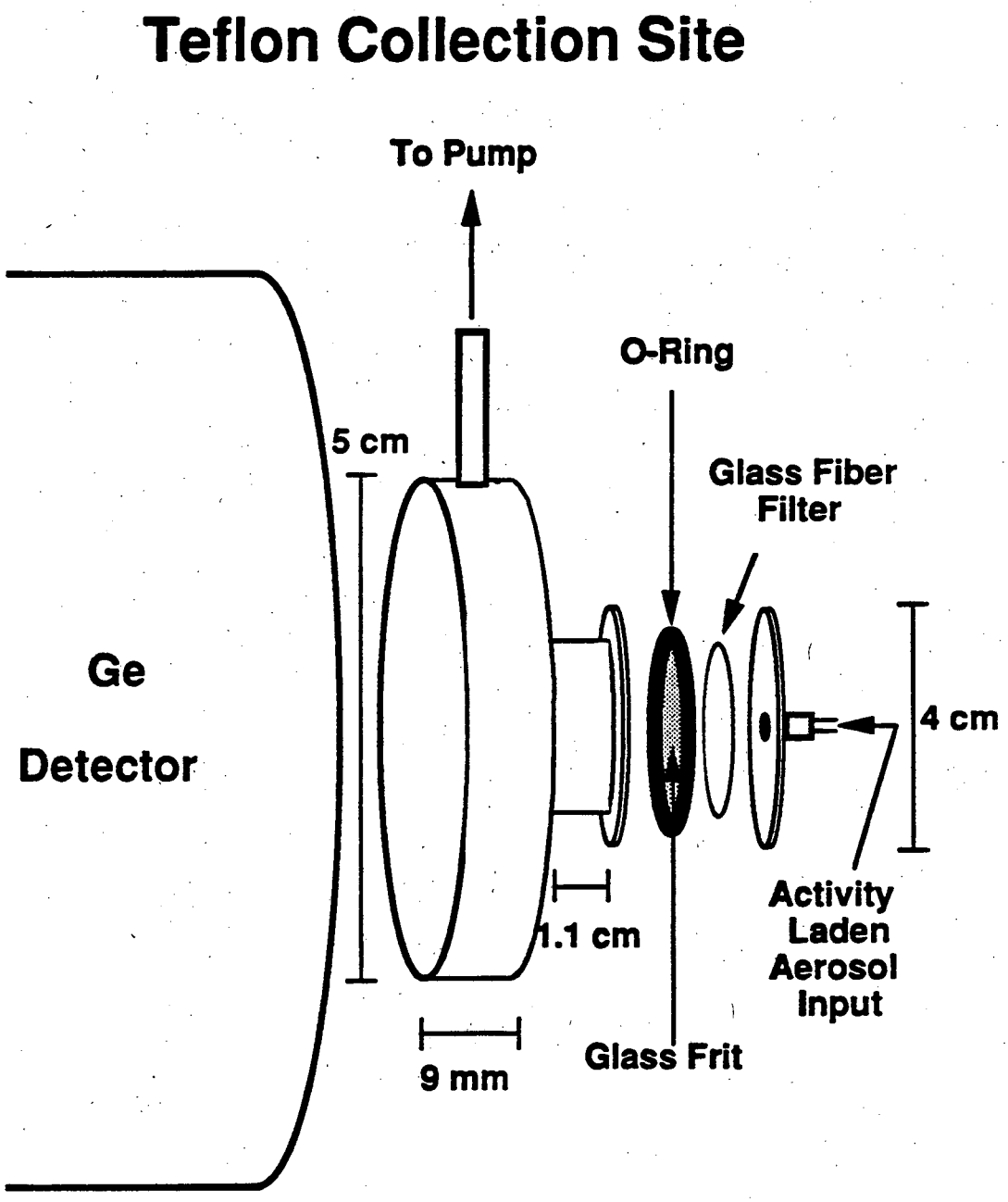

Fig. 4.7 Illustration of the Teflon collection site and detector arrangement used for detection of gamma activities. The activity laden aerosols are collected on the glass fiber filter 4.5 cm from the Ge detector. The glass fiber filter is replaced after each experiment.

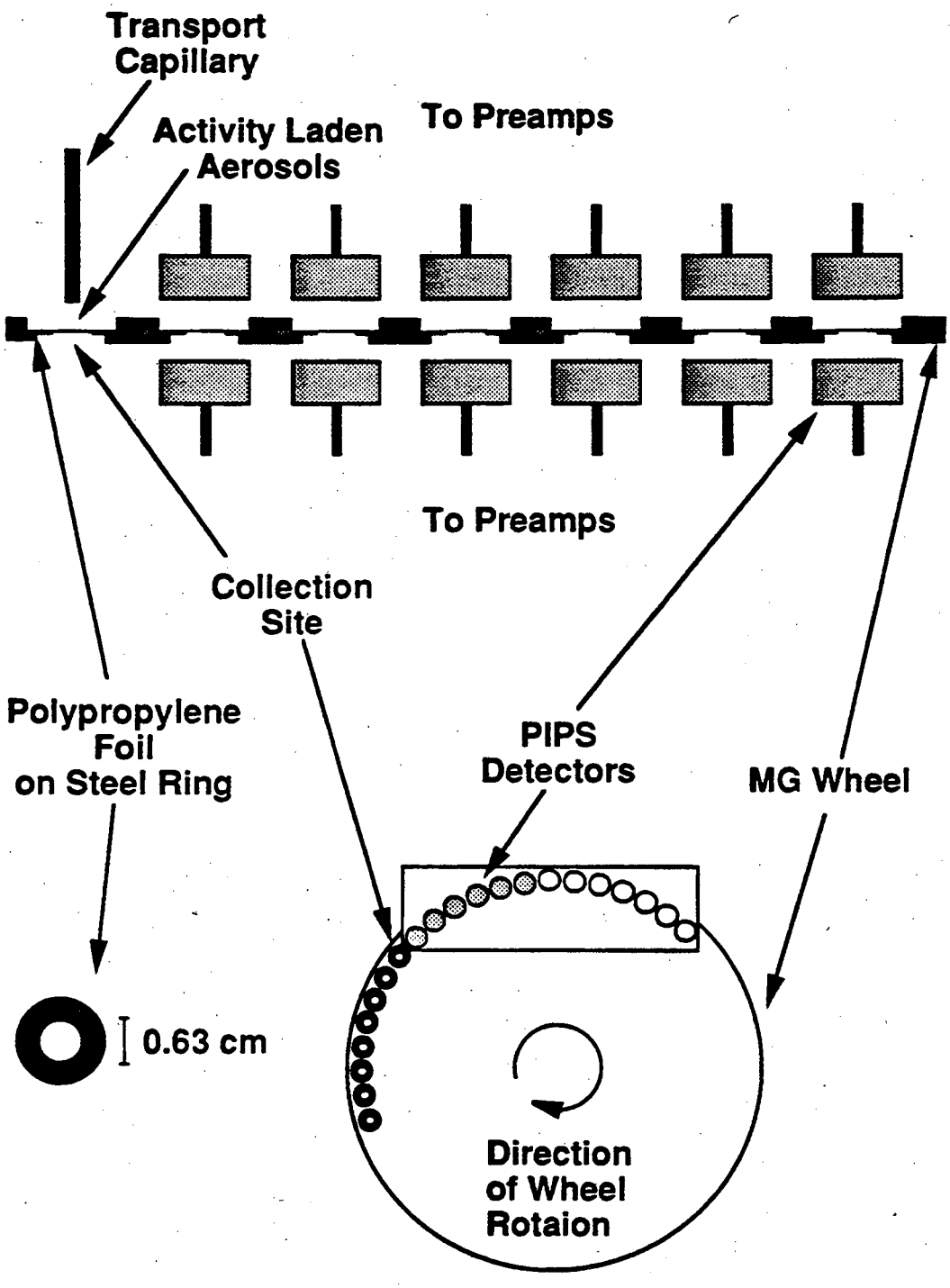

Fig. 4.8 The MG wheel system.

intervals so as to move the foils consecutively from the collection site into positions between pairs of passivated ion-implanted planar silicon detectors (PIPS). Because of the corrosive nature of the reactive gases used, PIPS detectors were required for this experiment, since they are chemically inert. The MG wheel was replaced with a new one after two complete revolutions in order to minimize the accumulation of any long-lived activities. Six pairs of detectors were used to measure the kinetic energies of coincident fission fragments and alpha particles. The efficiency for detection of alpha particles in each detector is 30%. Since in this configuration each detection station consists of two detectors, one above and the other below the wheel, the efficiency for the detection of alpha particles is about 60% and that for coincident fission fragments is about 60%. A second detector configuration was utilized in some measurements. In these experiments twelve detectors were placed above the MG wheel, and the stepping time was reduced to 30 s. Appropriate efficiency corrections were applied in consideration of the two detector configurations. The MG chamber was evacuated with an inert vacuum pump. The exhaust gases, still containing the reactive halogenating agents, were neutralized in a NaOH (*Mystaire Venturi 2 Series Source) scrubber system before release to the building exhaust.

Fig. 4.9 illustrates the RAGS electronics schematic. RAGS is an LSI-11/73 computer-controlled data acquisition system. The amplified output signals of the PIPS detectors from alpha or spontaneous fission events are digitized by ORTEC AD811 analog-to-digital-converters (ADC). The ADC's are controlled by a Standard Engineering CAMAC crate controller. All events were stored on a hard disk in list mode. Each event was tagged with a time, channel number, and a detector number.

* Heat Systems, Inc., 1938 New Highway, Farmingdale, New York 11735.

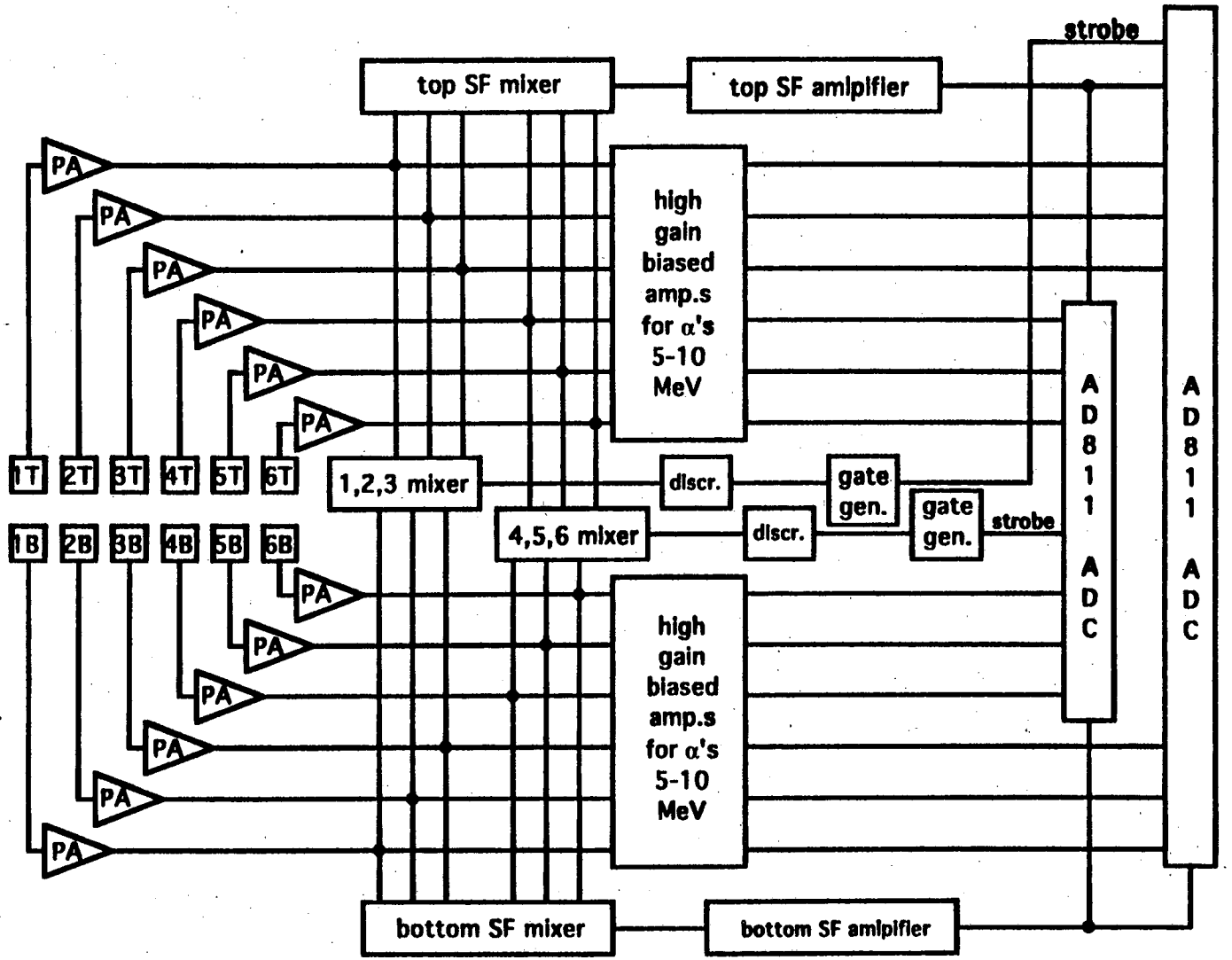

Fig. 4.9 RAGS electronic schematic.

4.4.3 OLGA II Tape System

The OLGA II Tape System [GAG 91] was used for the detection of alpha and SF activities from the (^{18}O,4n and 5n) reactions with ^{249}Bk at the GSI UNILAC accelerator. The tape system consisted of a modified magnetic tape station (cypher Mod. 900X) and seven chambers (Fig. 4.10), the first one of which acted as a collection site and the other six as detector stations. Activity-laden aerosols were deposited at the collection site on a regular computer tape, and subsequently stepped in front of six 450 mm^2 PIPS detectors. One tape allowed the collection of approximately 15000 samples, free from activities deposited in previous measurements. The detector efficiency was 38% for alpha-particles and 76% for SF's. The system was pumped with an inert vacuum pump and the exhaust gases were neutralized in a scrubber system.

The PSI Tandem system [SCH 89] was used for the data acquisition. NIM linear amplifiers and timing modules were used to prepare the signals for input into CAMAC-ADCs and a 1 MHz timer was employed to define the event times. A CES "Starburst" controller acting as front-end processor was used to assemble the event packages for transmission over an ethernet link to a micro VAXII/GPX back end.

4.5 Data Processing and Calculations

4.5.1 Processing of Gamma-Ray Data and Calculation of Relative Yields

Each gamma-ray spectrum consisted of a 4096-channel histogram. During all measurements samples were collected for 5 min and surveyed during the collection period for characteristic photopeaks. All gamma-ray spectra from direct catch and

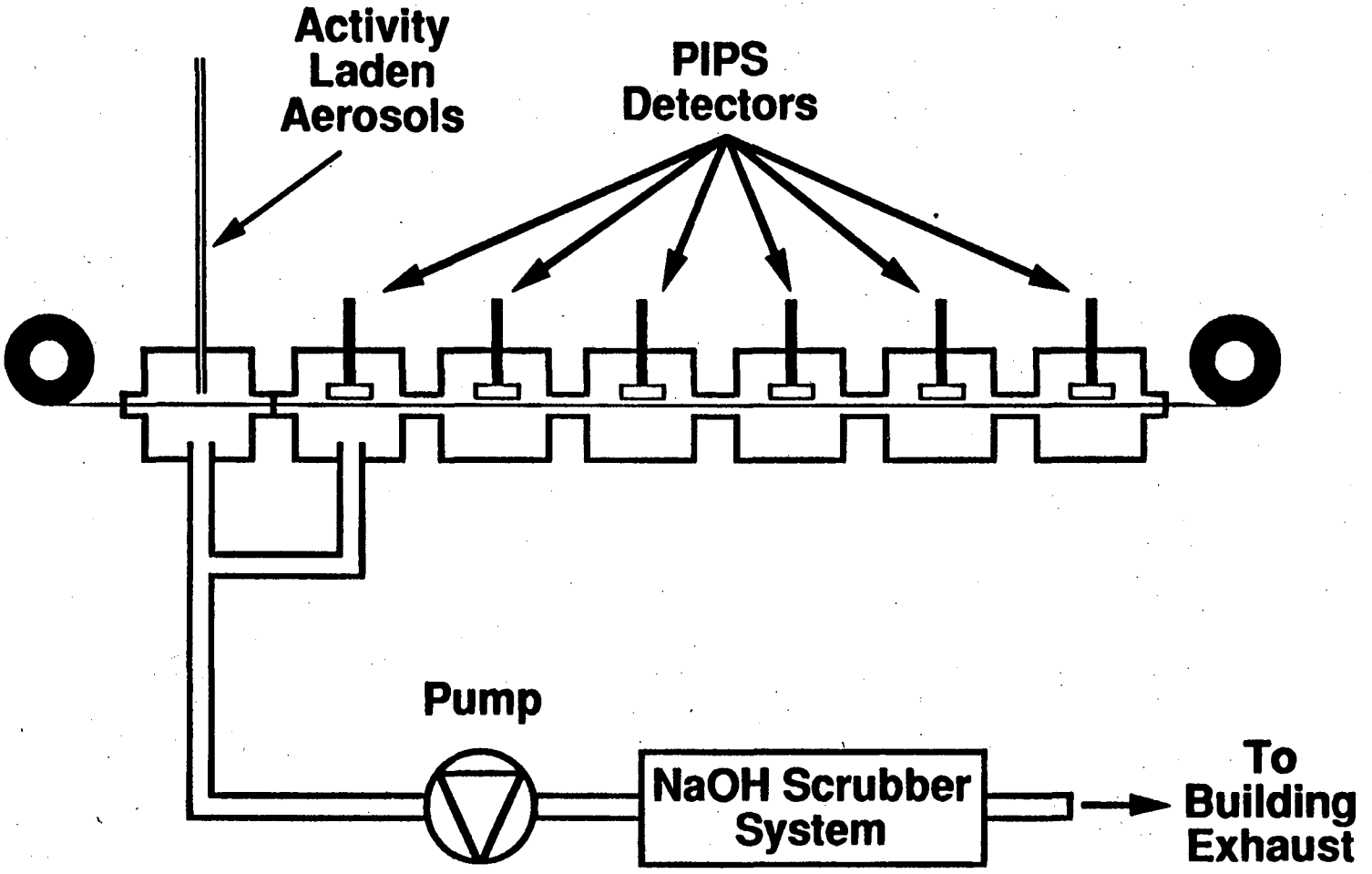

Fig. 4.10 Schematic of OLGA II tape system.

chemistry measurements were analyzed using the SAMPO computer code [ROU 69]. The SAMPO code contains algorithms for peak-shape, energy, and efficiency calibrations. It provides automatic peak-search and peak-fitting routines, and is capable of deconvoluting multiplet peaks. The output from SAMPO provided energy, total area, total activity, and the respective standard deviations on each value for each peak in the spectrum. In a typical experiment at a certain column temperature, two chemistry measurements were preceded and followed by a direct catch measurement. Corrections were made to peak area values to account for fluctuations in accelerator beam currents and dead time during data collection. Dead times of approximately 17%-20%, and 2%-4% were observed for direct catch and chemistry measurements, respectively. No neutron flux fluctuation corrections were made for the Zr and Nb experiments conducted at the PSI **SAPHIR** reactor since the flux remained constant. Photopeak areas and their corresponding statistical errors were calculated for the full-energy peaks corresponding to each isotope. All peak areas from chemistry measurements conducted at the same temperature were averaged together. At each temperature, the relative yield for each isotope was calculated by a direct comparison of the average areas from the chemistry measurements and the corresponding direct catch measurements. Values from the direct catch measurements represented a 100% chemical yield.

4.5.2 Processing of Alpha Data and Calculation of Relative Yields

The MG RAGS was used with two different detector configurations and stepping times. In order to combine the results of the experiments, corrections had to be made for all isotopes to normalize for the difference in decay between a 30-s and a 60-s stepping time. Appropriate corrections were also applied for detector efficiency. Alpha spectra

from all chemistry measurements were analyzed for the number of events in the 8.15-8.38 MeV energy region. This region contains all events due to ^{261}Rf and its 25±2-s daughter ^{257}No (Fig. 3.8). A weak alpha line at 8.305 MeV (0.25%) from the 25.2-s ^{211}Po^{m} also falls into this region. For all chemistry measurements the number of events in the 8.15-8.35 MeV range, due to ^{211}Po^{m}, was calculated, based on the intensity of the 7.275-MeV (91.05%) ^{211}Po^{m} alpha line, and subtracted from each spectrum. Corrections were made to account for fluctuations in accelerator beam currents for all measurements. Results from all chemistry measurements conducted at the same temperature were summed together and a plot of relative yield versus temperature was constructed for ^{261}Rf. The same procedure was followed to construct similar plots for ^{211}Bi and ^{211}Po^{m}. The 6.62-MeV and the 7.27-MeV alpha lines were used for ^{211}Bi and ^{211}Po^{m}, respectively.

To calculate the half-life of ^{261}Rf, all chemistry data were summed together (Fig. 3.8) and sorted into one-minute intervals. A two-component maximum likelihood [GRE 91] decay-curve fit was performed on the 7.275 MeV region of the spectrum. The two components consisted of 25.2-s ^{211}Po^{m} and 3.24-h ^{254}Fm. In this fit half-lives of both isotopes were fixed. The initial activity for the ^{211}Po^{m} from this fit was used to calculate an initial activity for the 8.305 MeV (0.25%) alpha line of the same isotope. A growth and decay plus one component fit was then performed on the 8.15-8.38 region of the spectrum consisting of ^{261}Rf, its daughter ^{257}No, and ^{211}Po^{m} to arrive at a half-life value for ^{261}Rf. In this fit, half-lives of Po and No and the initial activity of Po (calculated from the first fit) were fixed; all other parameters were allowed to vary.

A similar procedure was followed to process and calculate relative yields for the Ha experiments. The stepping time of the OLGA II tape machine was 20-s. Results from this experiment are presented in section 6.3.3.

4.5.3 Adsorption Enthalpy Calculations

On-line gas chromatography was used to determine the adsorption enthalpies of inorganic chlorides on solid SiO_2 and KCl surfaces. The theory for the calculation of these values from experimental data will be discussed in chapter 5. A Monte Carlo simulation program, also discussed in chapter 5, was used in these calculations. This program was able to simulate the chromatography process in our isothermal column. Yield versus temperature plots at given adsorption enthalpy values were generated for each halide molecule. A number of such plots at various adsorption enthalpy values were produced to compare to the experimental data. The adsorption enthalpy value was found by using a weighted least-squares procedure to find the generated plot which best represented the experimental data.

Chapter 5

Theory

Presently there are various types of gas-solid chromatography procedures to investigate the chemical properties of inorganic compounds. Some of these techniques include isothermal and temperature-programmed gas chromatography [RUD 79], thermochromatography [JON 79, ZVA 69], and on-line gas chromatography [RUD 76, GAG 85, 92, TUR 90]. The objectives of the different gas chromatography methods used are different. Some aim to develop separation methods for trace elements. Others aim to determine thermodynamic data, such as adsorption enthalpies [LAU 78, CON 79], to study chemical behavior of new artificial elements and their compounds [GAG 85, 92, TUR 90].

5.1 Calculation of Adsorption Enthalpy

Two methods could possibly be utilized to determine adsorption enthalpies. One method uses retention time of the species inside the chromatography column, derived from experimental data, to calculate adsorption enthalpies [RUD 80, GAG 85]. There are possible problems with this method. A notable problem is that this method assumes uniform isothermal temperature profiles inside the chromatography column. In practice

(Figs 2.4 and 2.11), this assumption may not be valid. This can lead to inaccurate results in the calculation of the adsorption enthalpies. Another problem is that different procedures may be used to arrive at retention times. These problems make comparison of results from different works a difficult task.

The other method (utilized in this work) uses Monte Carlo simulations to arrive at the adsorption enthalpies. This method simulates the chromatography process for single molecules taking into consideration the adsorption enthalpy and the migration process of the molecule through the chromatography column. The most significant aspect is that the measured temperature profiles (section 2.2.3) inside the chromatography column are also utilized in the simulation. Adsorption enthalpies are calculated as explained in section 4.5.3.

5.1.1 Calculations Based on Retention Time

5.1.1.1 First Method (Gäggeler et al.)

In order to determine the experimental adsorption enthalpies the following equations are considered [GAG 85]. Within the model of ideal linear gas chromatography [LEI 70] the velocity of migration of a component along a column is given by

$$\frac{dz}{dt} = \frac{u}{1+k_i} \qquad \text{Equation 5.1}$$

where z is the downstream coordinate, t is the time, u is the linear velocity of the gaseous phase, and k_i is the corrected partition coefficient. The linear velocity u can be expressed as

$$u = \frac{\bar{v}_o T}{\Phi T_o} \qquad \text{Equation 5.2}$$

where $\bar{v}_o$ is the mean gas flow rate (cm^3/s) under standard conditions (STP), T is the temperature of the column, T_0=298 K, and ϕ is the cross section of the column. Using the assumption that the gaseous adsorbate is an ideal gas and that the reference state of the adsorbent is the state of zero coverage, the corrected partition coefficient k_i is given by [EIC 82]

$$k_i = \frac{a}{\nu}\frac{V}{A}\exp\left(\frac{-\Delta H_a^o}{RT}\right)\exp\left(\frac{\Delta S_a^o}{R}\right) \qquad \text{Equation 5.3}$$

where a and ν are the surface and the volume per unit length (cm) of the column, A and V are the standard molar surface and the standard molar volume respectively, and ΔH_a^o and ΔS_a^o are the adsorption enthalpy and entropy. In the model based on mobile adsorption of a monoatomic gas, a standard state with V/A = 1 cm is usually chosen [EIC 82]. Inserting eqns. 5.2 and 5.3 into 5.1 and integrating eqn. 5.1 along the z coordinate leads to the retention time,

$$t_r = (z_1 - z_2)\left\{\frac{T_o\phi\left(1+\frac{a}{\nu}\frac{V}{A}\exp\left(\frac{-\Delta H_a^o}{RT}\right)\exp\left(\frac{\Delta S_a^o}{R}\right)\right)}{\bar{v}_o T}\right\}$$

where (z_1-z_2) is the column length, and finally to

$$\Delta H_a^0 = -RT\ln\left\{\left(\frac{t_r\bar{v}_0 T}{(z_1-z_2)T_0\phi}-1\right)\frac{\nu}{a}\frac{A}{V}\exp\left(\frac{-\Delta S_a^0}{R}\right)\right\} \qquad \text{Equation 5.4}$$

In principle, both thermodynamic quantities ΔH_a^o and ΔS_a^o can be derived from measurements of retention times t_r at different temperatures of the chromatography column. This is usually done [EIC 82] by plotting t_r (or ln v_r, where v_r is the net retention volume) against T^{-1} (Arrhenius plot). The slope and intercept of a linear fit through the experimental data are then proportional to ΔH_a^o and ΔS_a^o [GAG 85],

respectively. However, since the on-line technique only permits the measurement of retention times in the vicinity of the half-life of the nuclide investigated, adsorption entropies deduced in this way have large uncertainties in general . The adsorption entropy can be estimated from the model of mobile adsorption [EIC 82] given by

$$\Delta S_a^0 = R \ln \frac{A}{V \nu_B} \left(\frac{kT}{2\pi m} \right)^{1/2} + 1/2R \qquad \text{Equation 5.5}$$

where the standard state is V/A=1 cm, ν_B is the characteristic frequency of the adsorbent B, k is the Boltzmann constant and m is the atomic mass of the adsorbate. The characteristic frequency ν_B is given by

$$\nu_B = k\theta_{298} / h \qquad \text{Equation 5.6}$$

where h is Planck's constant, and θ_{298} is the characteristic temperature of the adsorbent B. The adsorption enthalpy can be determined by the measurement of only one value of retention time. At the temperature where the measured activity of the species is 50% of saturation, t_r is assumed to be equal to the half-life of the species. The adsorption enthalpy can then be calculated using the half-life of the species, the experimental $T_{50\%}$-values, the estimated ΔS_a° from eqn. 5.5, along with eqn. 5.4.

5.1.1.2 Second Method (Rudolph et al.)

The variables a and v in this section are not the same variables as in section 5.1.1.1. In order to keep the same nomenclature as the references cited, these variables have been given new definitions. The frame of reference has also been changed from $\frac{dz}{dt}$ to $\frac{dx}{dt}$.

If short-lived nuclides are used for the determination of retention times in a chromatographic system, three conditions have to be met [RUD 80]:

1. All losses of the short-lived nuclide within the chromatographic system must be due to radioactive decay.
2. The retention time distribution (shape of the chromatographic elution peak) has to be small compared with the half-life of the short-lived radionuclide.
3. The retention time should be of the same order of magnitude as the half-life of the radionuclide used in order to keep the error of the retention time, which is caused by the statistical counting errors, within reasonable limits.

The retention time t_r^o can be calculated from the following simple relation:

$$t_r^o = \frac{t_{1/2}}{\ln 2} \ln \frac{A_o}{A} \qquad \text{Equaiton 5.7}$$

where A_0 and A are the activities of the short-lived nuclide introduced into and eluted from the chromatographic system, respectively.

Determination of A_0 is simple if a constant source for the short-lived nuclide is used. In this case eqn. 5.7 can be slightly modified:

$$t_r^o = \frac{t_{1/2}}{\ln 2} \ln \frac{I_o}{I} \qquad \text{Equation 5.8}$$

where I_0 is the counting rate for $t_r^o = 0$ and I is the counting rate for t_r^o. I_0 can be determined in the following way:

1. The counting rates at the end of the chromatographic column are measured for a number of different temperatures.
2. As a first approximation, a value I_o^* for I_0 is calculated in the following way. At a sufficiently high temperature, T_0, the retention time of a compound in a gas chromatographic column is not very different from the column dead time, t_0. The dead time can be calculated from the column dead volume and the gas flow rate. I_0 can then be calculated from the counting rate I at temperature T_0 and the dead time. This method is justified as long as the net retention time t_r at T_0 is very small compared with the retention times of the other experiments.

3. With the approximated value I_o^* the retention times are calculated.
4. From the retention times, the net retention volumes V_r are calculated:

$$V_r = t_r \dot{v} = (t_r^o - t_o)\dot{v} \qquad \text{Equation 5.9}$$

where $\dot{v}$ is the gas flow rate

5. The logarithms of the net retention volumes (ln V_r) are plotted against the inverse temperature.
6. From the straight line which fits the points, the net retention volume V_r^m at the maximum experimental temperature T_m is determined.
7. From V_r^m the retention time t_r at T_m is calculated using:

$$t_r^o = \frac{V_r}{\dot{v}} + t_o \qquad \text{Equation 5.10}$$

8. With this approximation a new value for I_o^* is calculated and the iteration is repeated from step 3 until a constant value for V_r^m (the net retention volume at T_m) is obtained.

This is the best estimate for V_r^m which can be obtained from the measurement series. The adsorption enthalpy is then calculated in the following manner [RUD 80b].

As in eqn. 5.1, the velocity of migration of a component along a column is given by

$$\frac{dx}{dt} = v = \frac{u}{1+k} \qquad \text{Equation 5.11}$$

using the model of ideal linear gas chromatography [LEI 70]. Where u is the linear velocity of the carrier gas. The partition coefficient, k, can be expressed as

$$k = \frac{as}{c_g V_g} = K_a \frac{s}{V_g} \qquad \text{Equation 5.12}$$

where K_a is a/c_g (cm), a=surface concentration, s=surface area, V_g is the free column volume and c_g is concentration in the gas-phase. To convert the gas-phase concentration into the partial pressure (p), as a first approximation for an ideal gas it is assumed that

$$k = \frac{asRT}{pV_g} = K_p \frac{sRT}{V_g} \qquad \text{Equation 5.13}$$

where K_p is a/p (mol N^{-1}).

The adsorption enthalpy can be determined from the temperature dependence of the partial pressure p in the gas phase at constant surface pressure π using

$$\Delta H_{ads} = -RT^2 \left(\frac{\partial \ln p}{\partial T} \right)_{\pi} \qquad \text{Equaiton 5.14}$$

In theory, the adsorption enthalpy can be determined from retention data by combining eqn. 5.11 (in the integrated form) for constant experimental conditions [$t_r^o = t_0(1+k)$] with eqns. 5.13 and 5.14:

$$-\left\{ \frac{\partial \ln \left[\frac{asRT}{V_g (t_r/t_0)} \right]}{\partial T} \right\}_{\pi} RT^2 = \Delta H_{ads} \qquad \text{Equation 5.15}$$

where t_r^o is total retention time, t_0 is dead time and $t_r = t_r^o - t_0$ is the net retention time.

The correlation between $(\partial \ln p/\partial T)\pi$ and $(\partial \ln p/\partial T)_a$ and the following expression, derived by Hill et al. [HIL 49]:

$$\Delta H_{ads} = -RT^2 \left(\frac{\partial \ln p}{\partial T} \right)_a + Ta \left(\frac{\partial \pi}{\partial T} \right)_{\theta} \qquad \text{Equation 5.16}$$

Where θ is relative surface coverage, may be used. The term $RT^2(\partial \ln p/\partial T)_a = q_{is}$ is often called the isosteric heat of adsorption.

For the case of immobile adsorbed molecules at low surface concentration the following equation holds:

$$\Delta H_{ads} = -R\left[\frac{d\ln\left(\frac{t_r}{t_o T}\right)}{d\left(\frac{1}{T}\right)}\right] = -R\left[\frac{d\ln\left(\frac{V_r}{TV_g}\right)}{d\left(\frac{1}{T}\right)}\right] \qquad \text{Equation 5.17}$$

where V_r is net retention volume. Since the net retention time, t_r, and the net retention volume, V_r, are independent of the surface concentration, the adsorption enthalpies do not depend on the surface concentration and it is no longer necessary to use partial differentials.

According to eqn. 5.17, the adsorption enthalpies can be determined from a graph of the logarithms of the net retention volumes at the column temperature versus the inverse of the absolute temperature. The adsorption enthalpies calculated are based on the assumption of immobile adsorbed molecules. The standard adsorption enthalpies are determined from the intercept of the curve with the $\ln V_r$ axis according to the following equation:

$$\Delta S^o_{ads} = \frac{\Delta H^o_{ads}}{T} - R\ln\left(\frac{a_s sRT}{V_r P_o}\right) \qquad \text{Equation 5.18}$$

where a_s is standard surface concentration (1.37×10^{-11} mole/cm^2 [DEB 53]) and P_o is standard gas phase pressure (1 atm).

5.1.2 Monte Carlo Method

The variables a and v in this section are not the same variables from section 5.1.1.1 or 5.1.1.2. In order to keep the same nomenclature as the references cited, these variables have been assigned new definitions.

A Monte Carlo simulation code (appendix A) was written [TUR 91] using the microscopic model of gas-solid thermochromatography in open columns with the laminar flow of the carrier gas, proposed by Zvara [ZVA 85]. This model describes the downstream migration of a sample molecule as a small number of some effective random displacements, and sequences of adsorption-desorption events. The simulation of the exact physical picture of these random migrations would necessitate too much computer time. Therefore, a simplified model is proposed that allows the downstream motion of a molecule in an open column to be reduced to much smaller numbers of effective displacements and adsorption residence events.

The real temperature profiles (Fig. 2.11) of the chromatography column are used in this simulation. A random life time is generated for each molecule in the simulation, using a random number generator and the half-life of the simulated molecule. The migration history of the molecule is traced down the column through a series of adsorption-desorption and jump steps. A time duration is generated for each step. If the retention time of the molecule (total time of migration) through the column is shorter than the generated life time, the molecule leaves the column and is detected. If the retention time is longer than the life time, the molecule decays inside the column and is not detected.

The retention time is related to the number of adsorption-desorption steps between the molecule and the column surface and also the period of time the molecule spends in the adsorbed state. The retention time is then dependent on the adsorption enthalpy, the column temperature, the true volume flow rate of the carrier gas and the column length.

For each temperature a large number (≈20,000) of sample molecules are modeled. The total number of detected and undetected molecules is recorded for each isothermal temperature. Relative yield versus temperature plots at given adsorption enthalpies are generated for comparison with experimental data.

5.1.2.1 Adsorption residence time

In the following discussion the term profile, $\rho(x)$, is used in the sense of the probability density distribution of coordinates along the column, at which the molecules are found. The isothermal gas phase chromatography is based on the reversible adsorption of the species to be separated on the chromatography surface [ZVA 85]. The period of time a molecule spends in the adsorbed state, τ_a, is a random quantity with the mean value, $\bar{\tau}_a$, given by [DEB 53],

$$\bar{\tau}_a = \tau_o \exp(-\Delta H_a / RT) \qquad \text{Equation 5.19}$$

Where τ_o is the period of oscillation of the molecule in an adsorbed state perpendicular to the surface, ΔH_a the enthalpy of adsorption, R the gas constant, and T the absolute temperature. An exponential probability distribution holds for τ_a:

$$\rho(\tau_a) = \left(\frac{1}{\bar{\tau}_a}\right)\exp\left(\frac{-\tau_a}{\bar{\tau}_a}\right) \qquad \text{Equation 5.20}$$

The quantities τ_o and ΔH_a are characteristics of the adsorbate.

5.1.2.2 Frequency of encounters with the column surface

The mean migration velocity of molecules down the column, at a given coordinate, is determined by $\bar{\tau}_a$, by the frequency of encounters with the surface, and by the flow velocity (profile) of the carrier gas. Let $\bar{\nu}$ be the mean number of collisions experienced between the column wall and a molecule with the mean speed c, when a gas with the true volume flow rate Q passes through a volume enclosed by the surface S. From the theory of molecular kinetics we find [ZVA 85],

$$\nu = cS / 4Q \qquad \text{Equation 5.21}$$

and, for the mean number of collisions per a unit length segment of a cylindrical tube, ν_1, we obtain,

$$\nu_1 = \left(\frac{r}{Q}\right)\sqrt{2\pi RT/M} \qquad \text{Equation 5.22}$$

where r is the radius of the column and M is the molar mass. It should be noted that $\nu_1(p,T) \alpha p/\sqrt{T}$ since $Q \alpha T/p$, where p is the pressure.

5.1.2.3 Displacements between two encounters

The migration distance, l, of a molecule along the column between two successive encounters with the column wall may vary over a wide range. Let us consider molecular diffusion as random jumps with lengths of approximately one mean free path. Then, for a molecule that has just been desorbed, there is a very high probability (≈100%) that the displacement from the column surface is very small. At this thin layer near the column wall the flow of the carrier gas with a laminar flow profile is vanishingly small. So, the occurrence of very short displacements of the order of a few mean free paths is very large. These displacements are both negative and positive in the coordinate along the length of the column. Very rarely does the molecule diffuse far enough from the wall to be carried by the gas flow over a large distance. We can expect the probability distribution, $\rho(l)$, as a function of jump length, l, to be of the shape shown schematically in Fig. 5.1a, with a small probability for long jumps. Some information on $\rho(l)$ may be extracted from the solution to the problem of diffusional deposition from a stream to absorbing walls of a channel [GOR 49]. For the laminar flow in a cylindrical tube, the following probability density distribution was derived for down-stream movement distance of molecules, l', before encountering the wall:

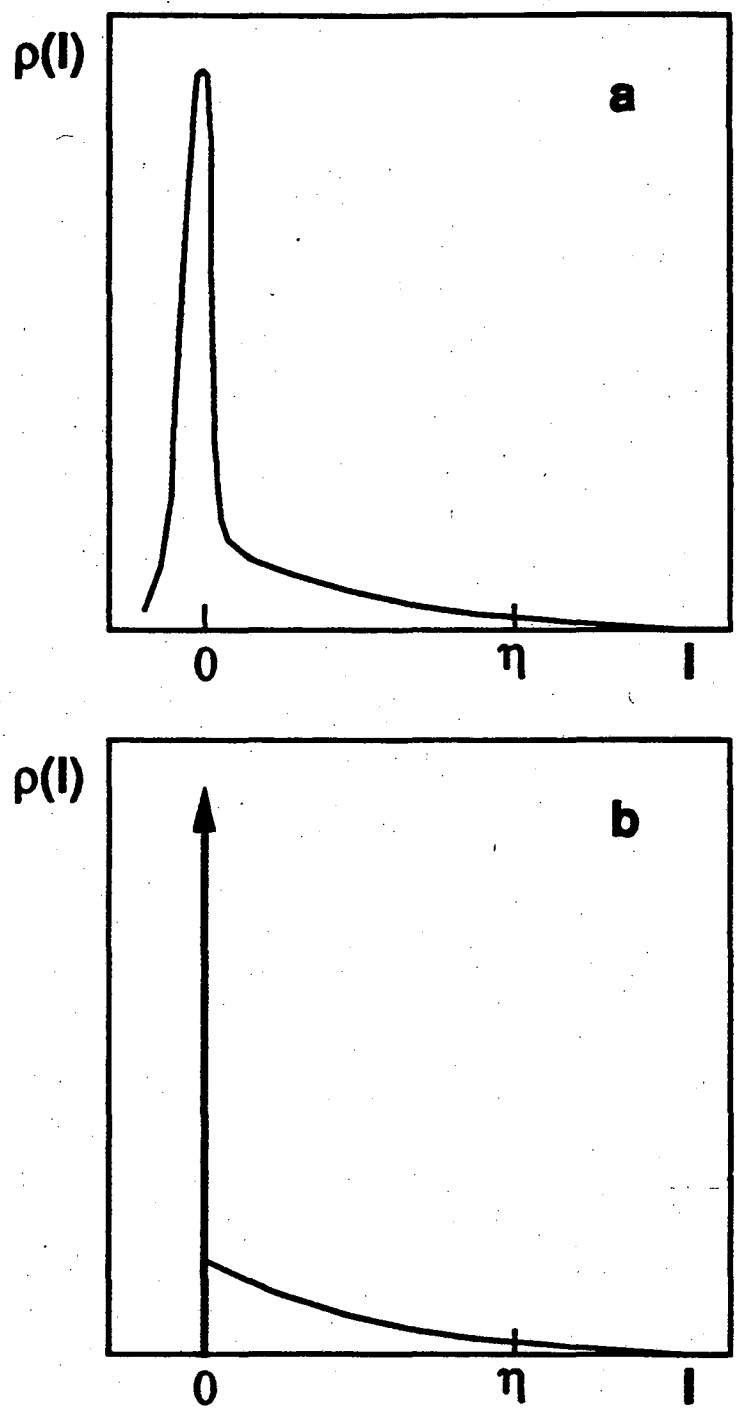

Fig. prepared from [ZVA 85]
Fig. 5.1 Graph of the probability density distributions for displacements l:
a - character of the real distribution;
b - the accepted approximation [GOR 49]

$$\rho(l') = \mu \sum_{m=1}^{\infty} \alpha_m \beta_m \exp(-\beta_m \mu l')$$

$$= \sum_{m=1}^{\infty} \left(\frac{\alpha_m}{\bar{\eta}_m}\right) \exp\left(\frac{-l'}{\bar{\eta}_m}\right) \qquad \text{Equation 5.23}$$

where

$$\mu = \frac{\pi D}{Q}; \qquad \bar{\eta}_m = \frac{1}{\beta_m \mu} = \frac{Q}{\beta_m \pi D}; \quad \sum_{m=1}^{\infty} \alpha_m = 1 \qquad \text{Equation 5.24}$$

Here D is the diffusion coefficient. The set of the eigen values β_m is invariant [GOR 49]:

$$\beta_1 = 3.65; \qquad \beta_2 = 22.3 \qquad \beta_3 = 56.9; \ldots., \qquad \text{Equation 5.25}$$

while the numerical coefficients α_m depend on the concentration distribution over the tube cross section, n(l',r), at the mouth of the tube (l'=0). In particular [GOR 49], for the uniform distribution, n(0,r)=constant:

$$\alpha_1 = 0.82; \qquad \alpha_2 = 0.098; \qquad \alpha_3 = 0.033; \ldots., \qquad \text{Equation 5.26}$$

The β_m values rapidly increase in the series; hence, at sufficiently large l', the shape of ρ (l') will be determined mostly by the first term in eqn. 5.23 for which

$$\bar{\eta}_1 = \frac{Q}{3.65 \pi D}. \qquad \text{Equation 5.27}$$

This might be expected since η(l',r) should no longer depend on η(0,r) if l' is much larger than the product of the linear flow velocity, $u = Q/\pi r^2$, and the characteristic time for diffusion across the tube section, $2r^2/D$.

The complete microscopic description (the knowledge of the exact ρ(l)) is not helpful in the Monte Carlo simulation, because ν_1 is a large number. A reasonable approximation of ρ(l) is proposed which is convenient for computer calculations. The following form appears to be appropriate (Fig. 5.1b):

$$\rho(l) = (1-a)\delta(l) + \left(\frac{a}{\bar{\eta}}\right)\exp\left(\frac{-l}{\bar{\eta}}\right), \qquad a = \frac{1}{\nu_1 \bar{\eta}}. \qquad \text{Equation 5.28}$$

Here $\delta(l)$ is Dirac's delta function, $\bar{\eta}$ is the adjustable parameter which can be chosen as discussed below, and a is the fraction undergoing jumps in the exponential distribution.

The corresponding variance of l is

$$\sigma_l^2 = a\bar{\eta}^2(2-a) = \left(\frac{\bar{\eta}}{\nu_1}\right)\left[2 - \left(\frac{1}{\nu_1 \bar{\eta}}\right)\right] \qquad \text{Equation 5.29}$$

This proposed approximation implies the following physical picture: Once the molecule encounters the surface, it experiences a series of adsorption-desorption events without a change in the x coordinate. These sequences are intermittent with rather long down-stream jumps,of length η, which have the exponential probability distribution

$$\rho(\eta) = \left(\frac{1}{\bar{\eta}}\right)\exp\left(\frac{-\eta}{\bar{\eta}}\right). \qquad \text{Equation 5.30}$$

5.1.2.4 Adsorption residence resulting from a series of encounters

The number of adsorptions in a sequence of adsorption-desorption steps with no change in coordinate, N, has the average value [ZVA 85]

$$\bar{N} = \frac{1}{a} = \nu_1 \bar{\eta}, \qquad \text{Equation 5.31}$$

and the probability distribution

$$\rho(N) = a(1-a)^{N-1} = \frac{(\nu_1 \bar{\eta} - 1)^{N-1}}{(\nu_1 \bar{\eta})^N}. \qquad \text{Equation 5.32}$$

The residence time, $\tau_{a,N}$, resulting from the series of N adsorptions has the probability distribution

$$\rho(\tau_{a,N}) = \left\{ \frac{\tau_{a,N}^{N-1}}{\left[\bar{\tau}_a^N (N-1)!\right]} \right\} \exp\left(\frac{-\tau_{a,N}}{\bar{\tau}_a} \right), \qquad \text{Equation 5.33}$$

and for $\tau_{a,s}$, the residence time with random N, we obtain

$$\rho(\tau_{a,s}) = \sum_{N=1}^{\infty} \rho(N)\rho(\tau_{a,N})$$

$$= \left(\frac{1}{\nu_1 \bar{\tau}_a \bar{\eta}} \right) \exp\left(\frac{-\bar{\tau}_{a,s}}{\nu_1 \bar{\eta} \bar{\tau}_a} \right). \qquad \text{Equation 5.34}$$

5.1.2.5 Mean jump length

Using eqn. 5.29, the variance of the simulated zone profile for the case of isothermal chromatography can be obtained

$$\sigma_x^2 = \nu_1 \bar{x} \sigma_1^2 = \bar{x}\bar{\eta}\left[2 - \left(\frac{1}{\nu_1 \bar{\eta}} \right) \right], \qquad \text{Equation 5.35}$$

where $\bar{x}$ is the center of gravity coordinate of the zone.

Since the value of a is much less than 1

$$\frac{\sigma_x^2}{\bar{x}} = 2\bar{\eta}. \qquad \text{Equation 5.36}$$

For open columns, the exact analytical solution in known [GID 65, GRU 72]:

$$\frac{\sigma_x^2}{\bar{x}} = 2\pi r^2 \frac{D}{Q} + \left(11 - 16\Re + 6\Re^2\right)\left(\frac{Q}{24\pi D} \right), \qquad \text{Equation 5.37}$$

where $\Re$ is the ratio of the velocity of the carrier gas to the mean migration velocity of the zone, or the ratio of the residence time in the gas phase to the overall residence time in the given segment of the column, i. e.,

$$\Re = \frac{\left(\frac{1}{u}\right)}{\left(\frac{1}{u + v_1 \bar{\tau}_a}\right)}. \qquad \text{Equation 5.38}$$

By definition, $0<\Re<1$. Equating the right hand sides of eqns. 5.36 and 5.37, gives

$$\bar{\eta} = \frac{\pi r^2 D}{Q} + \left(11 - 16\Re + 6\Re^2\right)\left(\frac{Q}{24\pi D}\right). \qquad \text{Equation 5.39}$$

Equation 5.39 solves the problem of choosing the value for $\bar{\eta}$ to be used in the Monte Carlo simulations. At large linear velocities of the carrier gas, the first term on the right hand sides of eqns. 5.37 and 5.39 can be neglected, since this term takes into account the longitudinal molecular diffusion. Therefore,

$$\bar{\eta} = \left(11 - 16\Re + 6\Re^2\right)\left(\frac{Q}{24\pi D}\right). \qquad \text{Equation 5.40}$$

In practice, the value for $\Re$ is often very close to zero, and the above equation reduces to

$$\bar{\eta} = \frac{11Q}{48\pi D}. \qquad \text{Equation 5.41}$$

Since $Q \approx T/p$ and $D \approx pT^{3/2}$ it follows that $\bar{\eta}$ is independent of p and r, and $\bar{\eta} \approx 1/\sqrt{T}$.

5.1.2.6 Calculations

A flow chart of the Monte Carlo code is shown in Fig. 5.2. At the start of the simulation several variables and constants, such as the value of pi, mass of helium, density of helium, and the gas constant R, are declared. The actual measured temperature profiles of the chromatography column are then read. Next the user is asked to provide the following information on the molecule under study: half-life, number of molecules to be used at each temperature, the actual flow rate of He through the column,

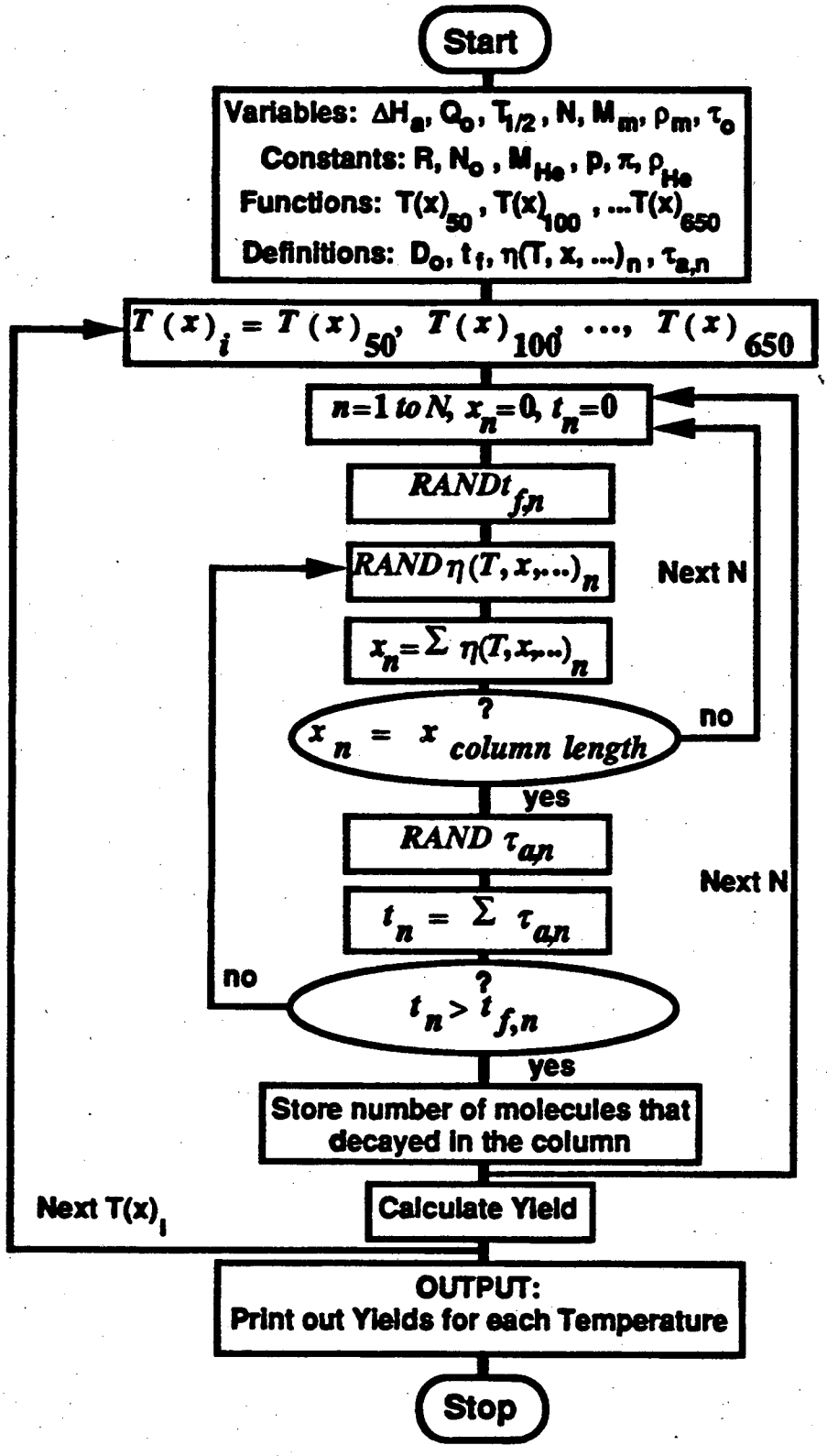

Fig. 5.2 Computer program flow chart

the molecular weight of the species, the density of the species, the period of oscillations of the molecule (on the order of 1×10^{-12}), the starting adsorption enthalpy, the ending adsorption enthalpy, and finally the step width between the two enthalpy values.

Molecules are then put through the simulation one by one. A random decay time is calculated for a molecule. A random jump is generated, the coordinate of the molecule after the jump is evaluated, and a flight time is calculated. The flight time is compared with the generated decay time of the molecule and the molecule coordinate is monitored to evaluate whether the molecule has left the column. If the molecule has decayed or left the column, the next molecule is sent through. If the molecule has not decayed, and is still in the column, a mean number of collisions with the column wall is calculated and a random adsorption time is generated. The total simulation time is updated and again compared with the generated decay time of the molecule. If the molecule has not decayed or left the column, it will go back to the random jump step until it has decayed or made it through the column. The number of molecules which decayed or made it through the column are recorded for each temperature and the yields for each temperature at various adsorption enthalpy values are printed. From these yields plots of relative yield versus temperature may be constructed to compare with the experimental data.

Figure 5.3 shows a relative yield versus temperature plot for a 30 second activity at various adsorption enthalpies. As expected, smaller adsorption enthalpies correspond to less volatile species. Figure 5.4 shows a relative yield versus temperature plot for 5-second and 35-second activities with the same adsorption enthalpy. This illustrates the case of two isotopes of an element with different half-lives. The program does not take into account the recluster time and transport time of the molecules to the detection system (≈20 to 25-s). The experimental data would show a decreased maximum yield for the shorter-lived species. To compare the simulations with the experimental data, the experimental data were normalized to 100% at maximum yield.

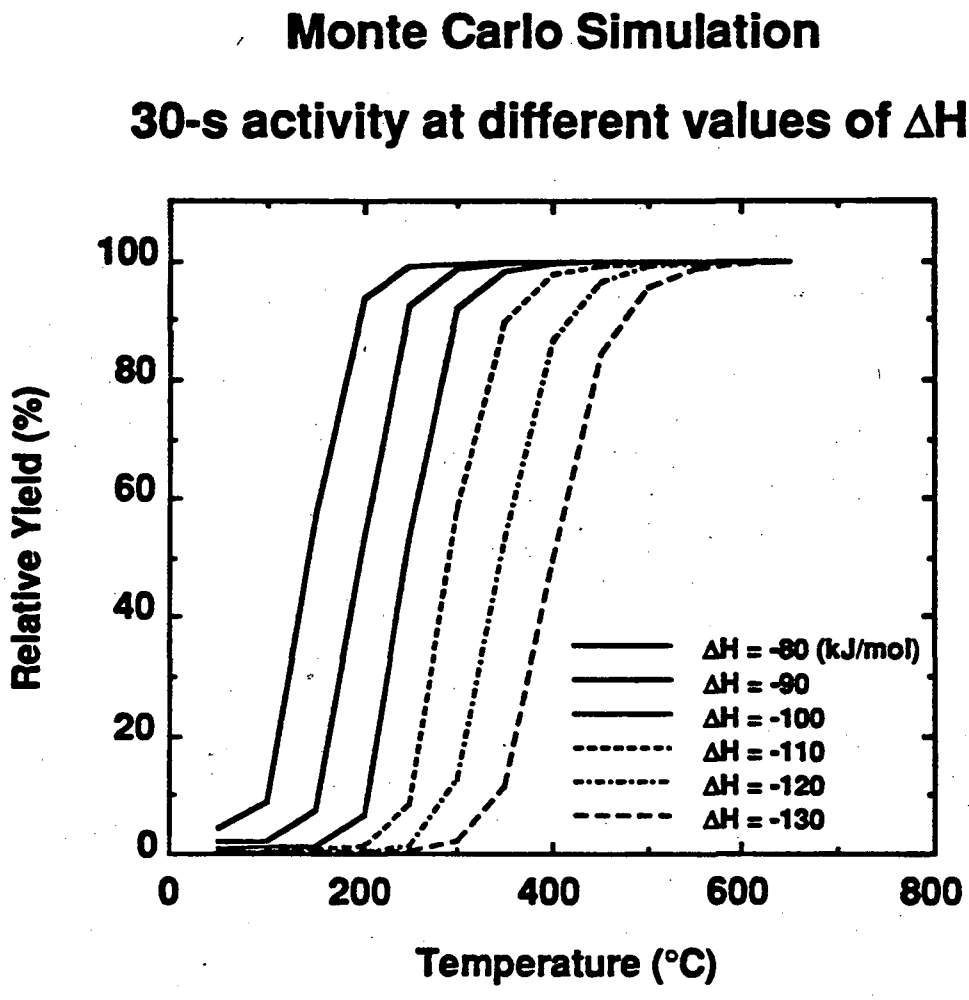

Fig. 5.3 Relative yield versus temperature plot for a 30-second activity at various adsorption enthalpies.

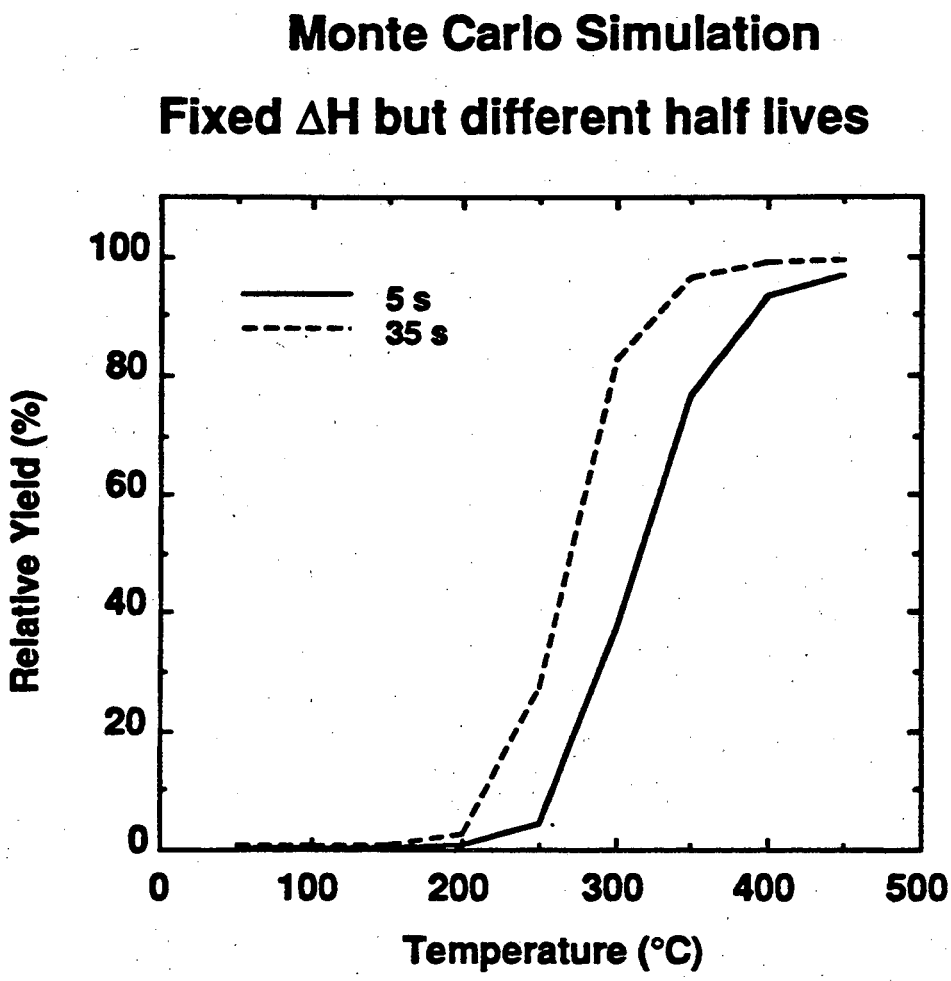

Fig. 5.4 Relative yield versus temperature plot for a 5-second and a 35-second activity with a fixed adsorption enthalpy.

Chapter 6

Results and Discussion

The volatilities of Bi- and Po-chlorides and the chlorides of Rf and its group 4 homologs, Zr and Hf, as well as Ha and its group 5 homologs Nb and Ta, have been measured. Adsorption enthalpies are calculated for the above mentioned species with various chromatography surfaces. Preliminary results are presented for Zr- and Nb-bromides. The volatility results are illustrated using relative yield versus temperature plots. Several halogenating agents were used as discussed in section 4.2. Figure 6.1 shows a yield curve for $^{99}NbCl_5$. HCl/CCl_4 was used as the halogenating agent and MoO_3 as transport aerosol. When the halogenating agents containing hydrogen (HCl, and HBr) were used, significant yields were unexpectedly observed at very low temperatures (50°C to ≈150°C). During the Zr and Nb experiments an isotope of strontium (^{94}Sr) was also produced. Strontium does not form volatile halides. However, significant yields are observed at 50°C and 100°C (Fig. 6.1) for ^{94}Sr. The yield then decreases with increasing temperature to acceptable levels. Therefore, transport by mechanisms other than isothermal chromatography is indicated at very low temperatures when using HBr or HCl as halogenating agents. This complicates the interpretation of the yield curves. When Cl_2/CCl_4 was used as the halogenating agent, the Sr yields at low temperatures were decreased to acceptable levels (Fig.6.2), resulting in yield curves which agree well with our Monte Carlo simulations of the isothermal chromatography process.

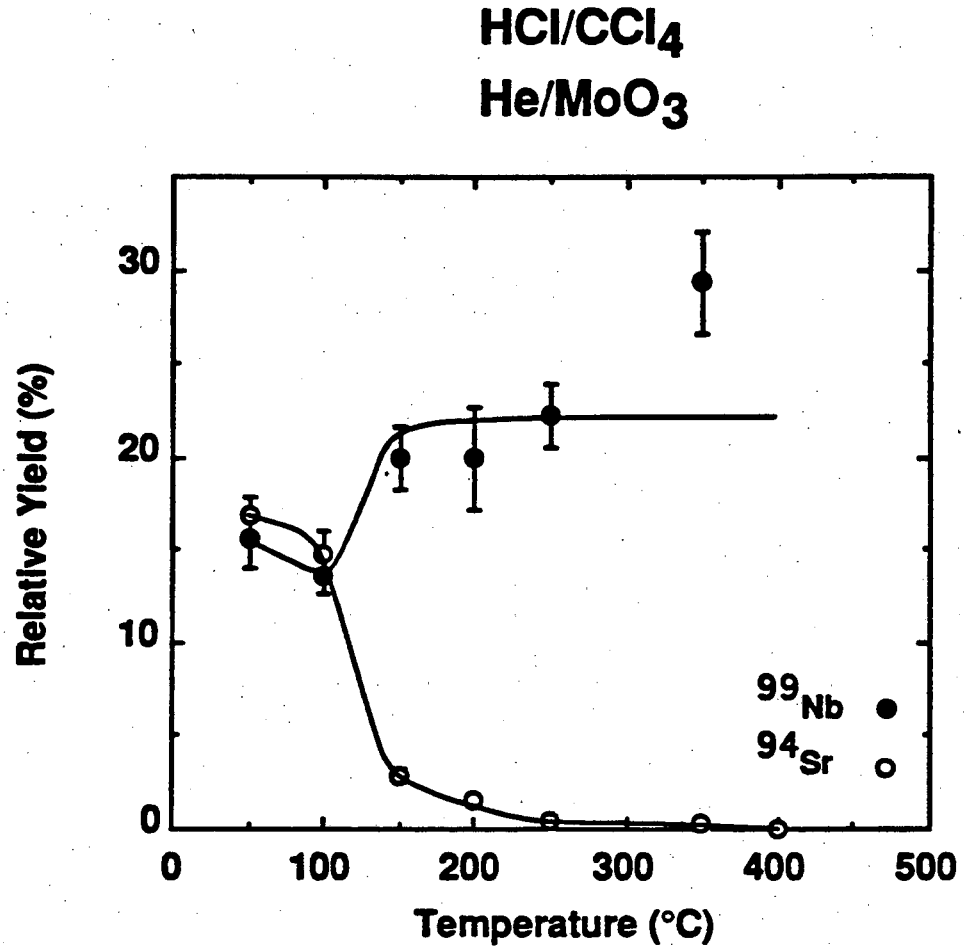

Fig. 6.1 Relative yield curves for ^{99}Nb- and ^{94}Sr-chloride molecules with a He/MoO_3 gas jet and HCl/CCl_4 as chlorinating agent.

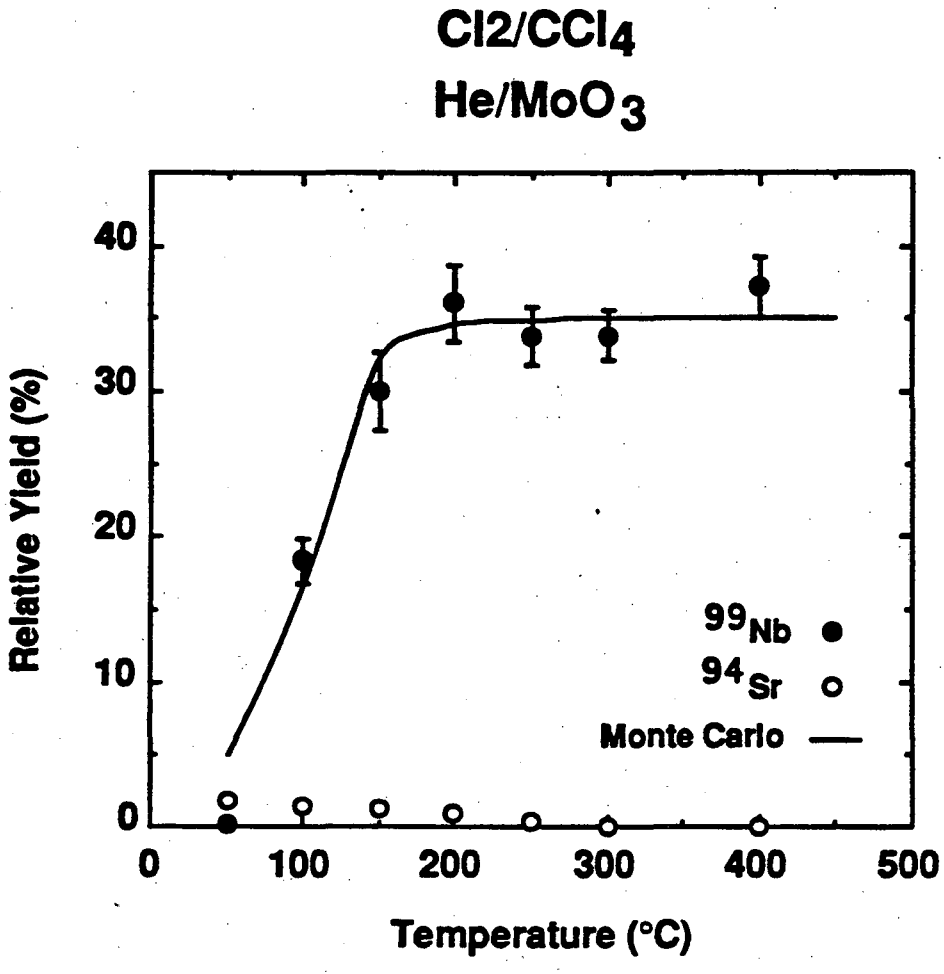

Fig. 6.2 Relative yield curves for ^{99}Nb- and ^{94}Sr-chloride molecules with a He/MoO_3 gas jet and Cl_2/CCl_4 as chlorinating agent. The solid line drawn through the data points is from the Monte Carlo computer program.

This high yield effect at low temperatures is not completely understood, but our results show a correlation between this effect and the presence of hydrogen in the system. The presence of hydrogen and even the smallest amount of oxygen may lead to the formation of water aerosols which transport the activity at very low temperatures. This, however, is a speculation and more research is required for a clear understanding of this problem.

Throughout this chapter, volatility results have been illustrated using relative yield versus temperature plots. The error bars shown in all yield curves represent one sigma uncertainties based on statistical fluctuations in the peak areas. Where no error bars are displayed, the error is smaller than the symbols. For many of the yield curves, the Monte Carlo lines through the data points are normalized to the maximum yield values.

Adsorption enthalpy results have been compared to Rudolph's values; however, the halogenating conditions used are not similar. Rulolph used a CCl_4 chlorinating agent at various vapor pressures.

6.1 Bi- and Po-Chlorides

Figure 6.3 shows a relative yield curve for 2.14-min $^{211}BiCl_3$ and 25.2-s $^{211}Po^{m}Cl_4$ with a He/MoO_3 gas-jet and HCl as chlorinating agent. The experimental data (Table 6.4) were normalized to 100% at maximum yield as explained in section 4.5.2. As illustrated, the high yield effect at low temperatures is observed at 50°C for Po. $BiCl_3$ is volatile at 100°C and $PoCl_4$ is volatile at 150°C, with respective adsorption enthalpies of -69±4 kJ/mol and -74±5 kJ/mol (Table 6.1).

The adsorption enthalpy for the Po species agrees well with Rudolph's value of

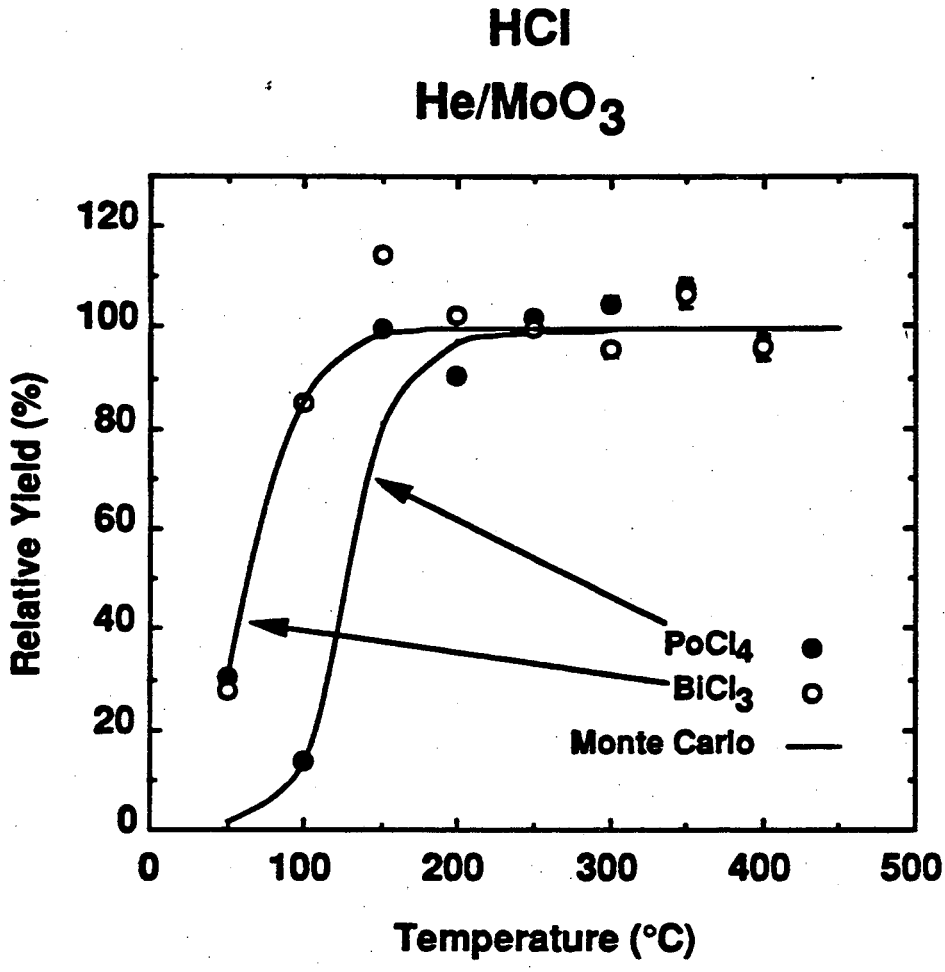

Fig. 6.3 Relative yield curves for ^{211}Bi- and ^{211}Po^{m}-chloride molecules with a He/MoO_3 gas jet and HCl as chlorinating agent. The solid lines drawn through the data points are from the Monte Carlo computer program.

-69±20 [RUD 79]; however, the Bi value does not. This disagreement may be a result of the large estimated errors in Rudolph's measurements.

Table 6.1 Adsorption enthalpies for Bi- and Po-chlorides. These compounds are probably the species which are formed.

Compound	Surface	Halogenating Agent	Transport Aerosol	ΔH^{o}_{ads} (kJ/mol)	$*\Delta H^{o}_{ads}$ (kJ/mol)
$BiCl_3$	SiO_2	HCl	MoO_3	-69 ± 4	-101 ± 20
$PoCl_4$	SiO_2	HCl	MoO_3	-74 ± 5	-69 ± 20

*Data from [RUD 79]

6.2 Group 4 Elements

The differences in maximum yield between different isotopes of the same element are due to their half-lives. The time-consuming process (on the order of 15 to 25 seconds) of reclustering separated halides on KCl aerosols and their subsequent transport to the detection system is the source of yield differences.

6.2.1 Zr-Chlorides and -Bromides

Figures 6.4 through 6.7 show relative-yield curves for 30.7-s ^{98}Zr and 7.1-s ^{100}Zr-halides with either a He/MoO_3 or He/KCl gas jet and various halogenating agents on a SiO_2 surface. As depicted in Figs 6.4 and 6.5, $ZrCl_4$ becomes volatile at temperatures between 100°C and 150°C. Table 6.2 lists the calculated adsorption enthalpies. In experiments performed with HCl, HCl/CCl_4, and HBr as chlorinating agents (Figs 6.5,

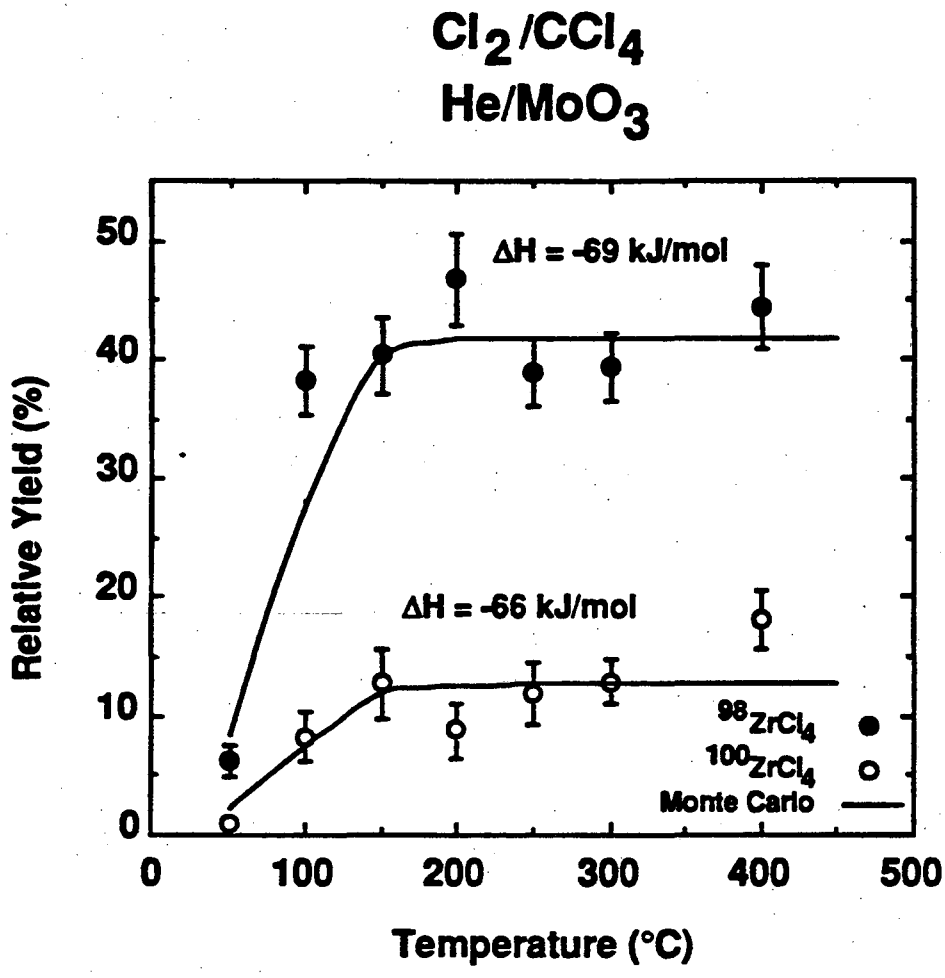

Fig. 6.4 Relative yield curves for ^{98}Zr- and ^{100}Zr-chloride molecules with a He/MoO_3 gas jet and Cl_2/CCl_4 as chlorinating agent. The solid lines drawn through the data points are from the Monte Carlo computer program.

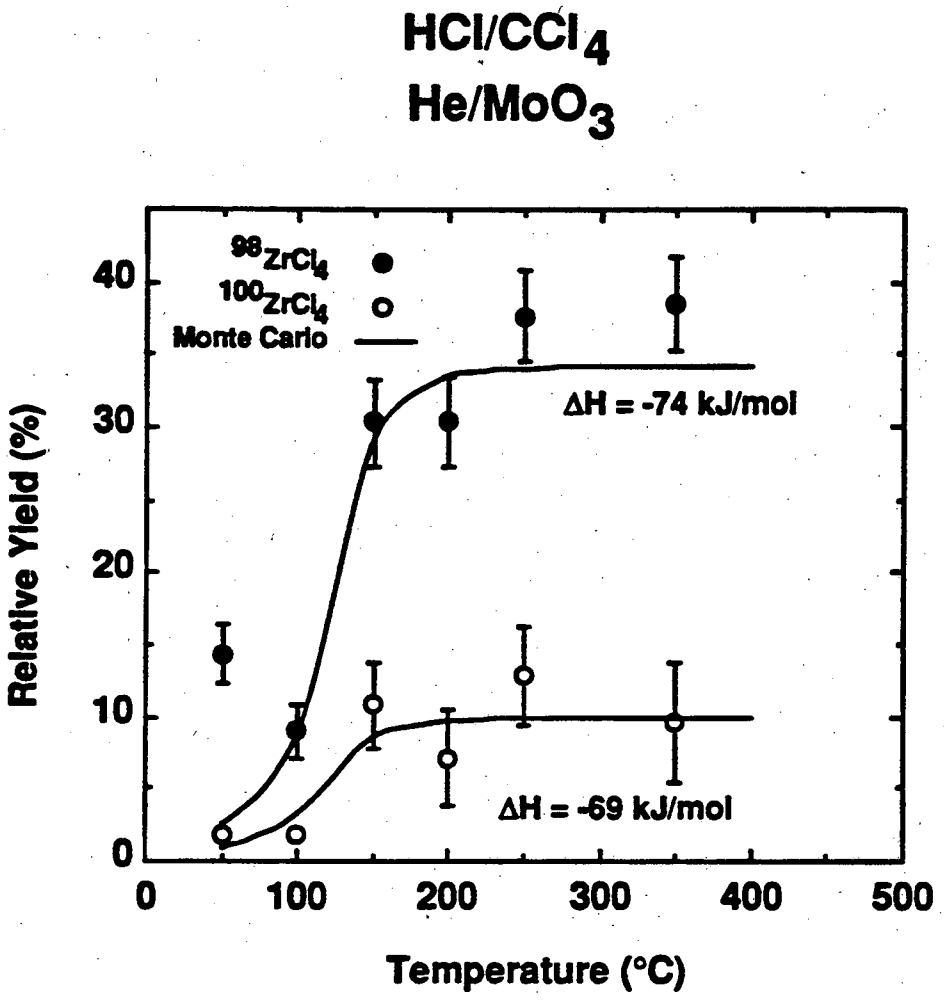

Fig. 6.5 Relative yield curves for ^{98}Zr- and ^{100}Zr-chloride molecules with a He/MoO_3 gas jet and HCl/CCl_4 as chlorinating agent. The solid lines drawn through the data points are from the Monte Carlo computer program.

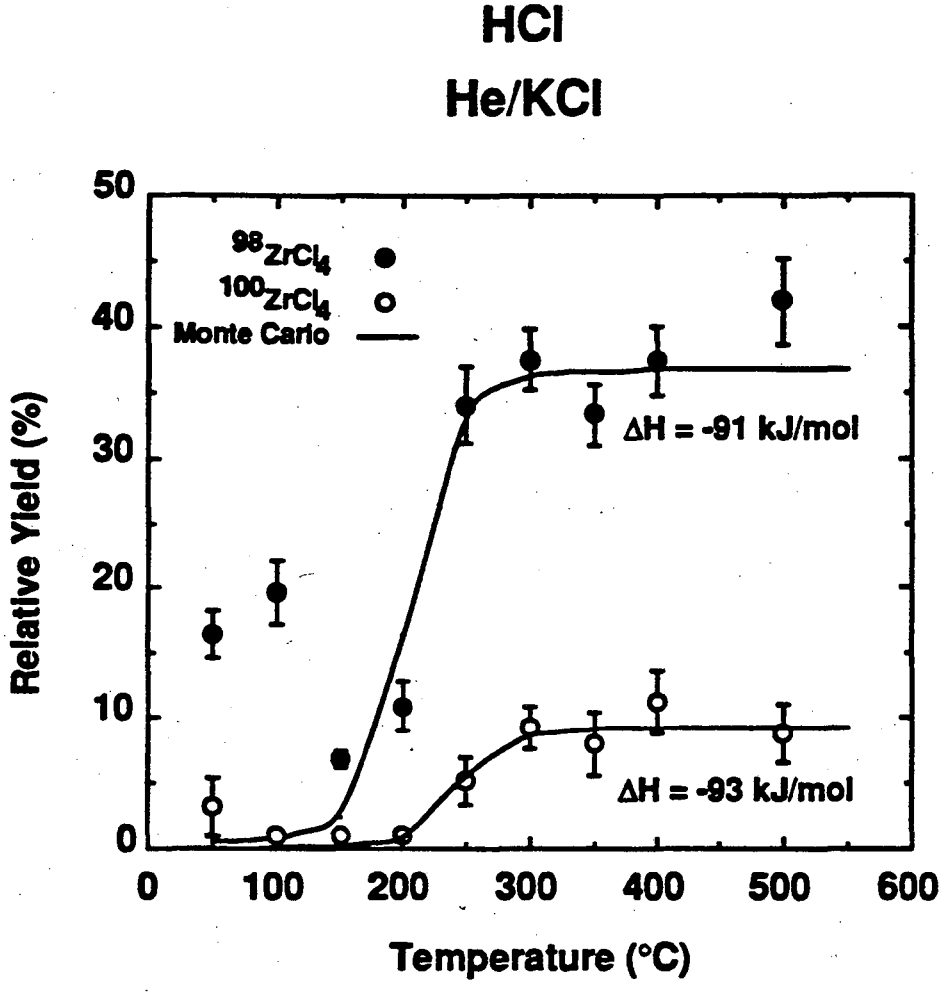

Fig. 6.6 Relative yield curves for ^{98}Zr- and ^{100}Zr-chloride molecules with a He/KCl gas jet and HCl as chlorinating agent. The solid lines drawn through the data points are from the Monte Carlo computer program.

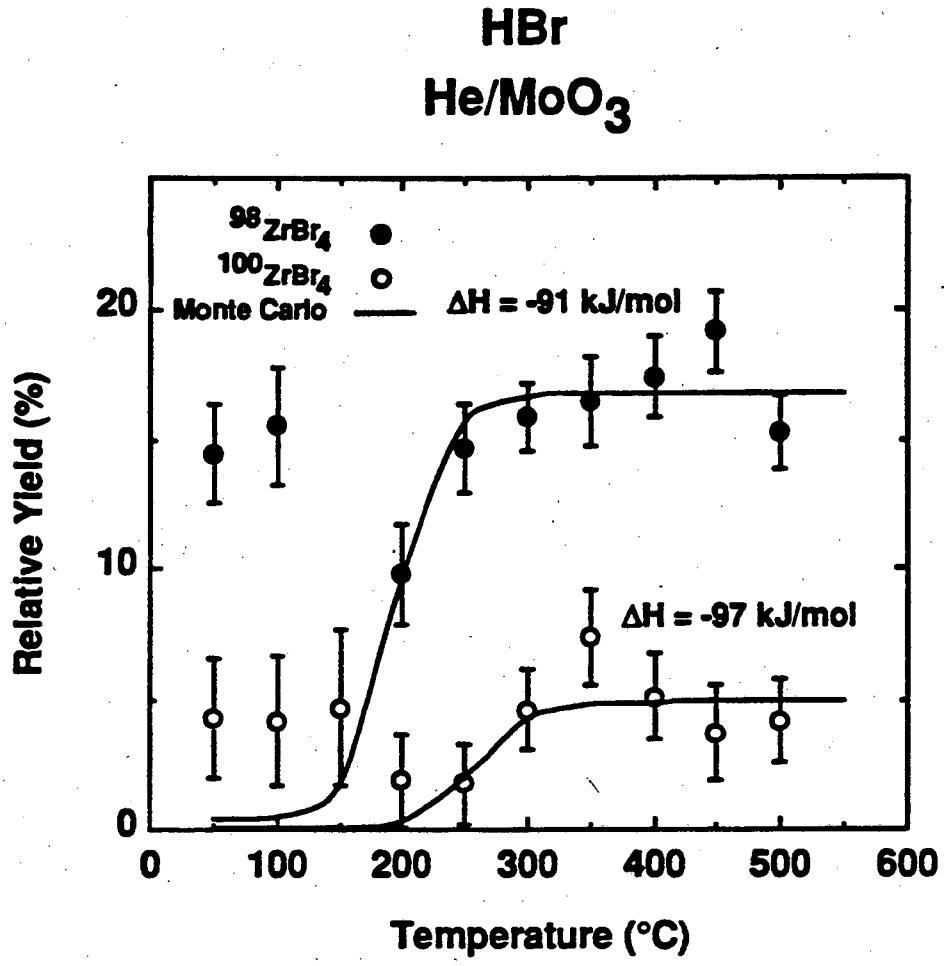

Fig. 6.7 Relative yield curves for ^{98}Zr- and ^{100}Zr-bromide molecules with a He/MoO_3 gas jet and HBr as chlorinating agent. The solid lines drawn through the data points are from the Monte Carlo computer program.

6.6, and 6.7), the high yield effect at low temperatures is present. Small deposits of MoO_2Cl_2 were observed inside the column for some experiments (Table 6.2); yet, the adsorption enthalpies agree well with values calculated for quartz (SiO_2) surface. When using KCl as transport aerosol material, one third of the column was coated with KCl. A decreased volatility on the order of 100°C (Fig. 6.6) was observed for $ZrCl_4$ since the separation was conducted on a partially KCl coated column and is consistent with results of Rudolph [RUD 79] for a NaCl surface. As expected, a more negative adsorption enthalpy value was observed. Our results show a lower volatility for $ZrBr_4$ in comparison to $ZrCl_4$. The results shown for $ZrBr_4$ are preliminary.

Table 6.2 Adsorption enthalpies for Zr-chlorides and bromides. These compounds are probably the species which are formed.

Compound	Half-life (sec)	Surface	Halogenating Agent	Transport Aerosol	ΔH^o_{ads} (kJ/mol)	$*\Delta H^o_{ads}$ (kJ/mol)
$^{98}ZrCl_4$	30.7	SiO_2	Cl_2/CCl_4	MoO_3	-69 ± 6	-97 ± 20
$^{100}ZrCl_4$	7.1	SiO_2	Cl_2/CCl_4	MoO_3	-66 ± 9	
$^{98}ZrCl_4$	30.7	SiO_2 (MoO_2Cl_2)	HCl/CCl_4	MoO_3	-74 ± 5	
$^{100}ZrCl_4$	7.1	SiO_2 (MoO_2Cl_2)	HCl/CCl_4	MoO_3	-71 ± 6	
$^{98}ZrCl_4$	30.7	SiO_2(KCl)	HCl	KCl	-91 ± 7	•-99±20
$^{100}ZrCl_4$	7.1	SiO_2(KCl)	HCl	KCl	-93 ± 8	
$^{98}ZrBr_4$	30.7	SiO_2 (MoO_2Br_2)	HBr	MoO_3	-91 ± 6	
$^{100}ZrBr_4$	7.1	SiO_2 (MoO_2Br_2)	HBr	MoO_3	-97 ± 8	

*Data from [RUD 79]

•Adsorption enthalpy on NaCl surface.

The best value of adsorption enthalpy on a SiO_2 surface for $ZrCl_4$ is -69±6 kJ/mol from experiments performed with a He/MoO_3 gas-jet and Cl_2/CCl_4 as chlorinating agent, since the quartz surface was free of any contaminations.

6.2.2 Hf-Chlorides

For this study, 38-s ^{162}Hf and 102-s ^{165}Hf were used. Various halogenating agents (Cl_2, HCl/CCl_4, and HCl/$SOCl_2$) were utilized. Unfortunately, the chlorine gas used (99.99% pure) did not yield any volatile Hf-chloride species. According to Türler [TUR 93], the gas may not have been pure enough (99.9999% pure) to produce Hf-chloride species. Due to the scarcity of accelerator time, we were unable to repeat these experiments with high purity chlorine gas. Therefore, all results presented here have the high yield problem at low temperatures discussed in section 6.

As shown in Figs 6.8 through 6.11, $HfCl_4$ begins to be volatile at temperatures between 200°C and 250°C. Table 6.3 lists the calculated adsorption enthalpies. As observed in section 6.2.1, when using KCl as transport aerosol material (Figs 6.12 and 6.13) decreases in volatility (on the order of 150°C) and adsorption enthalpies (Table 6.2) are expected.

The best value of adsorption enthalpy on a SiO_2 surface for $HfCl_4$ is -96±5 kJ/mol from experiments performed with a He/MoO_3 gas-jet and HCl/CCl_4 as chlorinating agent.

Table 6.3 Adsorption enthalpies for Hf-chlorides. These compounds are probably the species which are formed.

Compound	Half-life (sec)	Surface	Halogenating Agent	Transport Aerosol	ΔH^o_{ads} (kJ/mol)	$*\Delta H^o_{ads}$ (kJ/mol)
$^{162}HfCl_4$	38	SiO_2	HCl/CCl_4	MoO_3	-96 ± 5	
$^{165}HfCl_4$	102	SiO_2	HCl/CCl_4	MoO_3	-104 ± 9	
$^{162}HfCl_4$	38	SiO_2	$HCl/SOCl_2$	MoO_3	-101 ± 7	
$^{165}HfCl_4$	102	SiO_2	$HCl/SOCl_2$	MoO_3	-109 ± 7	
$^{162}HfCl_4$	38	$SiO_2(KCl)$	$HCl/SOCl_2$	KCl	-127 ± 6	•-99±20
$^{165}HfCl_4$	102	$SiO_2(KCl)$	$HCl/SOCl_2$	KCl	-130 ± 9	

*Data from [RUD 79]

•Adsorption enthalpy on NaCl surface.

6.2.3 Rf-Chlorides

A new half life of 78^{+11}_{-6} s has been measured for ^{261}Rf as explained in section 4.5.2. Decay curves of the 7.275 MeV and the 8.15 to 8.38 MeV regions are shown in Figs 6.14 and 6.15, respectively. A yield curve (Fig. 6.16) for $^{261}RfCl_4$ was constructed as explained in section 4.5.2. Table 6.4 contains the data used in constructing yield curves for $BiCl_3$, $PoCl_4$, and $RfCl_4$. As illustrated in Fig. 6.16, $RfCl_4$ becomes volatile at temperatures between 100°C and 150°C, corresponding to an adsorption enthalpy value of -77 ± 6 kJ/mol.

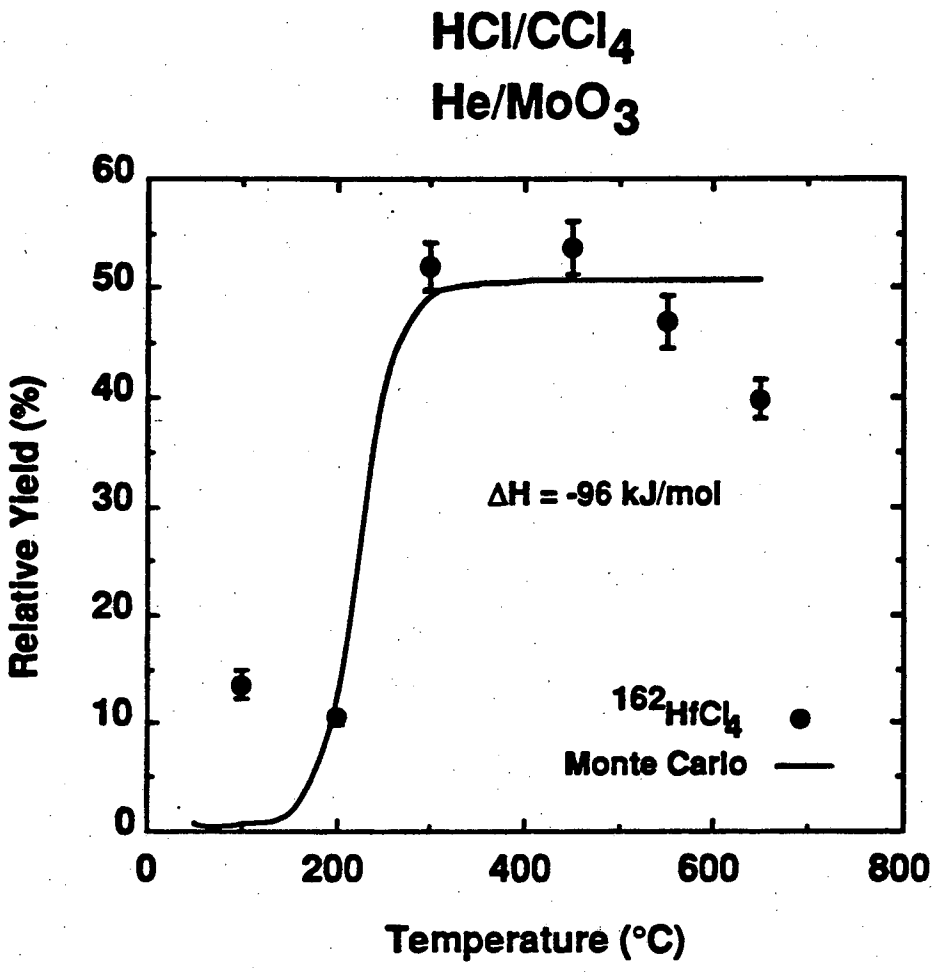

Fig. 6.8 Relative yield curve for Hf-chloride molecules with a He/MoO_3 gas jet and HCl/CCl_4 as chlorinating agent. The solid line drawn through the data points is from the Monte Carlo computer program.

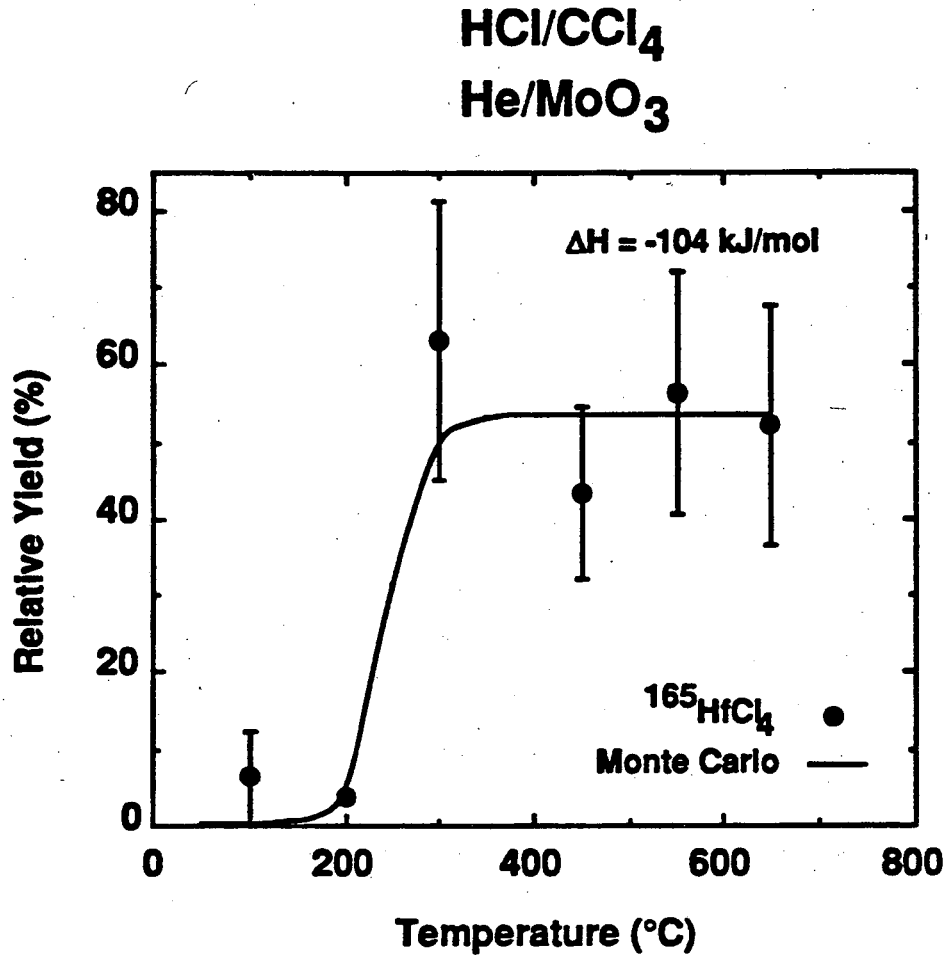

Fig. 6.9 Relative yield curve for Hf-chloride molecules with a He/MoO_3 gas jet and HCl/CCl_4 as chlorinating agent. The solid line drawn through the data points is from the Monte Carlo computer program.

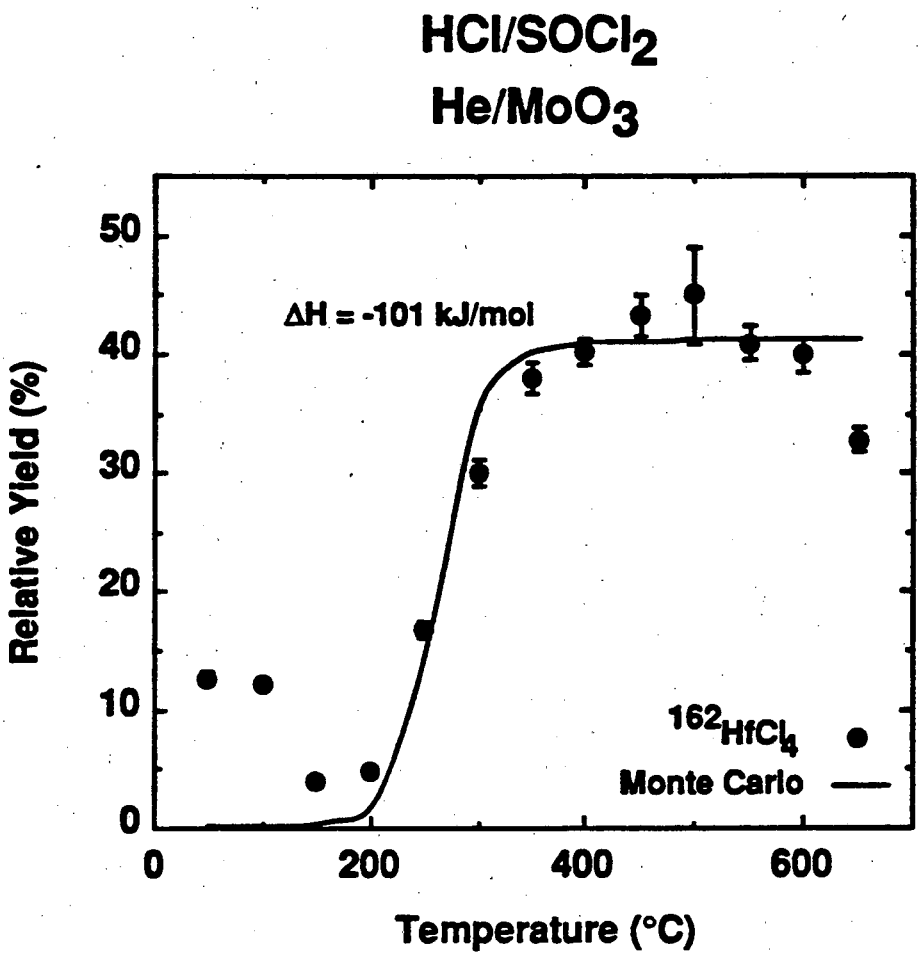

Fig. 6.10 Relative yield curve for Hf-chloride molecules with a He/MoO_3 gas jet and $HCl/SOCl_2$ as chlorinating agent. The solid line drawn through the data points is from the Monte Carlo computer program.

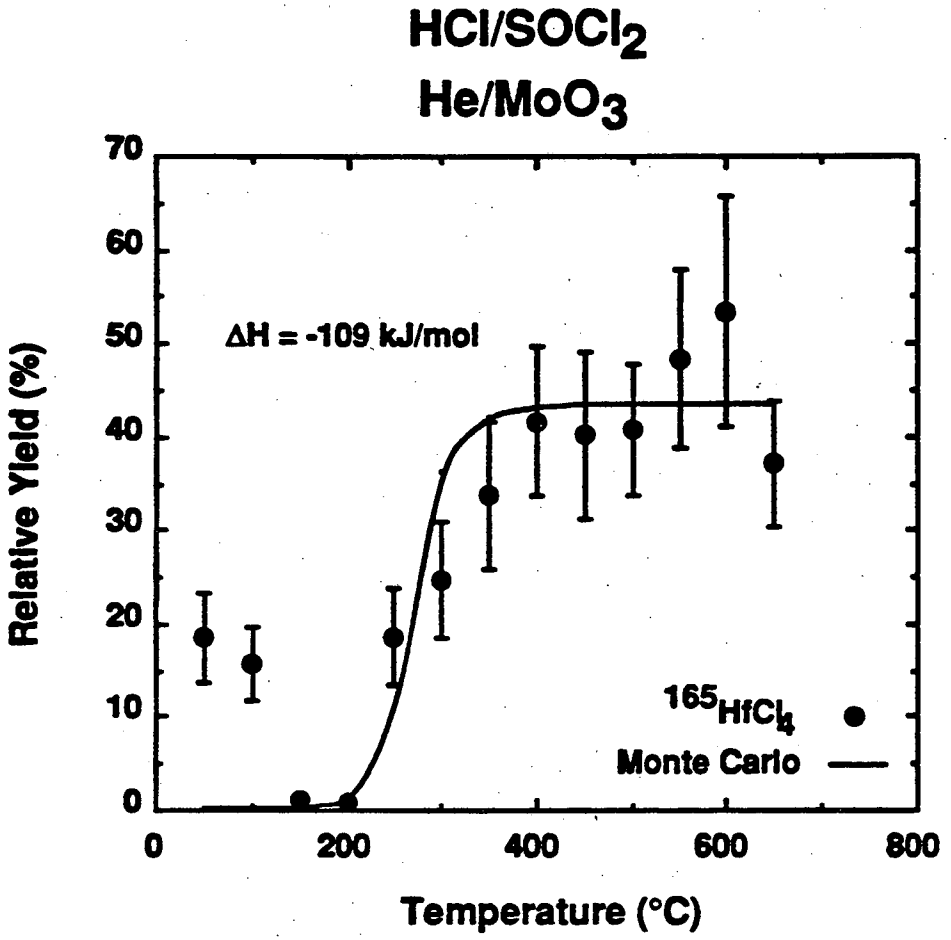

Fig. 6.11 Relative yield curve for Hf-chloride molecules with a He/MoO_3 gas jet and $HCl/SOCl_2$ as chlorinating agent. The solid line drawn through the data points is from the Monte Carlo computer program.

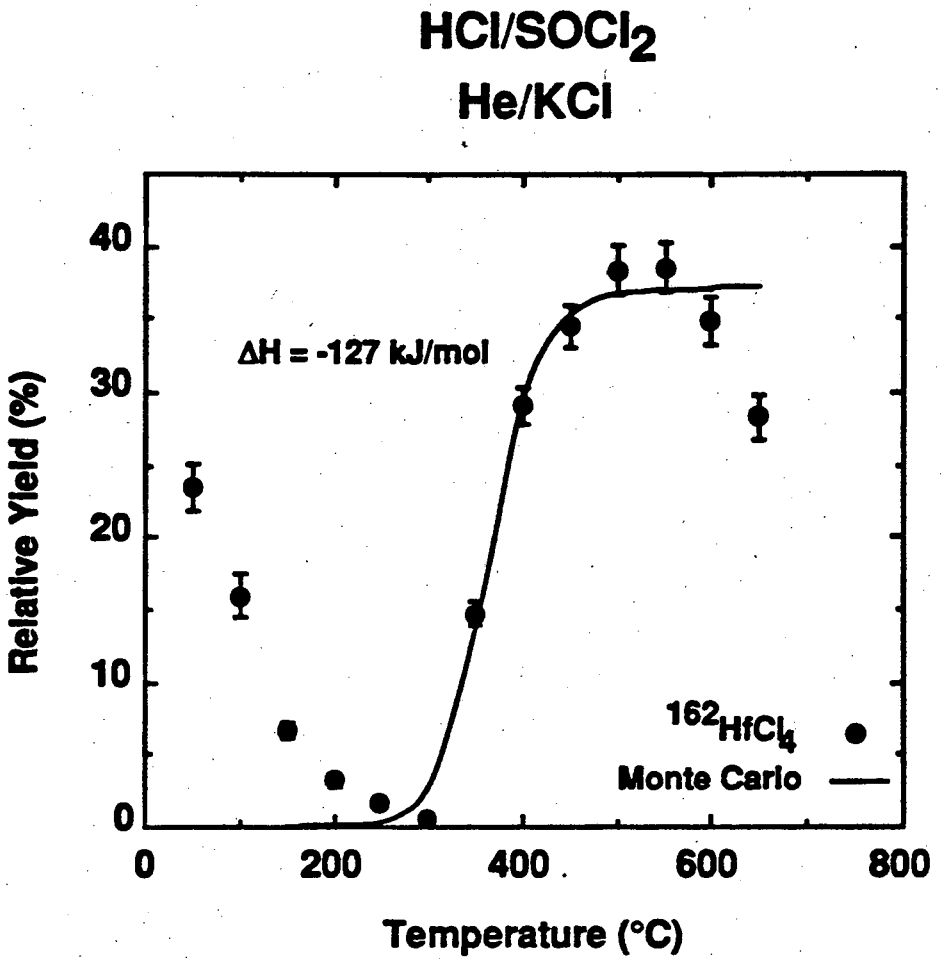

Fig. 6.12 Relative yield curve for Hf-chloride molecules with a He/KCl gas jet and $HCl/SOCl_2$ as chlorinating agent. The solid line drawn through the data points is from the Monte Carlo computer program.

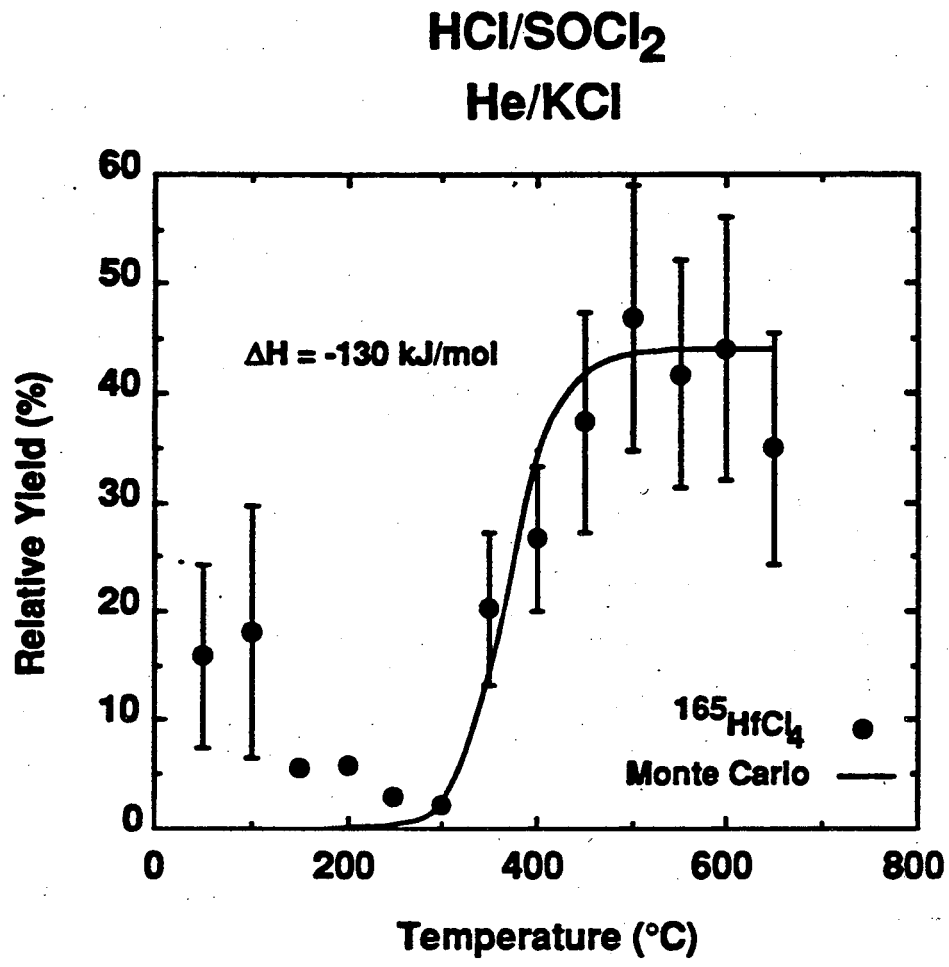

Fig. 6.13 Relative yield curve for Hf-chloride molecules with a He/KCl gas jet and $HCl/SOCl_2$ as chlorinating agent. The solid line drawn through the data points is from the Monte Carlo computer program.

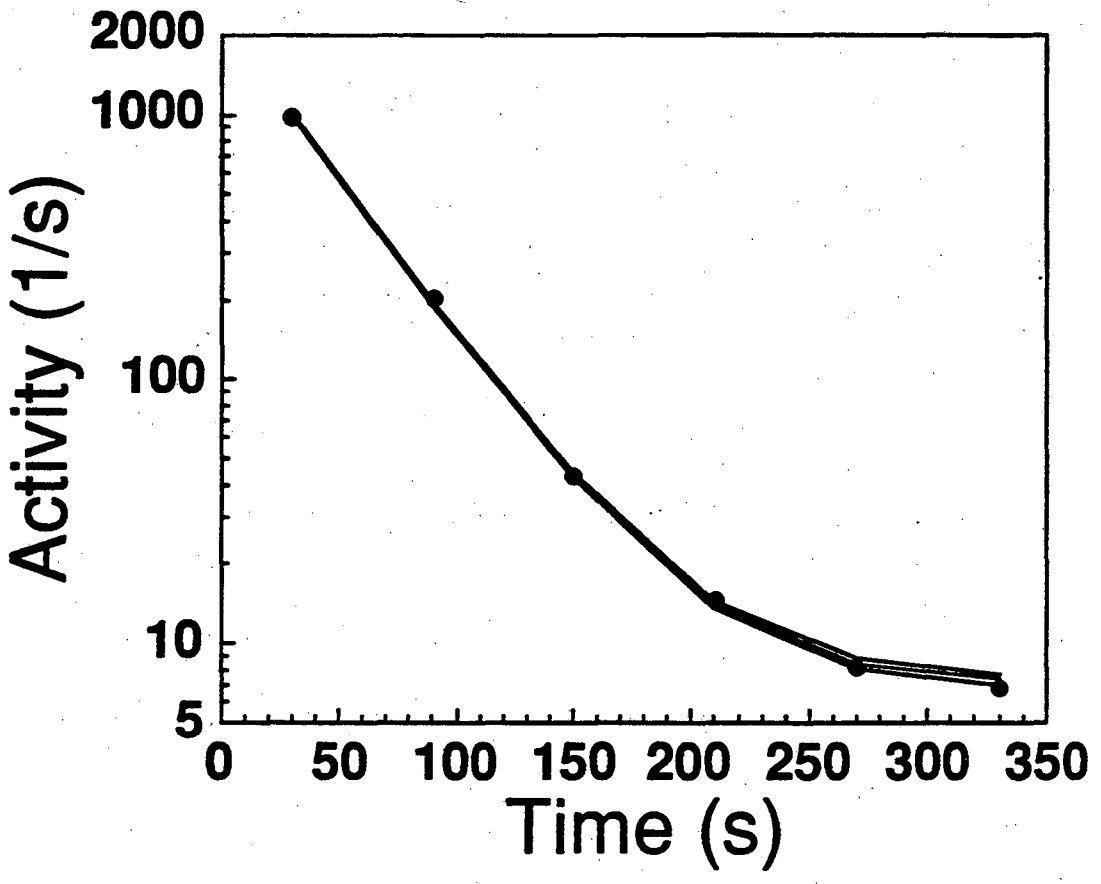

Fig. 6.14 Two component decay curve fit to the 7.275 MeV region. The half-lives of $^{211}Po^{m}$ and ^{254}Fm isotopes were fixed at 25.2 s and 3.24 h, respectively. The initial Po activity from this peak was used to calculate an initial activity for the 8.305 MeV (0.25%) alpha line of the same isotope in the fit to the ^{261}Rf - ^{257}No decay curve. A maximum likelihood decay curve fit has been used. The upper and lower limits on the decay curve correspond to a confidence level of 68% [GRE 91].

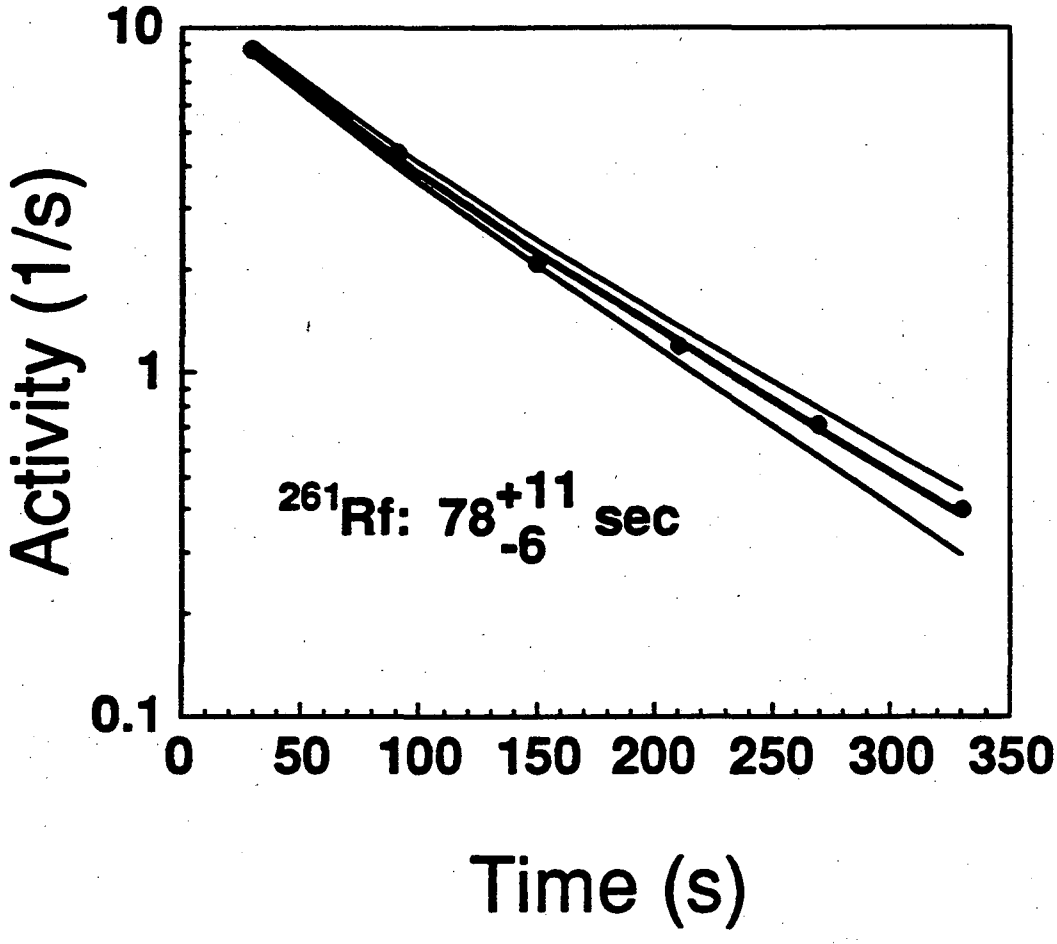

Fig. 6.15 Growth (^{261}Rf) and decay (^{257}No) plus one component (^{211}Po^{m}) fit to the 8.15 to 8.38 MeV region. In this fit half-lives of Po and No and the initial activity of Po were fixed; all other parameters were allowed to vary. A maximum likelihood decay curve fit has been used. The upper and lower limits on the half-life interval correspond to a confidence level of 68% [GRE 91].

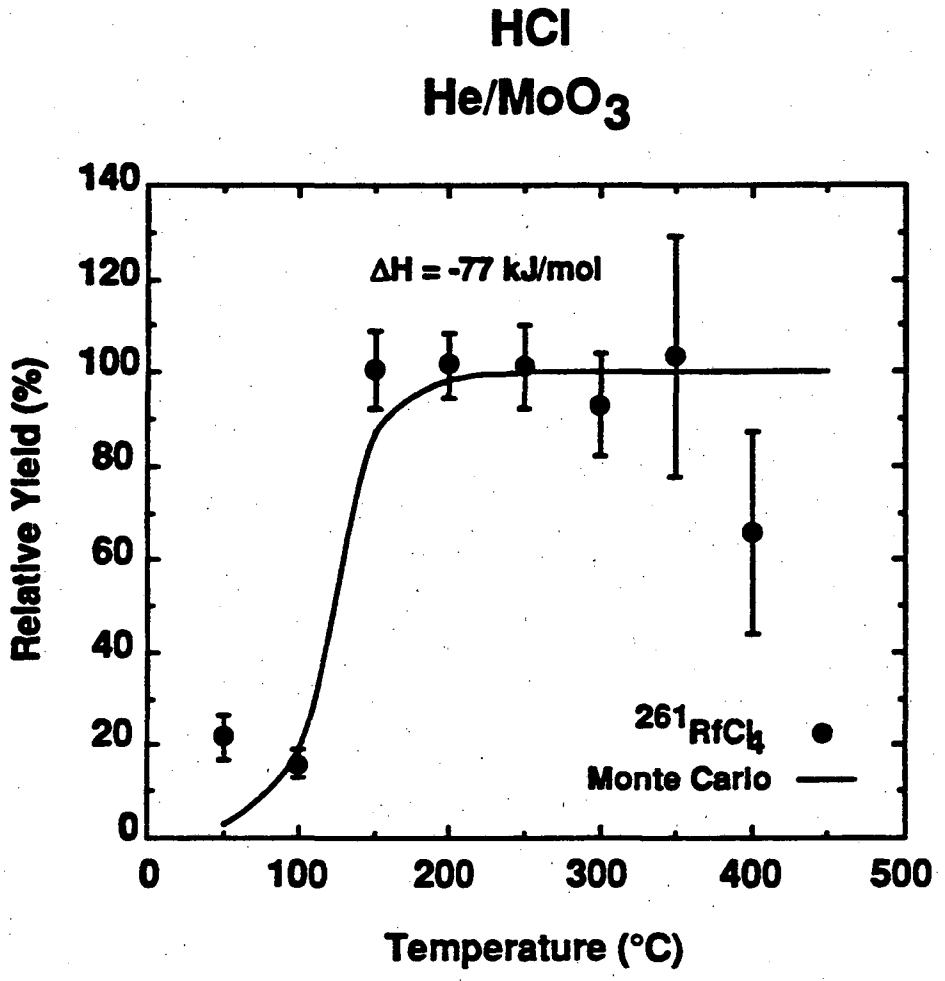

Fig. 6.16 Relative yield curve for Rf-chloride molecules with a He/MoO_3 gas jet and HCl as chlorinating agent. The solid line drawn through the data points is from the Monte Carlo computer program.

Table 6.4 Experimental data used in constructing relative yield curves for $BiCl_3$, $PoCl_4$, and $RfCl_4$.

Temperature (°C)	Beam (μC)	Total Events $^{211}Po^m$ 7.27 MeV	Total Events ^{211}Bi 6.62 MeV	Total Events $^{261}Rf + ^{257}No + ^{211}Po^m$ 8.18-8.38 MeV	Expected $^{211}Po^m$ Events 8.305 MeV	^{261}Rf Events 8.18-8.38MeV
50	54393	2753	1821	40	8	32
100	68280	1516	7045	34	4	30
150	68792	11435	9519	222	31	191
200	92113	13869	11412	296	38	258
250	59063	10010	7142	193	28	165
300	42171	7337	4867	128	20	108
350	11495	2056	1482	39	6	33
400	11315	1803	1315	25	5	20

6.2.4 Discussion

Within the group 4 elements, the lighter species ($ZrCl_4$) is more volatile and has a larger adsorption enthalpy than the heavier species ($HfCl_4$). Assuming this trend continues and there are similar molecular structures for chloride complexes within a periodic table group, $RfCl_4$ should be the least volatile of the group 4 chlorides and have the smallest adsorption enthalpy.

The volatility of Rf-chlorides, which has been determined with high accuracy, can be compared with the volatility of Zr- and Hf-chlorides measured under identical conditions. The following volatility series has been established for the group 4 element chlorides: $ZrCl_4 \geq RfCl_4 > HfCl_4$. The Zr- and Rf-chlorides are similar in volatility and more volatile than Hf-chlorides. The order observed in the volatilities does not correspond to the expected trend for the group 4 chlorides. The adsorption enthalpies are as follows: $ZrCl_4 > RfCl_4 > HfCl_4$.

Preliminary results indicate that the Zr-chlorides are more volatile than their bromides.

6.3 Group 5 Elements

6.3.1 Nb-Chlorides

Figures 6.17 through 6.21 show relative yield curves for 15-s ^{99}Nb-chlorides with either a He/MoO_3 or He/KCl gas jet and various halogenating agents on SiO_2 or KCl surfaces. As depicted in Figs 6.17 and 6.18, $NbCl_5$ becomes volatile at temperatures between 100°C and 150°C. Table 6.5 lists the calculated adsorption enthalpies. Our adsorption enthalpies agree very well with Rudolph's values. A 100°C change is again

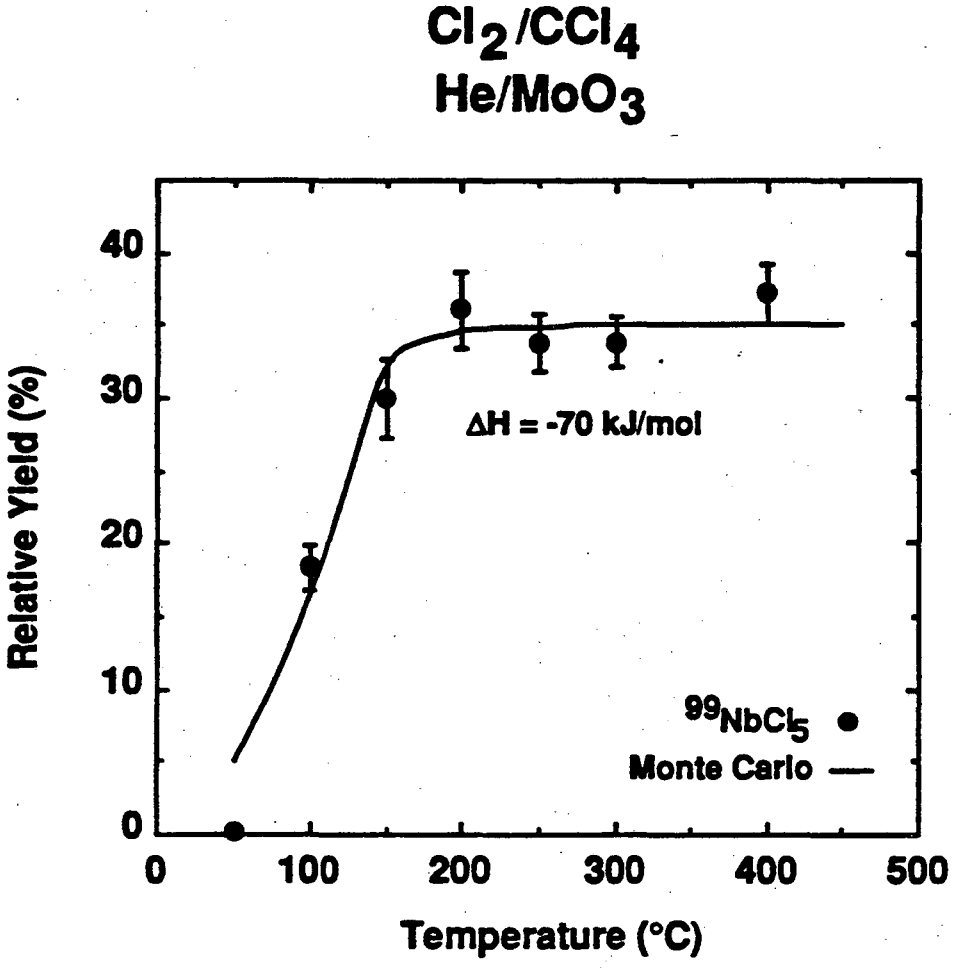

Fig. 6.17 Relative yield curves for ^{99}Nb-chloride molecules with a He/MoO_3 gas jet and Cl_2/CCl_4 as chlorinating agent. The solid line drawn through the data points is from the Monte Carlo computer program.

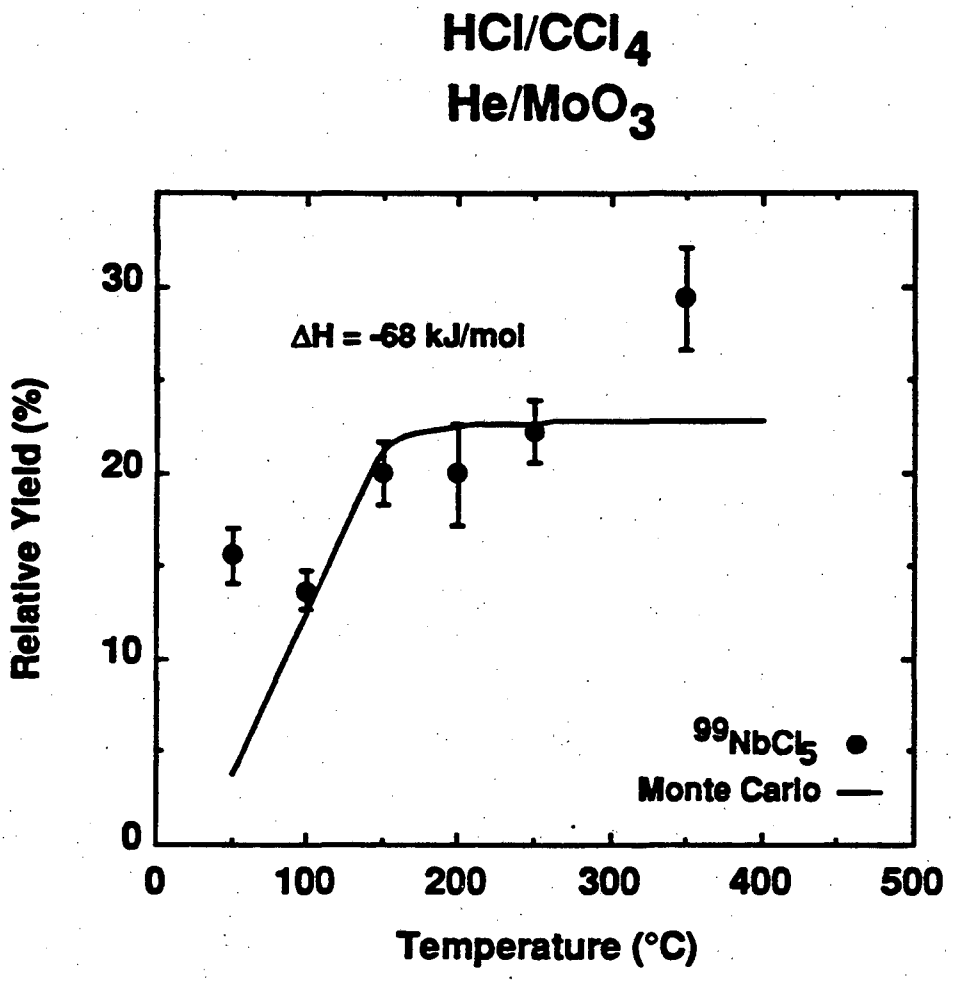

Fig. 6.18 Relative yield curves for ^{99}Nb-chloride molecules with a He/MoO_3 gas jet and HCl/CCl_4 as chlorinating agent. The solid line drawn through the data points is from the Monte Carlo computer program.

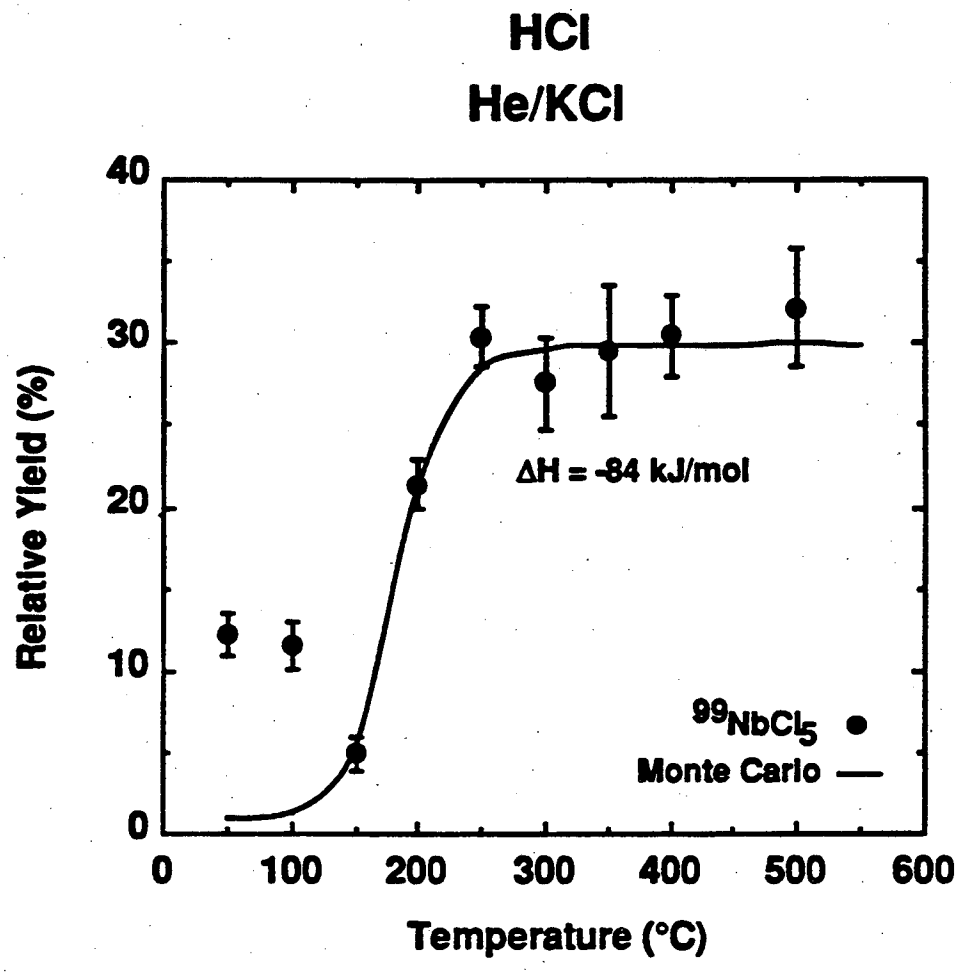

Fig. 6.19 Relative yield curves for ^{99}Nb-chloride molecules with a He/KCl gas jet and HCl as chlorinating agent. The solid line drawn through the data points is from the Monte Carlo computer program.

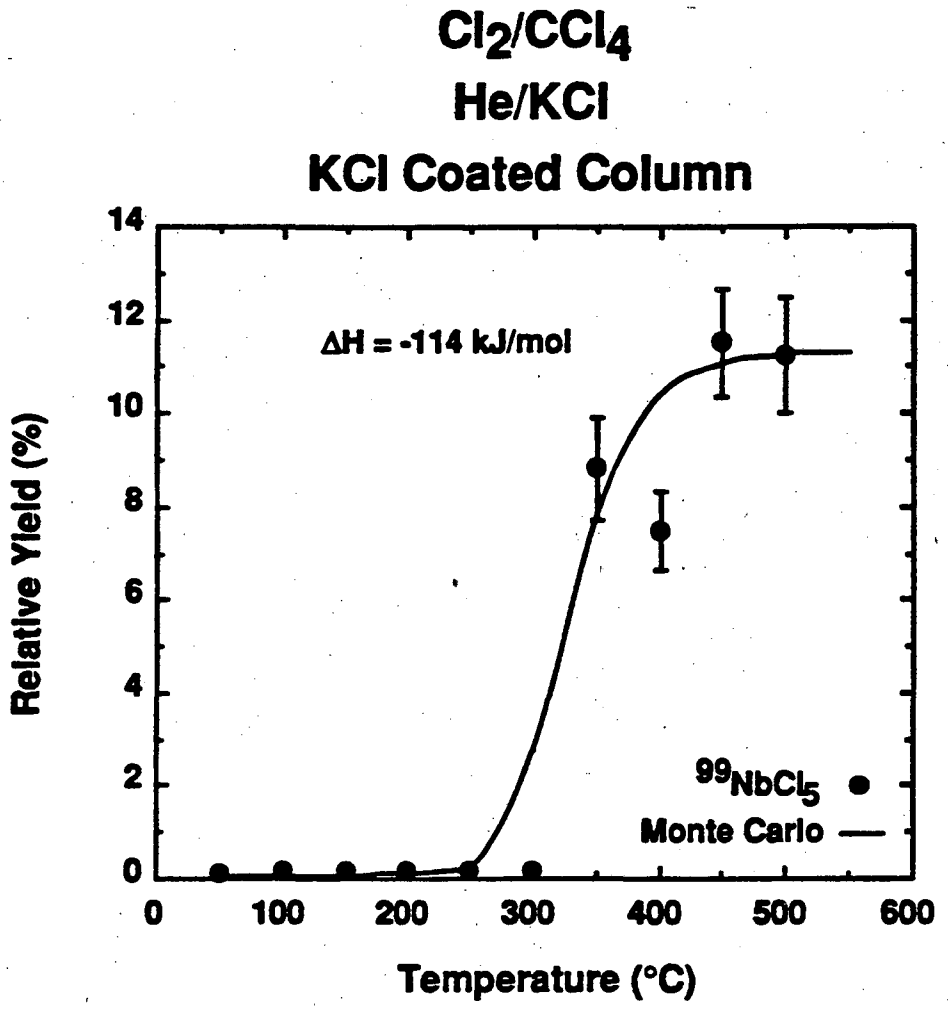

Fig. 6.20 Relative yield curves for ^{99}Nb-chloride molecules with a He/KCl gas jet and Cl_2/CCl_4 as chlorinating agent on a KCl surface. The solid line drawn through the data points is from the Monte Carlo computer program.

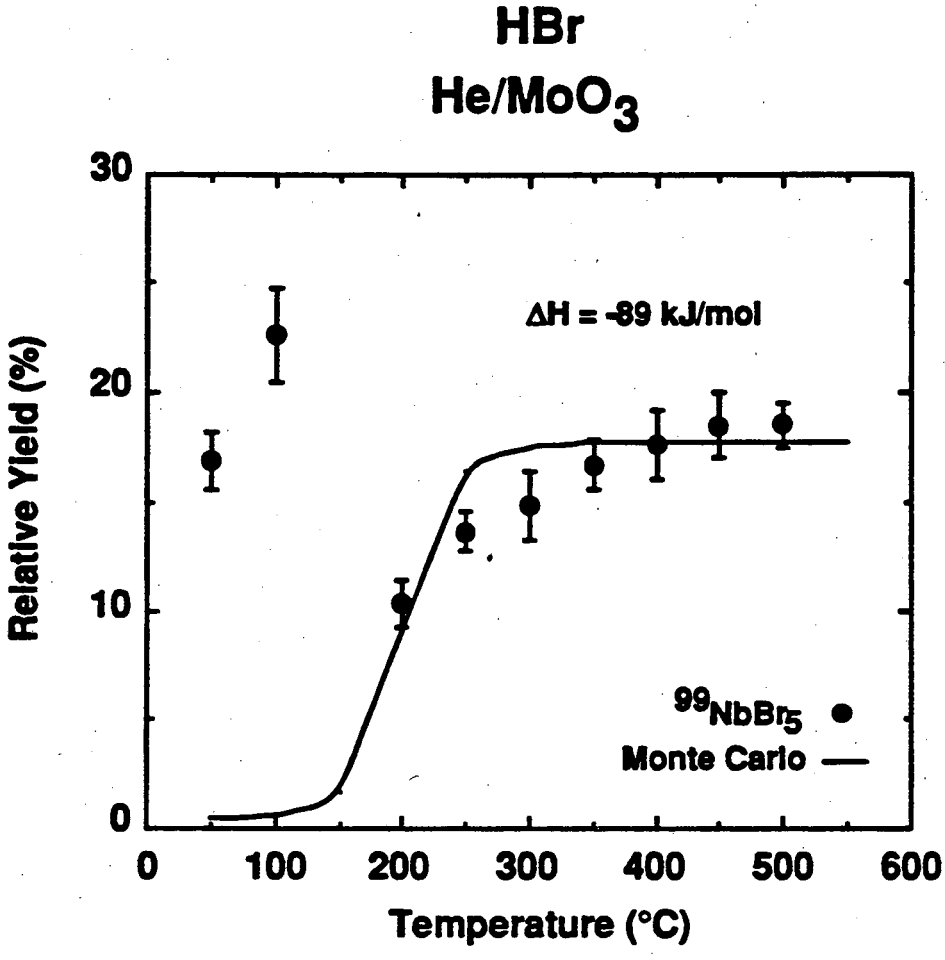

Fig. 6.21 Relative yield curves for ^{99}Nb-bromide molecules with a He/MoO_3 gas jet and HBr as chlorinating agent. The solid line drawn through the data points is from the Monte Carlo computer program.

observed when a He/KCl gas-jet was used (Fig. 6.19) because of the partially KCl-coated column surface. The volatility of $NbCl_5$ was investigated on a KCl surface, prepared as explained in section 4.3, and a 250°C decrease in volatility was observed. The decrease in adsorption enthalpies for $NbCl_5$ observed between experiments on a SiO_2 surface and on a KCl surface, is also observed by Rudolph (Table 6.5). The KCl surface was created as explained in section 4.3. Our results show a lower volatility for $NbBr_5$ than for $NbCl_5$. The results shown for $NbBr_5$ are considered preliminary.

Table 6.5 Adsorption enthalpies for Nb-chlorides and -bromides. These compounds are probably the species which are formed.

Compound	Surface	Halogenating Agent	Transport Aerosol	ΔH^o_{ads} (kJ/mol)	$*\Delta H^o_{ads}$ (kJ/mol)
$^{99}NbCl_5$	SiO_2	Cl_2/CCl_4	MoO_3	-70 ± 5	-69 ± 5
$^{99}NbCl_5$	SiO_2 (MoO2Cl2)	HCl/CCl_4	MoO_3	-68 ± 5	
$^{99}NbCl_5$	SiO_2(KCl)	HCl	KCl	-84 ± 5	
$^{99}NbCl_5$	KCl	Cl_2/CCl_4	KCl	-114 ± 7	-102 ± 2
$^{99}NbBr_5$	SiO_2 (MoO_2Br_2)	HBr	MoO_3	-89 ± 5	

*Data from [RUD 80b]

6.3.2 Ta-Chlorides

For this study, the 34-s ^{166}Ta and 84-s ^{167}Ta were used. Various halogenating agents (Cl_2, HCl/CCl_4, and $HCl/SOCl_2$) were utilized. Similar to the Hf results discussed in section 6.2.2, chlorine gas did not yield any volatile Ta-chloride species.

The results presented here have the high-yield problem at low temperatures discussed in section 6.

Most probably the Ta species under study here is $TaOCl_3$ rather than $TaCl_5$ because of the unusually low volatility. As shown in Figs 6.22 through 6.25, $TaOCl_3$ becomes volatile at temperatures between 550°C and 600°C. Table 6.6 lists the calculated adsorption enthalpies. Rudolph's work [RUD 79] shows an increase in adsorption enthalpy (or volatility) for $TaOCl_3$ between experiments performed on a SiO_2 surface ($\Delta H = -133 \pm 20$ kJ/mol) and experiments done on a NaCl surface ($\Delta H = -96 \pm 20$ kJ/mol). An increase in volatility (on the order of 50°C) is observed (Fig. 6.26 and 6.27) when KCl is used as the transport aerosol because the column is partially coated with KCl.

Table 6.6 Adsorption enthalpies for Ta-chlorides. These compounds are probably the species which are formed.

Compound	Half-life (sec)	Surface	Halogenating Agent	Transport Aerosol	ΔH^o_{ads} (kJ/mol)	$*\Delta H^o_{ads}$ (kJ/mol)
$^{166}TaOCl_3$	34	SiO_2	HCl/CCl_4	MoO_3	-152 ± 12	-133 ± 20
$^{167}TaOCl_3$	84	SiO_2	HCl/CCl_4	MoO_3	-153 ± 11	
$^{166}TaOCl_3$	34	SiO_2	$HCl/SOCl_2$	MoO_3	-166 ± 9	
$^{167}TaOCl_3$	84	SiO_2	$HCl/SOCl_2$	MoO_3	-162 ± 7	
$^{166}TaOCl_3$	34	SiO_2(KCl)	$HCl/SOCl_2$	KCl	-149 ± 5	•-96±20
$^{167}TaOCl_3$	84	SiO_2(KCl)	$HCl/SOCl_2$	KCl	-160 ± 12	

*Data from [RUD 79]

•Adsorption enthalpy on NaCl surface.

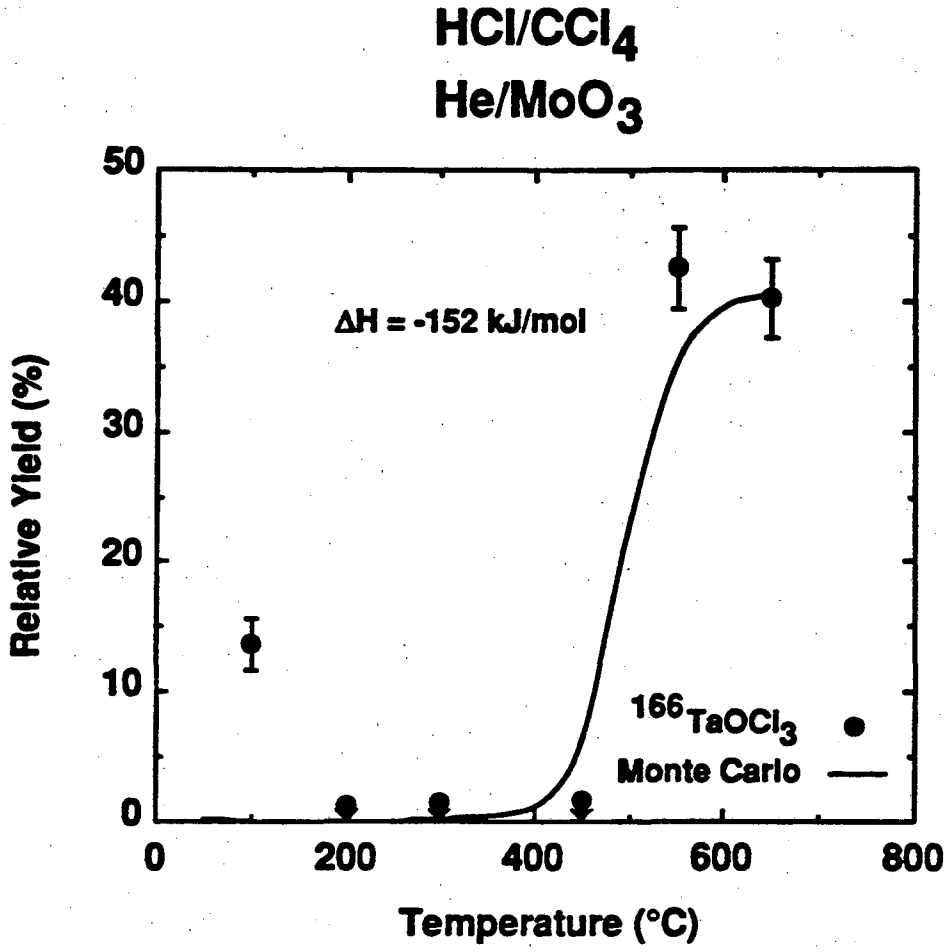

Fig. 6.22 Relative yield curve for Ta-chloride molecules with a He/MoO_3 gas jet and HCl/CCl_4 as chlorinating agent. The solid line drawn through the data points is from the Monte Carlo computer program.

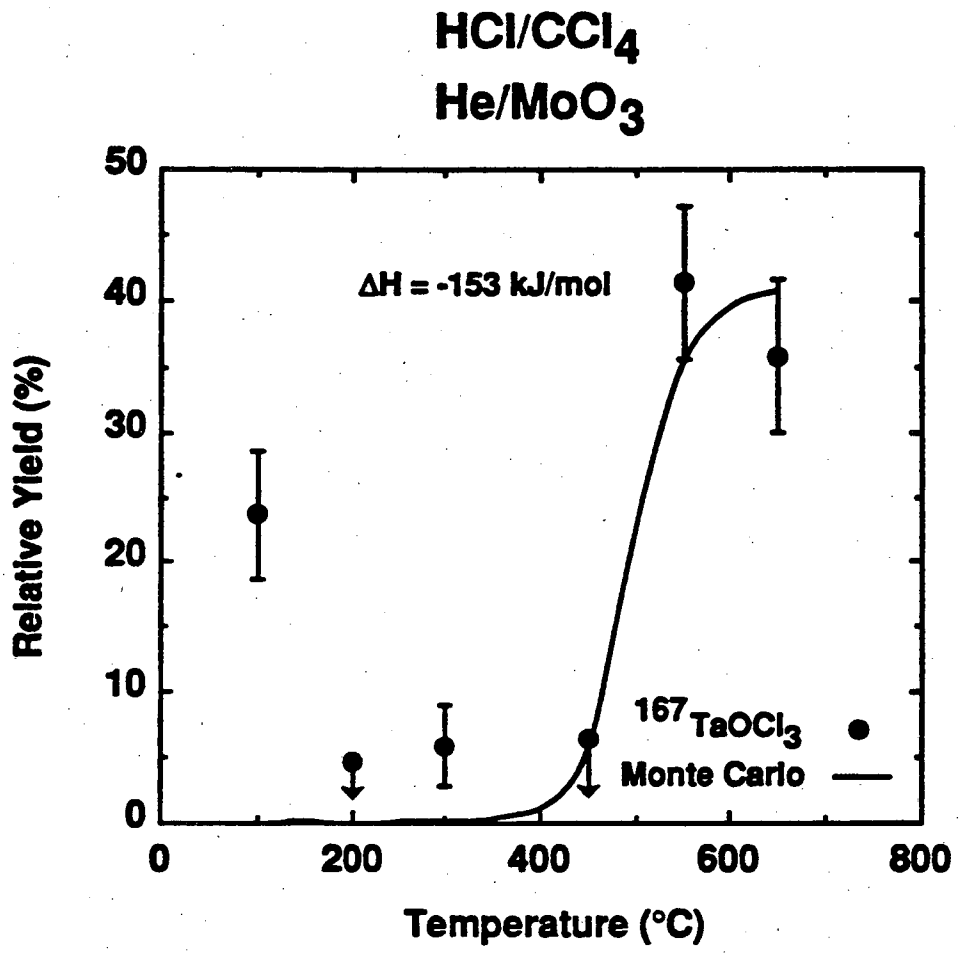

Fig. 6.23 Relative yield curve for Ta-chloride molecules with a He/MoO_3 gas jet and HCl/CCl_4 as chlorinating agent. The solid line drawn through the data points is from the Monte Carlo computer program.

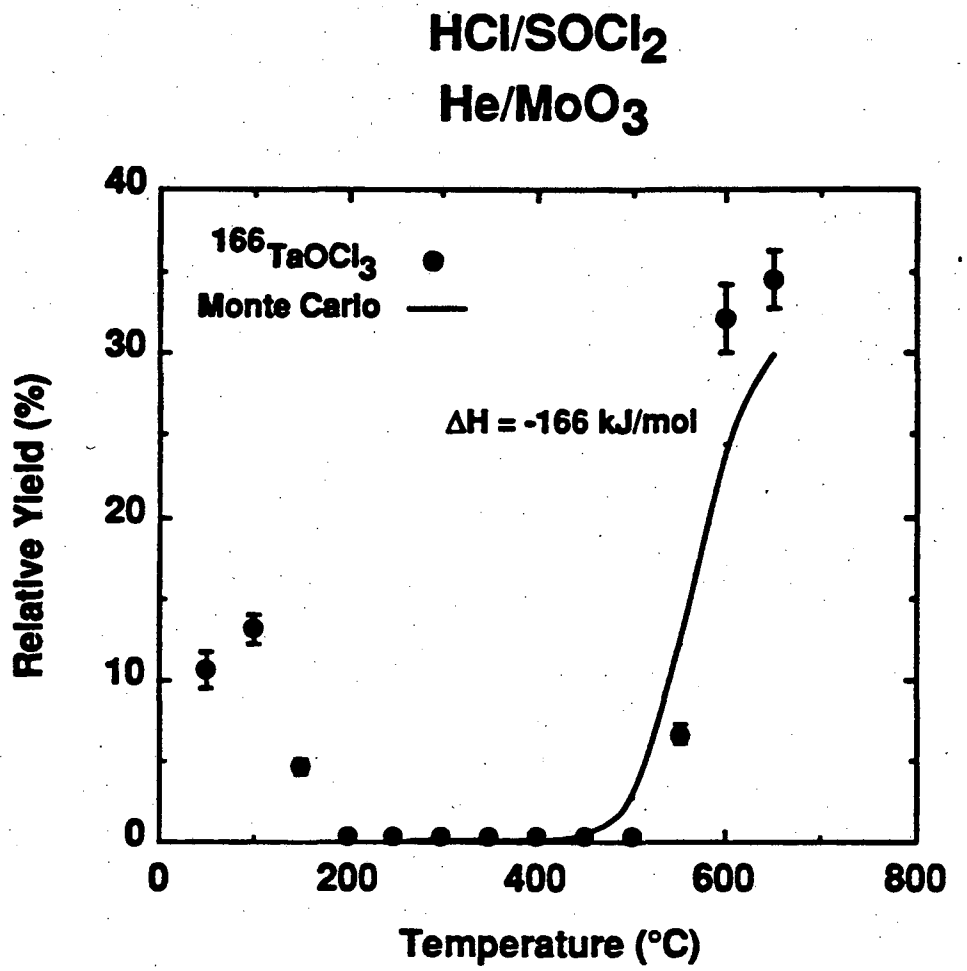

Fig. 6.24 Relative yield curve for Ta-chloride molecules with a He/MoO_3 gas jet and $HCl/SOCl_2$ as chlorinating agent. The solid line drawn through the data points is from the Monte Carlo computer program.

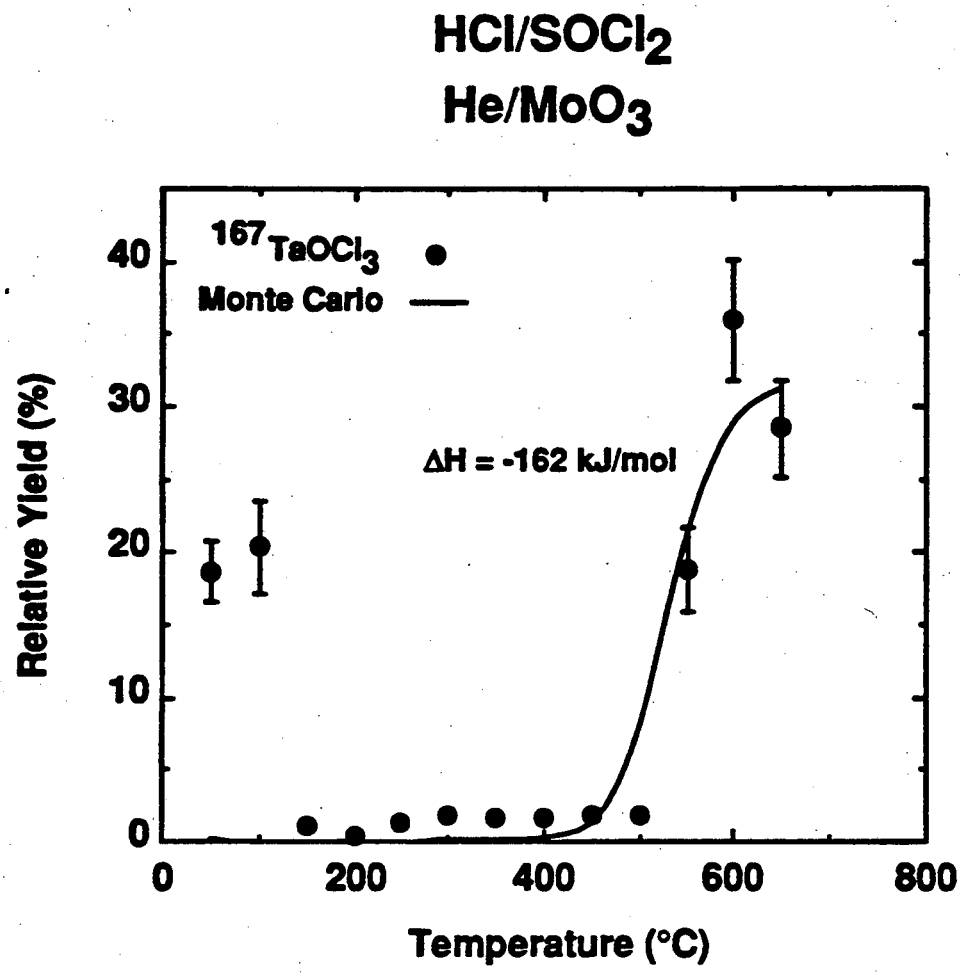

Fig. 6.25 Relative yield curve for Ta-chloride molecules with a He/MoO_3 gas jet and $HCl/SOCl_2$ as chlorinating agent. The solid line drawn through the data points is from the Monte Carlo computer program.

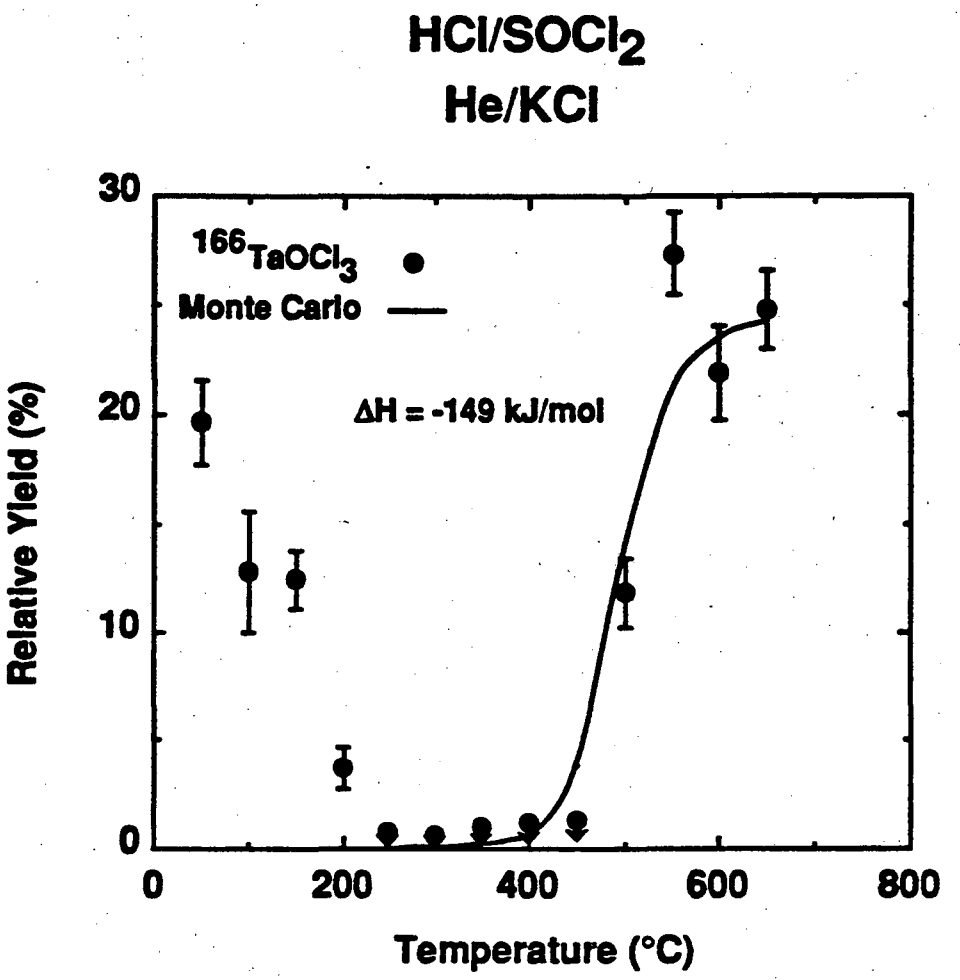

Fig. 6.26 Relative yield curve for Ta-chloride molecules with a He/KCl gas jet and $HCl/SOCl_2$ as chlorinating agent. The solid line drawn through the data points is from the Monte Carlo computer program.

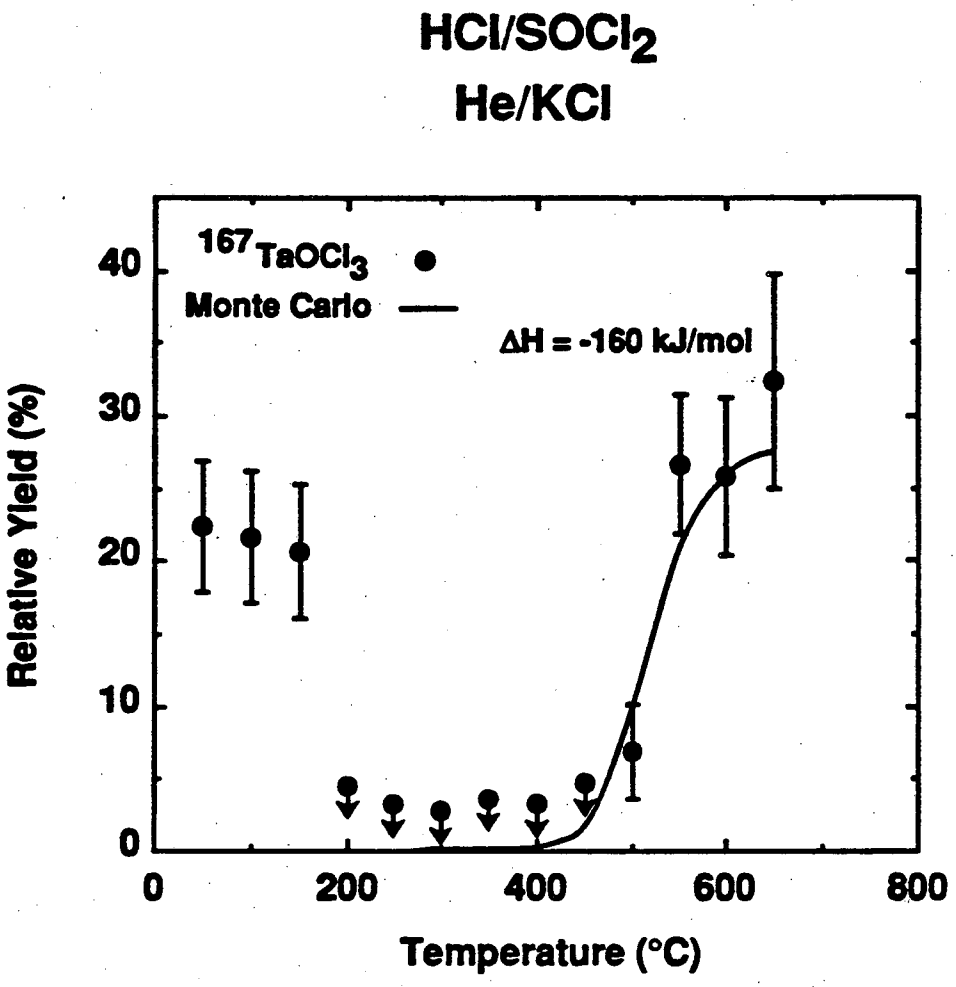

Fig. 6.27 Relative yield curve for Ta-chloride molecules with a He/KCl gas jet and HCl/$SOCl_2$ as chlorinating agent. The solid line drawn through the data points is from the Monte Carlo computer program.

6.3.3 Ha-Chlorides

^{262}Ha decays 67% by α-emission and 33% by spontaneous fission (SF) [KRA 92]. A decay-curve analysis of SF activities observed in all gas chemistry experiments resulted in a half-life of 47^{+11}_{-8} s, assuming a minor contamination from ^{256}Fm (^{256}Md). This half-life is long compared to the literature value of 34-s, but agrees well with the 44^{+19}_{-12}s half-life observed by Gäggeler et al. in earlier gas chemistry experiments [GAG 92]. The analysis of α-spectra revealed 7 correlated α-α pairs, which resulted from the decay of 34-s ^{262}Ha followed by α-decay of its 3.93-s ^{258}Lr daughter. Half-lives of 28^{+17}_{-8} s and $3.8^{+2.3}_{-1.0}$ s resulted for the mother and the daughter nuclides, respectively, in good agreement with the literature values. The observation of correlated mother-daughter pairs furnishes positive proof that ^{262}Ha was observed after chemical separation. Figure 6.28 shows the yield curve constructed for $HaCl_5$. The relative yield of Ha-chlorides at 100°C is considerably lower than that measured at 250°C and higher temperatures. Unfortunately, no data exist for temperatures between 100 and 250°C and additional experiments need to be performed to obtain a more accurate determination of the $HaCl_5$ volatility. An adsorption enthalpy of -73±10 kJ/mol was calculated for $HaCl_5$; however, the point at 100°C was heavily weighted in this calculation. The Monte Carlo line was forced to go through this point.

6.3.4 Discussion

Our results indicate that Nb- and Ha-chlorides are more volatile than their respective bromides [GAG 92]. $HaCl_5$ is probably similar in volatility to $NbCl_5$. However, additional experiments need to be performed for a more accurate determination of the

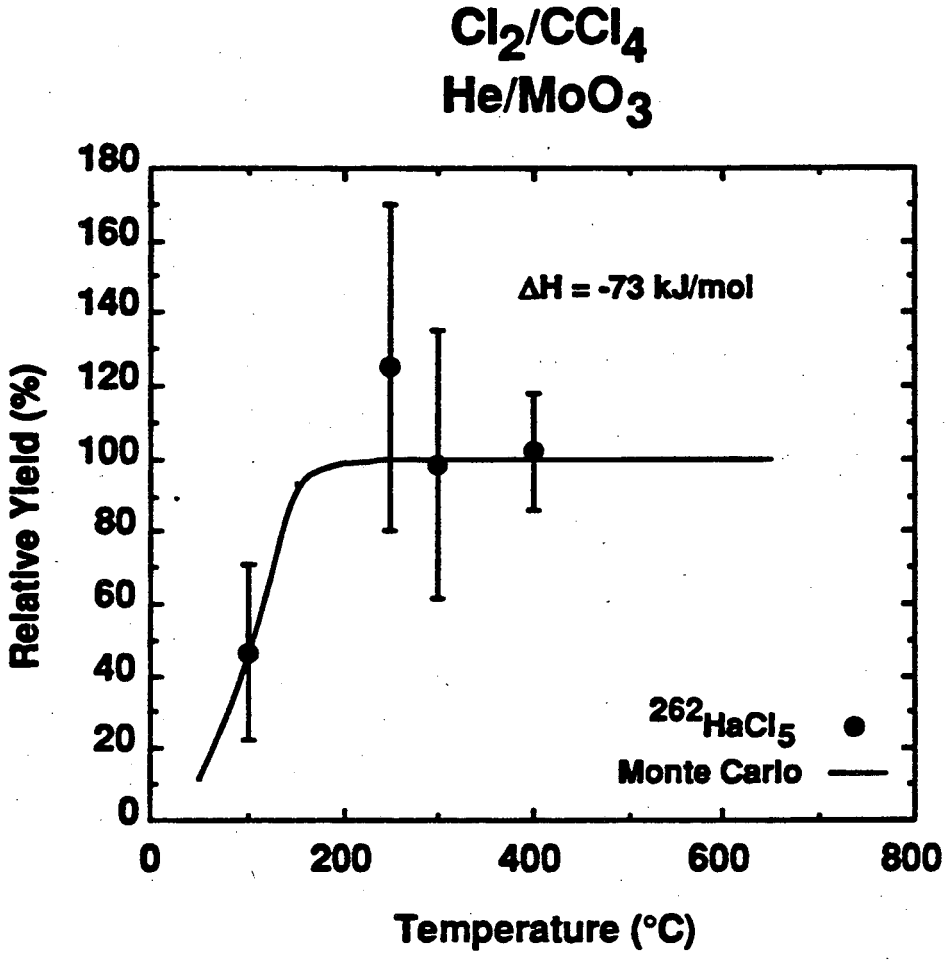

Fig. 6.28 Relative yield curve for Ha-chloride molecules with a He/MoO_3 gas jet and Cl_2/CCl_4 as chlorinating agent. The solid line drawn through the data points is from the Monte Carlo computer program.

volatility of Ha-chlorides. As explained in section 6.3.2, results were obtained for $TaOCl_3$ and not the pure chloride species ($TaCl_5$). Therefore, we are unable to arrive at any conclusions concerning volatility trends in the group 5 chlorides.

Chapter 7

Conclusions

We have constructed the Heavy Element Volatility Instrument (HEVI), an on-line gas chromatography system which continuously separates halide species of short-lived nuclides according to their volatilities. Volatility measurements have been performed on chlorides of Rf and its group 4 homologs, Zr and Hf, as well as Ha and its group 5 homologs, Nb and Ta. Adsorption enthalpies have been calculated for all species using a Monte Carlo code simulation based on a microscopic model for gas thermochromatography in open columns with laminar flow of the carrier gas. There is good agreement between the experimental results and the simulation. Table 7.1 contains the best volatility and adsorption enthalpy values for all species studied on SiO_2 surfaces.

Table 7.1 The best volatility and adsorption enthalpy values for all species studied on SiO_2 surface. These compounds are probably the species which are formed.

Compound	Volatility (°C)	ΔH^{o}_{ads} (kJ/mol)
$BiCl_3$	100 - 150	-69 ± 4
$PoCl_4$	150 - 200	-74 ± 5
$ZrCl_4$	100 - 150	-69 ± 6
$HfCl_4$	200 - 250	-96 ± 5
$RfCl_4$	100 - 150	-77 ± 6
$NbCl_5$	100 - 150	-70 ± 5
$HaCl_5$	100 - 250	-73 ± 10
$TaOCl_3$	550 - 600	-153 ± 11
$ZrBr_4$	200 - 250	-91 ± 6
$NbBr_5$	200 - 250	-89 ± 5

7.1 Group 4

The following series for volatilities and adsorption enthalpies of the group 4 element chlorides have been established: $ZrCl_4 \approx RfCl_4 > HfCl_4$ and $ZrCl_4 > RfCl_4 > HfCl_4$, respectively. Assuming similar molecular structures for chloride complexes within group 4 of the periodic table, a trend of decreasing volatility and ΔH_{ads} is observed as one moves down the group (noticed in Zr- and Hf-chlorides). Following this trend, $RfCl_4$ would then be expected to be the least volatile of the group 4 chlorides with the smallest

ΔH_{ads} value. However, illustrated in Fig. 7.1, our results show a reversal in this expected trend. Further calculations are needed to assess whether this is due to relativistic effects in the transactinide region. Preliminary results indicate that Zr-chlorides are more volatile than Zr-bromides.

7.2 Group 5

Our results indicate that Nb- and Ha-chlorides are more volatile than their respective bromides [GAG 92]. $HaCl_5$ is probably similar in volatility to $NbCl_5$. Additional experiments need to be performed for a more accurate determination of the volatility of Ha-chlorides. In this work, results were obtained for $TaOCl_3$ rather than for the pure chloride species $TaCl_5$. Therefore, we are unable to arrive at any conclusions concerning trends in volatility for the group 5 pentachlorides. However, if as in group 4, the heavier species $TaCl_5$ is less volatile than the lighter $NbCl_5$, then a reversal in trend again occurs for group 5 since the chlorides of Ha, the heaviest element, has about the same volatility as that of Nb.

7.3 Future work

The future of on-line gas chromatographic studies in the actinide and transactinide region is both challenging and exciting. The challenging aspect of this research comes from the short half-lives and low production rates of the transactinides. Improvements in detection methods of the existing system (HEVI) can allow studies of elements with half-lives of a few seconds or even less. The time required for the chemical separation of the

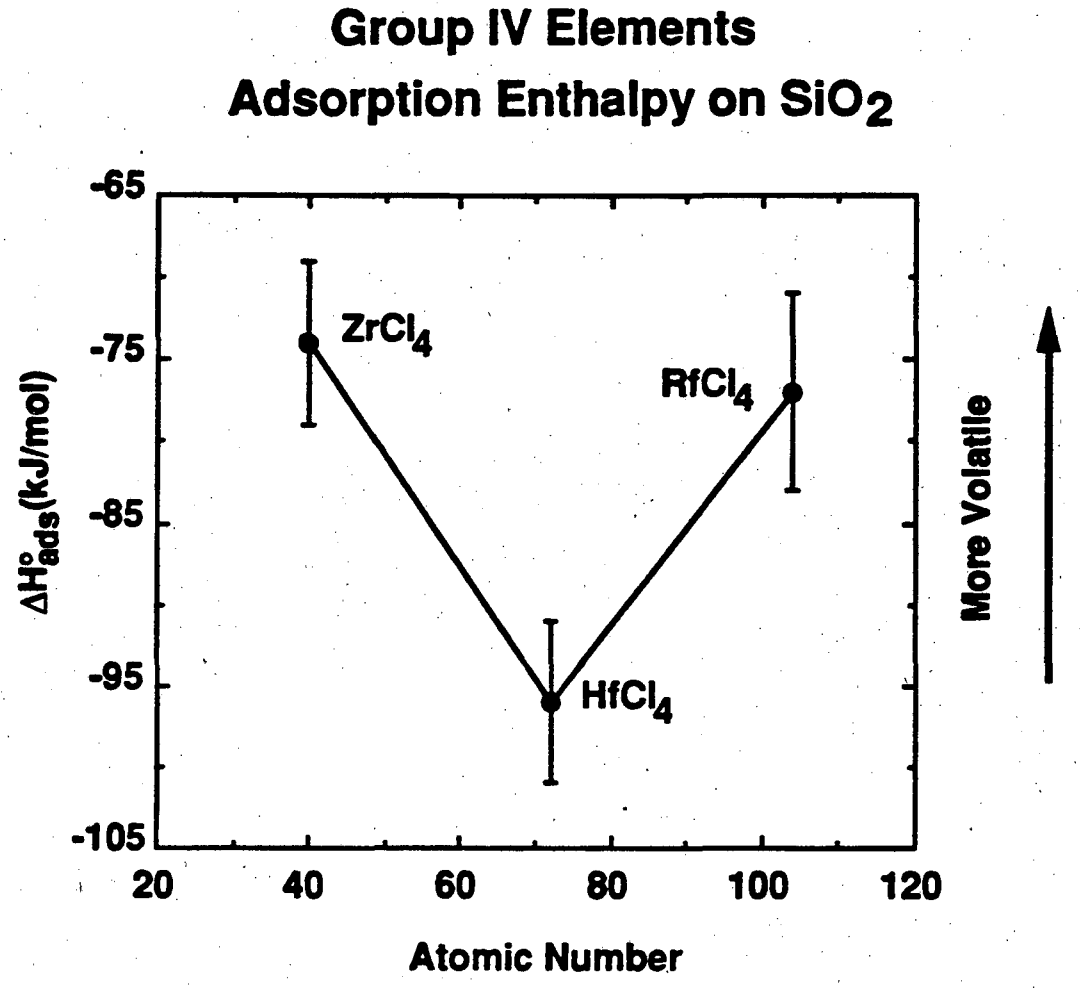

Fig. 7.1 A comparison of adsorption enthalpy values on SiO_2 for group 4 tetrachloride species.

halides is on the order of one second. As explained in section 6.2, the reclustering process for the separated halides on KCl aerosols and their transport to the detection system is a very time-consuming process (on the order of 15 to 25 seconds). Plans have been made for a new detection system design which will decrease the time between separation and detection to one or two seconds. This improvement will allow the investigation of the volatility of element 106 and its group 6 homologs, molybdenum and tungsten.

Presently, volatility studies are being conducted on the bromide systems of group 4 (Zr, Hf, and Rf) and group 5 (Nb, Ta, and Ha) elements. Collaborative efforts between Lawrence Berkeley Laboratory and Los Alamos National Laboratory have been planned to investigate the fluoride systems of group 4 and 5 elements. Elements with available 4^+ oxidation states such as cerium, thorium, plutonium and berkelium will also be investigated.

Finally, work is being done by theoretical chemists such as Valeria Perishina [PER 92], presently at GSI, B. Fricke, currently at University of Kassel in Germany, G. V. Ionova, currently at Institute of Physical Chemistry in Moscow, and Elijah Johnson, currently at Oak Ridge National Laboratory, to aid in the explanation of our experimental results.

Appendix A

```
'-------------------------------------------------------------------------
'MONTE CARLO SIMULATION OF ISOTHERMAL CHROMATOGRAPHY
'USING A MICROSCOPIC MODEL PROPOSED BY I. ZVARA
'
'AUTHOR: ANDREAS TÜRLER
'
'VERSION 1 FOR HEVI
'01/31/92
'-------------------------------------------------------------------------
SCREEN 0
CLS

'Declare variables and constants

DIM T(13, 59)
DIM LOSS(13)
DIM MADEIT(13)
CONST Pi = 3.141592653589#      'Nothing else put Pi
CONST M2 = 4.0026               'Molar mass of Helium (amu)
CONST d2 = .147                 'Density of Helium
CONST R = 8.31432E+07           'The gas constant (cgs)
```

```
'Read in the actual measured temperature profiles
OPEN "b:\heviprof.txt" FOR INPUT AS #1
FOR X = 0 TO 58 STEP 1
 INPUT #1, T(0, X), T(1, X), T(2, X), T(3, X), T(4, X), T(5, X), T(6, X), T(7, X), T(8,
X), T(9, X), T(10, X), T(11, X), T(12, X)
 NEXT X
CLOSE 1

'Read in information about molecule
INPUT "Half-life of the nuclide (sec)                    "; T.5
INPUT "Number of molecules for each temperature          "; I
INPUT "The flow rate of He through the column (Torr*l/sec STP)  "; Q
INPUT "The molecular weight of the species, i.e. TaBr5 (amu)    "; M1
INPUT "The density of the species, values from CRC Handbook     "; d1
INPUT "The period of oscillations of the molecule (1.0E-12)     "; p0
INPUT "The enthalpy of adsorption to start with          "; DHaSTART
INPUT "The enthalpy of adsorption to stop with           "; DHaSTOP
INPUT "The step width                                    "; DHaSTEP

Q = Q / 760 * 1000

OPEN "b:\hevi.dat" FOR OUTPUT AS #2
PRINT #2, "Monte Carlo Simulation for HEVI       "; DATE$, TIME$
PRINT #2, "=============================="
PRINT #2,
PRINT #2, "Half-life of the nuclide (sec)                "; T.5
```

```
PRINT #2, "Number of molecules for each temperature          "; I
PRINT #2, "The STP flow rate of He through the column (cm3/sec)    "; Q
PRINT #2, "The molecular weight of the species, i.e. TaBr5 (amu)    "; M1
PRINT #2, "The density of the species, values from CRC Handbook    "; d1
PRINT #2, "The period of oscillations of the molecule (1.0E-12)    "; p0
PRINT #2, "The enthalpy of adsorption to start with          "; DHaSTART
PRINT #2, "The enthalpy of adsorption to stop with          "; DHaSTOP
PRINT #2, "The step width                                   "; DHaSTEP
PRINT #2,
PRINT #2,

'Loop for different values of DHa
FOR DHa = DHaSTART TO DHaSTOP STEP DHaSTEP
PRINT #2, "Adsorption Enthalpy (kJ/mol)                     "; DHa
PRINT #2,
PRINT "Adsorption Enthalpy (kJ/mol)  "; DHa, TIME$

'Loop for different temperatures
FOR TX = 0 TO 12
 LOSS(TX) = 0              'The number of nuclides which didn't make it exit
 MADEIT(TX) = 0            'The number of nuclides which made it to the exit

PRINT "Temperature (øC)          "; (TX + 1) * 50

'Loop for I molecules
 FOR L = 1 TO I
 xi = 0                    'The distance variable in the column (cm)
```

```
tt = 0                    'The accumulated time (jump and sit) (s)

'Provide a primer for the random number generator
 RANDOMIZE TIMER

'Generate a random td (Decay Time)
'Since RND actually can be 0 use 1-RND as random number
 td = -T.5 / LOG(2) * LOG(1 - RND)

 DO

'Generate a random Ni (Jump Length)
'First calculate the Diffusion Coefficient using the Gilliland's equation
   D298 = .0043 * (298.15) ^ 1.5 * SQR(1 / M1 + 1 / M2) / (((M1 / d1) ^ (1 / 3) + (M2 /
d2) ^ (1 / 3))) ^ 2
   D = D298 * ((T(TX, CINT(xi)) + 273.15) / 298.15) ^ 1.75

'Then calculate N mean
   Nm = 11 * Q * (T(TX, CINT(xi)) + 273.15) / 273.15 / (48 * Pi * D)
'Generate random Ni
'Since RND actually can be 0 use 1-RND as random number
   Ni = -Nm * LOG(1 - RND)

'Evaluate the coordinate of the molecule
  xi = xi + Ni

'Calculate the flight time
```

```
'Assume that the flight time was Ni/Velocity and Velocity = Qi/Pi*r^2
  tf = 0
  IF xi - Ni > 53 THEN
    tf = 2 * Pi * .002025 * (INT(xi - Ni + 1) - (xi - Ni)) / ((Q * (T(TX, INT(xi - Ni)) +
273.15) / 273.15) + (Q * (T(TX, INT(xi - Ni + 1)) + 273.15) / 273.15))
    ELSE
    tf = 2 * Pi * .0841 * (INT(xi - Ni + 1) - (xi - Ni)) / ((Q * (T(TX, INT(xi - Ni)) +
273.15) / 273.15) + (Q * (T(TX, INT(xi - Ni + 1)) + 273.15) / 273.15))
  END IF
  FOR Z = INT(xi - Ni + 1) TO INT(xi - 1)
    IF Z > 57 THEN EXIT FOR
    IF Z > 52 THEN
      tf = tf + 2 * Pi * .002025 / ((Q * (T(TX, Z) + 273.15) / 273.15) + (Q * (T(TX, Z +
1) + 273.15) / 273.15))
    ELSE
      tf = tf + 2 * Pi * .0841 / ((Q * (T(TX, Z) + 273.15) / 273.15) + (Q * (T(TX, Z + 1)
+ 273.15) / 273.15))
    END IF
  NEXT Z
  IF xi > 53 AND xi < 58 THEN
    tf = tf + 2 * Pi * .002025 * (xi - INT(xi)) / ((Q * (T(TX, INT(xi)) + 273.15) /
273.15) + (Q * (T(TX, INT(xi + 1)) + 273.15) / 273.15))
  END IF
  IF xi <= 53 THEN
    tf = tf + 2 * Pi * .0841 * (xi - INT(xi)) / ((Q * (T(TX, INT(xi)) + 273.15) / 273.15) +
(Q * (T(TX, INT(xi + 1)) + 273.15) / 273.15))
  END IF
```

```
  tt = tt + tf

'Check if the nuclide has decayed ?
  IF tt > td THEN
   LOSS(TX) = LOSS(TX) + 1
   EXIT DO
  END IF

'Check if the molecule has left the column ?
  IF xi > 58 THEN
   MADEIT(TX) = MADEIT(TX) + 1
   EXIT DO
  END IF

'Generate a random time the molecule spent adsorbed
'Calculate t mean
   tm = p0 * 1E-12 * EXP((-DHa * 1E+10) / (R * (T(TX, CINT(xi)) + 273.15)))
   'Calculate vi (mean number of collisions)
   IF xi > 53 THEN
     vi = .045 / (Q * (T(TX, CINT(xi)) + 273.15) / 273.15) * SQR(2 * Pi * R * (T(TX,
CINT(xi)) + 273.15) / M1)
   ELSE
     vi = .29 / (Q * (T(TX, CINT(xi)) + 273.15) / 273.15) * SQR(2 * Pi * R * (T(TX,
CINT(xi)) + 273.15) / M1)
   END IF
```

```
'Generate a random ta
'Since RND actually can be 0 use 1-RND as random number
  ta = -vi * tm * Nm * LOG(1 - RND)

'Update total time
  tt = tt + ta

'Check if the nuclide has already decayed ?
  IF tt > td THEN
   LOSS(TX) = LOSS(TX) + 1
   EXIT DO
  END IF
 LOOP WHILE tt <= td AND xi <= 58
 NEXT L
 PRINT #2, (TX + 1) * 50, MADEIT(TX), LOSS(TX), (MADEIT(TX) / I) * 100
NEXT TX
PRINT #2,
PRINT #2,
NEXT DHa
CLOSE #2
```

References

[AND 90] Andreyev, A. N., Bogdanov, D. D., Chepigin, V. I., Kabachenko, A. P., Sharo, S., Ter-akopian,G. M., Yeremin, A. V., Z. Phys. A, 337, 231-232 (1990).

[AUM 74] Aumann, D. C., Müllen, G., Nucl. Instr. Meth. 115, 75 (1974).

[BEL 75] Belov, V. Z., Zvarova, T. S., Shalaevsky, M. R., Sov. Radiochem. 17, 86 (1975).

[BRE 71] Brewer, L. J., Opt. Soc. Am., 61, 1101 (1971).

[BRE 84] Brewer, L., High Temp. Sci. 17, 1 (1984).

[BRU 81] Bruchertseifer, H., Eichler, B., Radiochem. Radio-anal. Lett. 48, 391 (1981).

[BRU 86] Brüchle, W., Agarwal, Y. L., Armbruster, P., Brügger, M., Dufour, J. P., Gäggeler, H., Hessberger, F. P., Hofmann, S., Lemmertz, P., Münzenberg, G., Poppensieker, K., Reisdorf, W., Schädel, M., Schmidt, K. H., Schneider, J. H. R., Schneider, W. F. W., Sümmerer, K., Vermeulen, D., Wirth, G., Ghiorso, A., Gregorich, K., Lee, D., Leino, M., Moody, K. J., Seaborg, G. T., Welch, R. B., Wilmarth, P., Yashita, S., Frink, C., Greulich, N., Herrmann, G., Hickmann, U., Hildebrand, N., Kratz, J. V., Trautmann, N., Fowler, M. M., Hoffman, D. C., Daniels, W. R., von Gunten, H. R., Dornhöfer, H., J. Less Comm. Metals, 122, 425 (1986).

[CON 79] Conder, J. R., and Young, G. L., Physicochemical Measurement by Gas Chromatography, Wiley, New York (1979).

[DEB 53] Deboer, J. H., The Dynamical Character of Adsorption, Clarendon Press, Oxford (1953).

[DES 80] Desclaux, J. P., and Fricke, B., J. Phys. (paris) 41, 943 (1980).

[EIC 82] Eichler, B., Zvara, I., RAdiochim. Acta 30, 233 (1982).

[EVA 72] Evans, J. E., Lougheed, R. W., Coops, M. S., Hoff, R. W., Hulet, E. K., Nucl. Instr. Meth. 102, 389 (1972).

[FRI 69] Fricke, B., and Greiner, W., Phys. Lett. 30B, 347 (1969).

[FRI SUB] Fricke, B., Johnson, E., Radiochim. Acta, to be submitted.

[GAG 85] Gäggeler, H. W., Dornhöfer, H., Schmidt-Ott, W. D., Greulich, N., Eichler, B., Radiochim. Acta, 38, 103 (1985).

[GAG 88] Gäggeler, H. W., Report Paul Scherrer Institute, PSI-14 (1988).

[GAG 91] Gäggeler, H. W., Jost, D. T., Baltensperger, U., Weber, A., Kovacs, A., Vermeulen, D., Türler, A., Nucl. Instr. and Meth., A309, 201 (1991).

[GAG 92] Gäggeler, H. W., Jost, D. T., Kovacs, J., Scherer, U. W., Weber, D., Vermeulen, A., Türler, A., Gregorich, K. E., Henderson, R. A., Czerwinski, K. R., Kadkhodayan, B., Lee, D. M., Nurmia, M., Hoffman, D. C., Kratz, J. V., Gober, M. K., Zimmermann, H. P., Zvara, I., Radiochim. Acta, 57, 93-100 (1992).

[GHI 70] Ghiorso, A., Nurmia, M., Eskola, D., Eskola, P., Phys. Let., 32B, 95 (1970).

[GID 65] Giddings, J. C., Dynamics of Chromatography, Part I, Principles and Theory, Marcel Dekker, New York 154 (1965).

[GLE 89] Glebov, V. A., Kasztura, L., Nefedov, V. S., and Zhuikov, B. L., Radiochim. Acta 46, 117 (1989).

[GOR 49] Gormley, P. G., Kennedy, M., Proc. R. Ir. Acad. 52A, 163 (1949).

[GRE 90] Gregorich, K. E., Nucl. Instr. and Meth., A302, 135-142 (1991).

[GRU 72] Grushka, I., Manyard, V., J. Chem Educ. 49, 565 (1972).

[HIL 49] Hill, T. L., J. Chem. Phys., 17, 520 (1949).

[HOF 80] Hoffman, D. C., Lee, D., Ghiorso, A., Nurmia, M., Aleklett, K., Phys. Rev. C22, 1581 (1980).

[HOR 69] Horowitz, E. P., Bloomquist, C. A. A., Henderson, D. J., Nelson, D. E., J. Inorg. Nucl. Chem. 31, 3255 (1969).

[HYD 87] Hyde, E. K., Hoffman, D. C., Keller, O. L. Jr., Radiochim. Acta, 42, 57 (1987).

[JOS 88] Jost, D. T., Gäggeler, H. W., Vogel, C. H., Schädel, M., Jäger, E., Eichler, B., Gregorich, K. E., Hoffman, D. C., Inorg. Chim. Acta 146, 255 (1988)

[KAD 92] Kadkhodayan, B., Türler, A., Gregorich, K. E., Nurmia, M. J., Lee, D. M., Hoffman, D. C., Nucl. Instr. and Meth., A317, 254-261 (1992).

[KAT 86] Katz, J. J., Seaborg, G. T., and Morss, L. R., The chemistry of the Actinide elements, Chapman and Hall, Second ed., Vol. 2, 1629-1633 (1986).

[KEL 84] Keller, Jr., O. L., Radiochim. Acta 37, 169 (1984).

[KRA 89] Kratz, J. V., Zimmermann, H. P., Scherer, U. W., Schädel, M.,Brüchle, W., Gregorich, K. E., Gannett, C. M., Hall, H. L., Henderson, R. A., Lee, D. M., Leyba, J. D., Nurmia, M. J., Hoffman, D. C., Gäggeler, H. W., Jost, D., Baltensperger, U., Ya Nai-Qi, Türler, A., Lienert, C. H., Radiochim. Acta 48, 121 (1989).

[KRA 92] Kratz, J. V., Gober, M. K., Zimmermann, H. P., Schädel, M., Brüchle, W., Schimpf, E., Gregorich, K. E., Türler, A., Hannink, N. J., Czerwinski, K. R., Kadkhodayan, B., Lee, D. M., Nurmia, M. J., Hoffman, D. C., Gäggeler, H., Jost, D., Kovacs, J., Scherer, U. W., Weber, A., Phys. Rev. C., 45, 1064 (1992).

[LAU 78] Laub, R. J., and Pecsok, R. L., Physicochemical Applications of Gas Chromatography, Wiley, New York (1978).

[LEI 70] Leipnitz, E., Struppe, H. G., Handbuch der Gaschromatographie, Verlag Chemie, Weinheim, 40 (1970).

[LER 87] Leres, R. G., Lawrence Berkeley Laboratory report #24808, Engineering Division (1987).

[MOO 83] Moody, K. J., Ph.D. thesis, University of California, Berkeley, 1983).

[MUL 75] Müllen, G., Aumann, D. C., Nucl. Instr. Meth. 128, 425 (1975).

[PER 92] Perishina, V., Sepp, W. D., Bastug, T., Fricke, B., Ionova, G. V., J. Chem. Phys. 97, 1123 (1992).

[PER 93] Perishina, V., private communications (1993).

[ROU 69] Routti, J. T., Prussin, S. G., Nucl. Inst. Meth., 72, 125 (1969).

[RUD 79] Rudolph, J., Bächman, K., J. Chrom. 178, 459-469 (1979).

[RUD 80] Rudolph, J., Bächmann, K., Radiochim. Acta 27, 105-108 (1980).

[RUD 80b] Rudolph, J., Bächman, K., J. Chrom. 187, 319-329 (1980)

[PYY 88] Pyyko, P., Chem. Rev. 88, 563 (1988).

[SHI 78] Shihab-Eldin, A. A., Jardine, L. J., Tuli, J. K., Buyrn, A. B., Table of Isotopes, John Wiley & Sons, Inc., Vol. 7 (1978).

[TIM 89] Timokhin, S. N., Kim, U. Jin, Domanov, V. P., Chuburkov, Yu. T., Zhuikov, B. L., Gavrilov, K. A., and Zvara, I., Int. Conf. Actinides, '89, Tashkent, USSR, September, 1989, Abstracts, Nauka, Moscow, p.227.

[TUR 90] Türler, A., Gregorich, K. E., Lee, D. M., Nurmia, M. J., Czerwinski, K. R., Hannink, N. J., Henderson, R. A., Kacher, C. D., Kadkhodayan, B., Kreek, S. A., Leyba, J. D., Hoffman, D.C., Gäggeler, H., Jost, D. T., Weber, A., Kovacs, J., Scherer, U. W., Kratz, J. V., Gober, M., Zimmermann, H. P., Schädel, Brüchle, W., Schimpf, E., and Barth, H., J. Radioanal. Nucl. Chem. in press.

[TUR 91] Türler, A, Gregorich, K. E., Hoffman, D. C., Lee, D. M., and Gäggeler, H. W., Lawrence Berkeley Laboratory annual report #31855, Nuclear Science Division (1991).

[TUR 93] Türler, A, Private communication.

[YA 89] Ya Nai-Qi, Jost, D. T., Baltensperger, U., Gäggeler, H. W., Radiochemica Acta 47, 1-7 (1989).

[ZHU 89] Zhuikov, B. L., Chuburkov, Yu. T., Timokhin, S. N., Jin, K. U., Zvara, I., Radiochim. Acta 46, 113 (1989).

[ZHU 90] Zhuikov, B. L., Glebov, V. A., Nefedov, V. S., and Zvara, I., Int. Conf. Actinides '89, Tashkent, USSR; Radioanal. and Nucl. Chem. Articles, 143, 103 (1990).

[ZVA.66] Zvara, I., Chuburkov, Yu. T., Caletka, R., Zvarova, T. S., Shalaevsky, M.R., Shilov, B. V., At. Energ. 21, 81 (1966).

[ZVA 69] Zvara, I., Chuburkov, Yu. T., Caletka, R., Shalaevsky, M. R., Sov. Radiochem. 11, 161 (1969).

[ZVA 70] Zvara, I. Chuburkov, Yu. T., Belov, V. Z., Buklanov, G. V., Zakhvataev, B. V., Zvarova, T. S., Maslov, O. D., Caletka, R., Shalaevsky, M. R., J. Inorg. Nucl. Chem. 32, 1855 (1970).

[ZVA 76] Zvara, I., Belov, V. Z., Domanov, V. P., Shalaevski, M. R., Radiokhimiya 18, 371 (1976).

[ZVA 85] Zvara, I., Radiochimica Acta 38, 95-101 (1985).

[ZVA 89] Zvara, I., Int. Conf. Actinides '89, Tashkent, USSR, September, 1989, Abstracts, Nauka, Moscow, p.989.

LAWRENCE BERKELEY LABORATORY
UNIVERSITY OF CALIFORNIA
TECHNICAL INFORMATION DEPARTMENT
BERKELEY, CALIFORNIA 94720